IN VIVO CERVICAL SPINE KINEMATICS, ARTHROKINEMATICS AND DISC LOADING IN ASYMPTOMATIC CONTROL SUBJECTS AND ANTERIOR FUSION PATIENTS

by

William Anderst

BS in Mechanical Engineering, University of Notre Dame, 1991

MS in Kinesiology, Indiana University, 1993

Submitted to the Graduate Faculty of

Swanson School of Engineering in partial fulfillment

of the requirements for the degree of

Doctor of Philosophy in Bioengineering

University of Pittsburgh

2014

UNIVERSITY OF PITTSBURGH

SWANSON SCHOOL OF ENGINEERING

This dissertation was presented

by

William Anderst

It was defended on

July 16, 2014

and approved by

John Brigham, PhD, Assistant Professor, Department of Civil and Environmental Engineering

Richard Debski, PhD, Associate Professor, Department of Bioengineering

James Kang, MD, Professor, Department of Orthopaedic Surgery

Dissertation Director: Scott Tashman, Associate Professor, Department of Orthopaedic Surgery

IN VIVO CERVICAL SPINE KINEMATICS, ARTHROKINEMATICS AND DISC LOADING IN ASYMPTOMATIC CONTROL SUBJECTS AND ANTERIOR FUSION PATIENTS

William Anderst, PhD

University of Pittsburgh, 2014

Approximately 25% of cervical arthrodesis patients require reoperation within 10 years of the initial surgery due to degeneration of motion segments adjacent to the arthrodesis. Adjacent segment degeneration is believed to result from one or more of the following distinct causes: 1) the natural history of the adjacent disc; 2) biomechanical stress on the adjacent level following the fusion; and 3) disruption of the adjacent segment anatomy due to the initial surgery. The overarching hypothesis of this study is that, after fusion, mechanical factors initiate disc degeneration by exposing the disc tissue to novel, excessive loads. The aims of this study were to identify kinematic and arthrokinematic characteristics of cervical spine motion that differentiate asymptomatic subjects from single-level anterior fusion patients during *in vivo* functional loading, and to verify and validate a single-level, subject-specific finite element model of the sub-axial cervical spine. Twenty asymptomatic control subjects and 17 single-level ACDF patients of similar age performed dynamic flexion-extension of the cervical spine while biplane radiographs were collected at 30 images per second. A previously validated volumetric model-based tracking process matched subject-specific vertebral bone models to each pair of radiographs with sub-millimeter accuracy. Adjacent segment kinematics (total range of motion, contributions to motion, path of the center of rotation) were not significantly different between fusion and control groups. Adjacent segment arthrokinematics (disc and facet joint capsule

deformation) were significantly different between groups. Inverse dynamics and finite element computational models indicated that, relative to the static neutral position, the force applied to the C56 motion segment increased by five times head weight during full extension.

This study has identified differences in the mechanics of adjacent segments during dynamic functional loading. The results suggest that in order to evaluate the effects of fusion on adjacent segments, from a mechanical perspective and clinical perspective, it may be most beneficial to assess arthrokinematic factors such as disc deformation and facet joint capsule deformation, rather than more traditional kinematic parameters such as range of motion and center of rotation.

TABLE OF CONTENTS

LIST OF TABLES

LIST OF FIGURES

PREFACE

This work was supported in part by Grant R03-AR056265 from NIH/NIAMS and a 21st Century Development Grant from the Cervical Spine Research Society.

1.0 INTRODUCTION

1.1 BACKGROUND

1.1.1 Anterior Cervical Fusion

Anterior cervical fusion, introduced in the 1950s[1], has emerged as the most popular surgical treatment for cervical spine disorders. The number of anterior fusions increased eight-fold, from 9,578 to 78,007 per year[2] during the 1990's. By the year 2000, anterior fusion accounted for 69.5% of all cervical spine disease procedures, and it was the most common surgical procedure to treat degenerative cervical spine disease in the United States[2]. The dramatic rise in anterior fusion procedures has been attributed to numerous factors, including the increased number of older persons, improved diagnostic and imaging technology, increased access to spine surgeons, and changes in the preferred choice of surgical technique[2-4].

1.1.2 Adjacent Segment Disease

In spite of the widespread popularity of anterior cervical fusion, subsequent degeneration adjacent to the surgical site (adjacent segment disease) remains a concern for patients and

surgeons. A 21-year follow-up report has indicated 32% of anterior fusion patients developed recurrent pain an average of 7.2 years after surgery, and 16% required surgery for disc disease at an adjacent level[5]. It has also been reported that between 16%[6] and 25%[7] of patients who have anterior cervical fusion have new diseases at an adjacent level within 10 years of the operation. Even short-term follow-up (17 months) has revealed more pronounced degenerative changes adjacent to the fusion compared to remote levels[8]. Although degenerative changes adjacent to fused cervical vertebrae have been well documented[5-11], the etiology of adjacent segment disease remains unclear[12,13]. This has led to an unresolved controversy among clinicians. Some clinicians believe the disease may progress due to the underlying spondylosis[7,14]. Alternatively, the fusion may lead to increased motion in adjacent vertebrae, resulting in overload and instability[10,12,15-17].

1.1.3 In Vivo Cervical Spine Movement

This controversy remains unresolved, in part, due to the fact that a comprehensive understanding of cervical spine kinematics during functional movement in asymptomatic subjects (let alone fusion patients) does not yet exist. Although *in vivo* range of motion between adjacent vertebrae during flexion-extension in asymptomatic subjects has been widely reported[16,18-20, 21-23], it should be noted that all of these results were obtained by analyzing 2D lateral radiographs collected with subjects in static positions. A small number of studies have reported cervical kinematics during dynamic movements. One study reported the timing of movement initiation in the cervical spine[24], a second reported on translation and rotation range of motion in young subjects[25], while a third reported the averaged location of the intervertebral center of rotation during flexion-

extension[26]. These studies were all completed by manually identifying landmarks on the vertebrae in order to calculate spine motion. Manual identification of anatomical landmarks can lead to high variability in measurements, evident by the large standard deviations in these studies[22,23]. Additionally, only one study has reported the precision of their measurements[23], while none have reported the bias in their measurement techniques. Therefore, the true intervertebral kinematics during functional motion remain ill defined due to limitations inherent in previous measurement techniques.

More recently, automated measurements of 2D fluoroscopic images have been performed on data collected during very slow flexion-extension movements. However, in spite of the automated measurement software employed, only the pair of images collected at full flexion and extension were analyzed[27]. Unfortunately, even after the introduction of computer automated measurement techniques, insight into the dynamic behavior of the cervical spine during functional loading remains elusive. Numerous authors have noted the necessity for three-dimensional[16,28-32], *in vivo* [21,28,30,33] measurements of the cervical spine under dynamic load[16,27,33,34]. Currently there is a complete absence of data regarding in vivo, 3D movement of cervical vertebrae during functional loading. The present study addresses this shortcoming.

Arthrokinematics refers to the specific movements of joint surfaces. Normal joint surface movement is necessary to maintain long-term health of the joint. The arthrokinematic behavior of the cervical spine has yet to be described in the literature. Static measurements of disc height have been recorded from sagittal, static x-rays of the neck in the neutral position[23,35,36]. However, there are no reports describing changes in disc height during dynamic, functional motion. Likewise, there are no reports describing relative motion at the facet joints *in vivo*. The

proposed study will, for the first time, provide quantitative data revealing the relationship between vertebral body kinematics and disc and facet joint arthrokinematics.

1.1.4 Computational Models

Computational models are particularly useful because they can estimate tissue stress and strain without attaching or inserting measurement devices into the tissue. The first step toward the creation of a clinically useful computational model is to develop a process by which subject-specific models can be created and validated. These models can later be used to evaluate the efficacy of surgical and non-surgical interventions and, potentially, be used to predict impending tissue failure. Ultimately, this will lead to improved treatment for patients with cervical spine disorders.

Model credibility must be established before clinicians and scientists can be expected to extrapolate information and base decisions on model predictions[37,38]. In order to establish the credibility of a finite element model (as proposed in the current study) the model must be verified, validated, and a sensitivity analysis must be performed. The current study proposes to address this first, crucial step in the development of subject-specific finite element modeling of the cervical spine by performing convergence and sensitivity tests and by validating the kinematic output and disc pressure estimated by the model.

A model that can accurately estimate disc stress will be beneficial to clinicians. Clinically, it would be interesting to know how normal movement, degeneration, and surgical treatment affect the stress and strain in the disc because excessive disc loading may drive the degenerative process in the cervical spine. Internal disc stresses and strains are important for two reasons. High stress concentrations and stress gradients have the potential to disrupt the internal

tissue architecture, leading to progressive structural failure as seen in advanced disc degeneration[39]. Secondly, cell metabolism is sensitive to stresses and pressure in the surrounding matrix[39-41]. It is unclear which mechanical signals affect the cells most: stress or strain. While many studies have attempted to measure compressive forces in the spine, much less effort has been expended on trying to understand how the forces are distributed over the joint, even though it is stress (or pressure) that determines mechanical failure, and it is stress (and the resulting strain) that cells respond to[39]. It is clear that a model that can provide accurate estimates of disc stress and strain will have a significant clinical impact. Therefore, the model in the proposed study will be validated using normal values of disc pressure from the literature[42.]

The finite element model developed as part of this project will serve as the basis for future computational modeling of the cervical spine. The ultimate goal of this work will be to generate subject-specific computational models of the cervical spine. The single-level validated model will eventually be expanded to include the entire sub-axial cervical spine. Furthermore, the model may be improved to incorporate subject-specific kinematics and kinetics using motion data determined from the biplane x-ray system and head-mounted marker trajectories. In an effort to further individualize the models, efforts will be made to include subject-specific disc material properties derived from MRI data[43,44].

1.1.5 Basic Science Significance

The basic science portion of the present study proposes to quantify the movement of cervical vertebrae in asymptomatic subjects and fusion patients during *in vivo*, muscle-driven loading. This *in vivo*, dynamic data has not been reported previously. Identification of dynamic movement characteristics of "normal" and "abnormal" vertebral movement patterns is crucial for

future research focusing on improving surgical and non-surgical treatments leading to more successful clinical outcomes.

The computational models developed as part of this project will provide estimates of the in vivo forces applied to vertebrae and the associated stress within the disc during dynamic movement. This information is necessary for in vitro loading paradigms that assess disc response load. Additionally, forces applied to the disc may be used to apply realistic loading patterns to disc replacements in order to assess their feasibility.

1.1.6 Clinical Significance

This study will provide initial indications of specific *in vivo* vertebral movement patterns that may be detrimental to the health of vertebral discs following fusion. This information will be valuable to clinicians, allowing them to advise their patients on post-surgical behavior modification and rehabilitation treatments that will avoid movements potentially associated with adjacent segment disease.

Second, several new cervical artificial disc replacements have recently been approved for use in the United States. The effectiveness of these "motion preservation" devices and their *in vivo* behavior during muscle-driven movement is unknown. Although more expensive than a traditional fusion, the new disc replacements have not yet proven to be superior in reducing the occurrence of adjacent segment disease. For the clinician, it would be helpful to know the arthrokinematic changes that occur in adjacent segments following fusion, and if these changes can even be addressed by motion-preserving instrumentation. Although a complete answer to these questions will require a prospective, randomized clinical trial to properly evaluate the effectiveness of non-surgical options, traditional fusion, and "motion preserving" devices, the

current proposal will provide initial data on *in vivo* effects of fusion that the clinician can use to advise their patients as to the recommended surgical procedure for degenerative disc disease.

Finally, the information gained from the modeling portion of this study will form a basis for eventually evaluating the effects of surgical and non-surgical cervical spine interventions on spine tissue stress and strain. Ultimately, this will lead to improved treatment for patients with cervical spine disorders.

1.2 SPECIFIC AIMS

The proposed study employs a biplane radiographic system capable of tracking *in vivo* bone motion with sub-millimeter accuracy during functional loading. The biplane radiographic system will be used to record precise, three-dimensional, *in vivo*, muscle-driven movement of cervical vertebrae in asymptomatic subjects and single-level anterior cervical fusion patients while they perform flexion-extension movements. Three-dimensional relative motion between adjacent vertebrae (joint kinematics), the corresponding small amplitude motion between articulating surfaces (joint arthrokinematics), and disc stress determined from computational modeling will provide a unique set of information to characterize cervical spine mechanics.

Each specific aim intends to identify distinct mechanical characteristics that may affect cervical disc degeneration following single level anterior fusion. It is hypothesized that kinematic data will provide evidence of *in vivo* motion patterns following fusion that are detrimental to adjacent segment intervertebral discs. The arthrokinematic data is expected to reveal how modifications in joint kinematics following fusion lead to novel and destructive

adjacent segment surface interactions. Finally, the computational model will be verified and validated as a first step in the process of identifying tissue loading that may negatively affect intervertebral disc homeostasis adjacent to the fused motion segment.

1.2.1 Specific Aim 1

The first Specific Aim is to identify kinematic characteristics of cervical spine motion that differentiate asymptomatic subjects from single-level anterior fusion patients during in vivo functional loading.

Hypothesis 1: Six months after fusion surgery, vertebrae adjacent to the fused segment will move through significantly greater range of motion, exhibit a change in location of their center of rotation, and display a change in the order of sequential motion during flexion-extension when compared to asymptomatic control subjects.

1.2.2 Specific Aim 2

The second Specific Aim is to identify arthrokinematic characteristics of cervical spine motion that differentiate asymptomatic subjects from single-level anterior fusion patients during in vivo functional loading.

Hypothesis 2: Six months after fusion surgery, the compression and expansion of discs and the relative velocity between facet joint surfaces adjacent to the fused segment will be significantly different from corresponding discs and facets in asymptomatic control subjects.

1.2.3 Specific Aim 3

The third specific aim is to verify and validate a single-level, subject-specific finite element model of the sub-axial cervical spine.

A subject-specific finite element model, with tissue geometry and material properties derived from medical images, will be developed. Convergence tests will be performed on disc and vertebra components of the models. A sensitivity analysis of bone, disc and ligament mechanical properties will be completed. The model will be validated using subject-specific in vivo kinematic data and previously published experimental results for disc stress.

1.2.4 Summary of Aims

The overarching hypothesis of this study is that mechanical factors initiate disc degeneration following fusion by exposing the disc tissue to novel, excessive loads. In fact, measurable changes in the mechanical environment may precede perceptible alterations in the biological environment. Thus, mechanical factors may be superior to biological or chemical indicators of impending disc degeneration. By identifying mechanical characteristics that are potentially harmful to the disc, the information gained from this study may eventually be applied to evaluate the efficacy of surgical and non-surgical interventions. Ultimately, this will lead to improved treatment for patients with cervical degenerative disc disease.

2.0 INTERVERTEBRAL KINEMATICS

2.1 RANGE OF MOTION

2.1.1 Introduction

Degenerative changes adjacent to fused cervical vertebrae have been well documented[5-11], and may occur as early as 17 months following surgery[8]. These degenerative changes occur in 16% (out of 112 patients)[6] to 25% (out of 374 patients)[7] of patients within 10 years of the operation, and require adjacent level surgery in 6% to 10% of patients[11,45-48] (out of 38 to 180 patients). A 21-year follow-up report of 50 patients has indicated 32% of anterior arthrodesis patients developed recurrent pain an average of 7.2 years after surgery, and 16% required surgery for disc disease at an adjacent level[5]. The literature is inconclusive as to the most likely location for adjacent segment degeneration, as one study suggested progressive degeneration occurs with equal frequency superior and inferior to the fused segment[49] while another determined adjacent segment degeneration is level-dependent and most prevalent at the C5/C6 and C6/C7 discs[7]. The etiology of adjacent segment disease following cervical arthrodesis remains controversial. The disease may progress due to the underlying spondylosis[7,14,50], the arthrodesis may lead to

increased motion in adjacent vertebrae, resulting in overload[10,12,15-17], or adjacent segment degeneration may result from a combination of these two factors[9,11].

Investigations designed to identify mechanical factors that may expedite adjacent segment degeneration have primarily focused on excessive motion adjacent to the fused segment during flexion-extension. In order to identify excessive motion, the normal range of motion (ROM) in asymptomatic subjects must first be defined. This has been previously accomplished by manually identifying anatomic landmarks on 2D lateral radiographs[16,18-23,51]. These measurements have inherent limitations including potential differences between ROM calculated from radiographs collected in static positions versus during dynamic, muscle-driven movement[30], the high measurement variability associated with manual digitization[22,23,25,27,52], and the inability to assess motion that occurs out of the film plane. Numerous authors have noted the necessity for three-dimensional[16,28-32], in vivo[21,28,30,33] measurements of the cervical spine under dynamic load[16,27,33,34].

The overall objective of the current study was to evaluate cervical intervertebral range of motion during dynamic flexion-extension in single-level anterior cervical discectomy and fusion (ACDF) patients and asymptomatic control subjects. The first aim was to assess differences between control subject intervertebral ROM and intervertebral ROM following single-level ACDF in terms of all six degrees of freedom (3 translations and 3 rotations). The second aim was to compare static ROM measurements to those obtained during dynamic, functional movement.

2.1.2 Materials and Methods

2.1.2.1 Subjects

Following Institutional Review Board (IRB) approval, subjects who were at least 18 years of age and scheduled to undergo (or recently received) single-level ACDF surgery were identified during clinic visits. Pregnant women, patients diagnosed with osteoporosis, and patients with any other injury or disease that interferes with spine function were excluded. Asymptomatic controls were recruited to approximately match the age and gender distribution of the arthrodesis subjects. Control subject recruitment was accomplished through an advertisement in an employee newsletter and word of mouth. Data from 30 subjects (10 C5/C6 arthrodesis patients and 20 controls) who provided informed consent to participate in this study was included in the present analysis.

2.1.2.2 Data Collection and Processing

High-resolution CT scans (0.29x0.29x1.25 mm voxels) of the cervical spine (C2-C7) were acquired on each participant (GE Lightspeed 16, GE Medical Systems, Waukesha, WI). Bone tissue was segmented from the CT volume using a combination of commercial software (Mimics software, Materialise, Leuven, Belgium) and manual segmentation[53]. A three-dimensional (3D) model of each vertebra was generated from the segmented bone tissue[54]. Markers were interactively placed on the 3D bone models to define bone-specific anatomic coordinate systems.

Subjects performed continuous full ROM flexion-extension to the beat of a metronome set at a rate of 40 to 44 beats per minute to complete one full movement cycle in approximately 3 seconds. Biplane radiographs were collected at 30 images per second for 3 seconds for two to three dynamic movement trials per subject (Figure 1). A total of 78 dynamic flexion-extension

trials were included in this analysis. Three static trials were also collected for each subject: one in the neutral position, one in full flexion, and one in full extension. For the flexion radiograph, subjects were instructed and encouraged to flex their head down as far as possible, pushing the chin into the chest if possible. For the extension radiograph, they were instructed and encouraged to look up and back as far as possible. For the neutral radiograph, they were instructed to look directly forward. A previously validated tracking process determined three-dimensional vertebral position in each pair of radiographs with sub-millimeter accuracy[55] for all static and dynamic trials (Figure 2). Details describing the model-based tracking process, including hardware and software specifications, calibration and distortion correction procedures, and computational algorithms have been described previously[55-58].

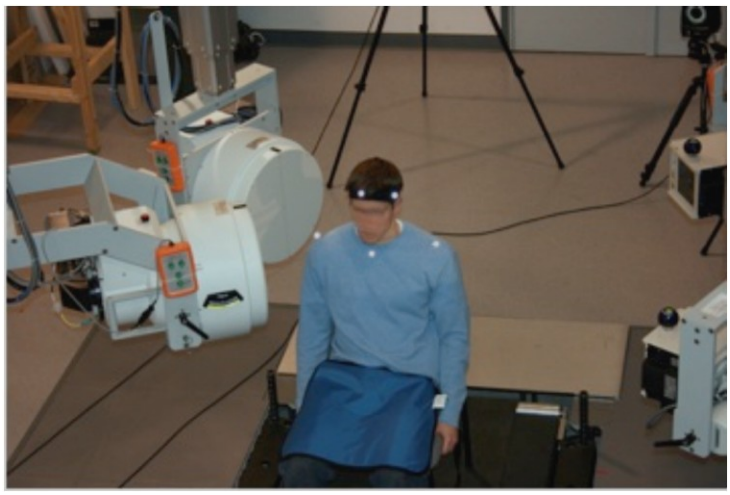

Figure 1: Biplane X-ray data collection system.

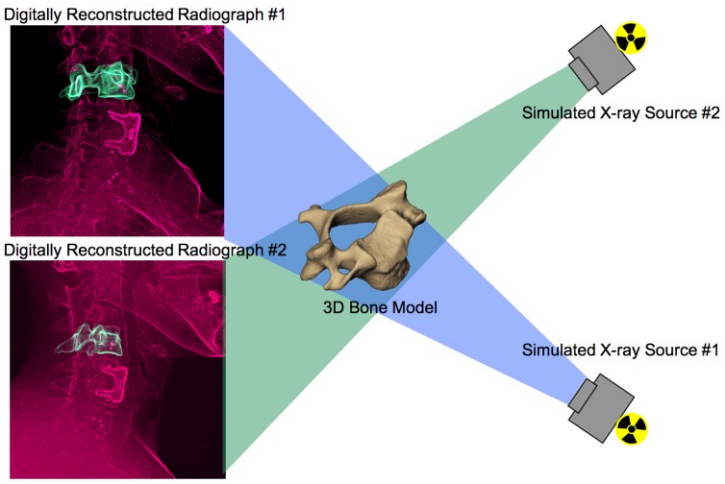

Figure 2: Virtual X-Ray system for model-based tracking.

Tracked data was filtered at 1.7 Hz using a fourth-order, low-pass Butterworth filter with the filter frequency determined using residual analysis[59]. Six degree-of-freedom (DOF) kinematics between adjacent vertebrae (3 translations: medial-lateral (ML), superior-inferior (SI) and anterior-posterior (AP); 3 rotations: flexion-extension (FE), twist (TW) and lateral bend (LB)) were calculated for every frame in each trial in accordance with established standards for reporting spine kinematics[60,61] (Figure 3).

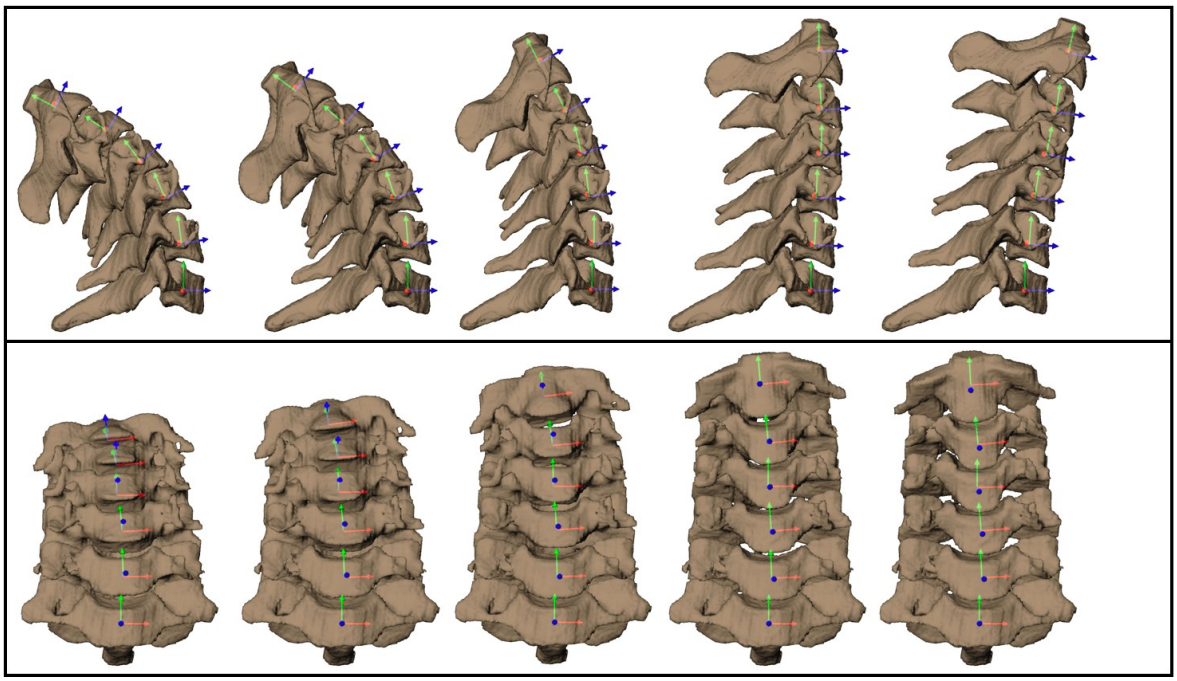

Figure 3: Three-dimensional bone models at five instants of the flexion cycle.

Three-dimensional motion data for C2 was not available for four arthrodesis subjects, either because the CT scan did not include enough of this bone or because the subject was positioned incorrectly within the field-of-view of the biplane X-ray system. These oversights in data collection were corrected prior to testing any asymptomatic control subjects. Thus, C2/C3 data is presented only for the asymptomatic control group.

2.1.2.3 Analyzed Parameters

Six degree-of-freedom (DOF) ROM was calculated from the maximum and minimum values for each of the six kinematic parameters describing relative motion between adjacent bones (3 translations and 3 rotations) for each motion segment for each trial (Figure 4). The standard deviation of these ROM values over all trials for a given subject defined the trial-to-trial variability. It is important to note that these maximum and minimum values may have occurred

at any point of the movement cycle; they did not necessarily occur at the end of the head flexion-extension range of motion. This was especially true for parameters describing motion out of the flexion-extension plane. The maximum overall ROM for each parameter was then calculated by finding the maximum and minimum value of each parameter over all dynamic movement trials for a given subject (the dynamic ROM).

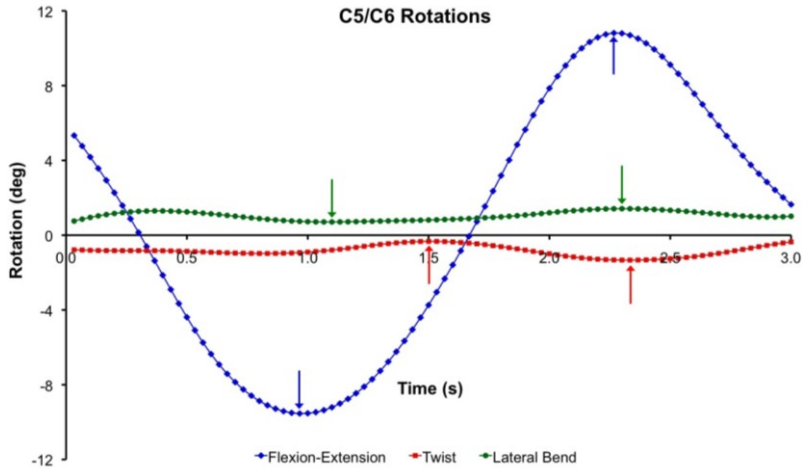

Figure 4: Intervertebral angles during the flexion-extension motion.

Intervertebral range of motion was also calculated from the static full-flexion and static full-extension images for each subject (the static ROM). An additional measurement, termed "clinical anterior-posterior ROM", was calculated using the inferior-posterior edge of the superior vertebral body and the superior-posterior edge of the inferior vertebral body. This measurement was similar to a previous method used to quantify anterior-posterior translation as is typically measured clinically[62].

Static alignment between adjacent vertebrae was determined from the static neutral trial from each subject. The maximum amount of flexion and anterior translation as well as the

maximum amount of extension and posterior translation were determined relative to this static neutral position for the dynamic flexion-extension trials.

Disc height in the anterior annulus, nucleus, and posterior annulus regions was determined for each subject in order to assess disc degeneration. Nucleus and annulus regions were defined on the bone model endplate surfaces according to previous reports[49,50] and disc height measurements were acquired within the central 1/3rd of the disc width (Figure 5). Average disc height within the nucleus, anterior annulus, and posterior annulus region was determined from the static trial with the subject in an upright neutral position (Figure 6).

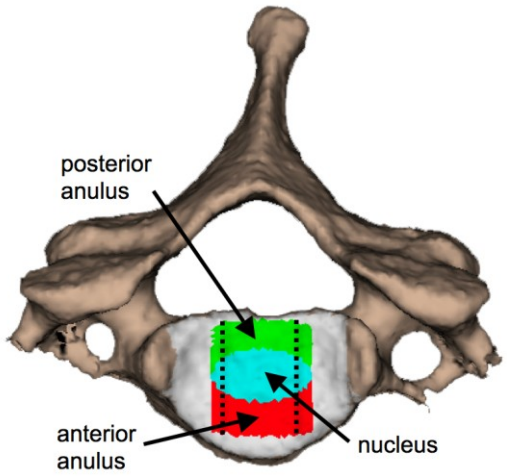

Figure 5: Disc regions.

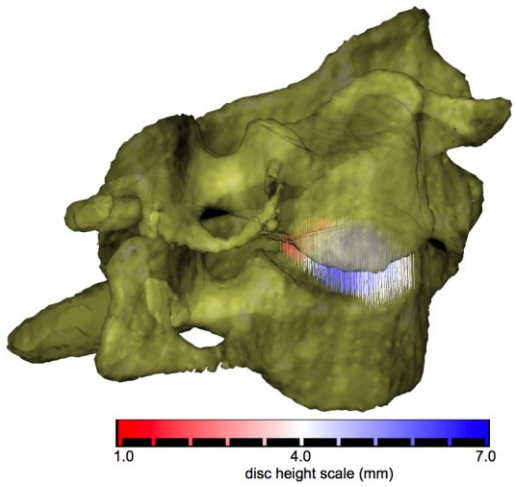

Figure 6: Color-coded disc height on a C6/C7 motion segment.

2.1.2.4 Statistical Design and Analysis

Sample size was determined using variability estimates from previous studies that used CT model-based tracking and kinematic measurement techniques that were similar to the current study[56,58], and power set at 0.80, so that differences between groups as small as 1.0º in rotation could be detected[63]. Analysis of variance was used to assess all differences between the control and arthrodesis groups. Paired t-tests were used to identify differences between static and dynamic six DOF ROM within all subjects. Significance was set at $p < .05$ for all tests and significance levels were adjusted for multiple comparisons using the False Discovery Rate[64]. P-values listed in all tables were significant after adjusting for multiple comparisons.

2.1.3 Results

2.1.3.1 Rotational Range of Motion

Dynamic ROM in asymptomatic controls during the flexion-extension movement was largest in the flexion-extension direction, followed by the lateral bend direction, and smallest in the twist direction at every motion segment (Appendix A, Table 2). Significant differences between the control group and C5/C6 arthrodesis group were identified at the operated motion segment, with flexion-extension ROM significantly less in the arthrodesis group (average difference: -11.8º, 95% CI -14.9º to -8.7º, $p < .001$). Twist rotation was also significantly larger inferior to the operated segment ($p < .001$) in comparison to controls. The total ROM in the flexion-extension direction was not significantly different between the control and arthrodesis groups at any non-operated motion segment (all $p > .370$).

Flexion-extension ROM was further characterized by separating the total flexion-extension ROM into flexion ROM and extension ROM using the static neutral trial as a reference. In the control group, the flexion ROM was larger than the extension ROM at each motion segment, however, this difference did not reach statistical significance at any level ($p = .096$) (Appendix A, Table 3). The distribution of flexion and extension ROM in C5/C6 arthrodesis subjects was opposite that of the controls. In arthrodesis subjects, the extension ROM was larger than the flexion ROM at each non-operated motion segment. In fact, for the C4/C5 motion segment, the extension ROM was significantly greater in C5/C6 arthrodesis patients in comparison to asymptomatic control subjects (average difference 3.8º, 95% CI 0.9º to 6.6º, $p = .011$) while the flexion ROM was significantly less in C5/C6 arthrodesis patients in comparison to asymptomatic control subjects (average difference -2.9º, 95% CI -5.3º to -0.5º, $p = .019$) (Appendix A, Table 3; Figure 7). Overall head ROM relative to the trunk was 40.9º ± 9.7º

in flexion and 45.3º ± 12.8º in extension for the control group, while overall head ROM relative to the trunk was 35.3º ± 8.5º and 43.5º ± 11.6º in flexion and extension, respectively, for the arthrodesis group.

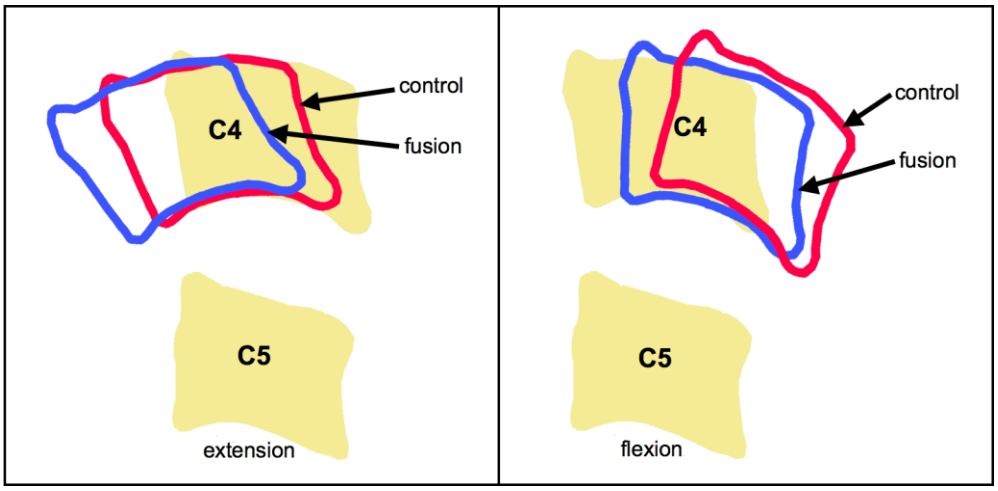

Figure 7: Representation of flexion-extension ROM in C5/C6 fusion and control groups.

2.1.3.2 Translation Range of Motion

The only significant difference between the control and C5/C6 arthrodesis groups in total dynamic translation ROM was at the fused motion segment, with anterior-posterior ROM significantly less in the arthrodesis group (average difference: -2.6 mm, 95% CI -3.2 to -2.0 mm, $p < .001$) (Appendix A, Table 4). The total anterior-posterior ROM was larger superior to the C5/C6 motion segment in comparison to controls, however, this difference did not reach statistical significance ($p = .063$).

When the total anterior-posterior ROM was divided into anterior ROM and posterior ROM using the static neutral trial as a reference, trends were similar to those found when analyzing flexion and extension components of the total dynamic ROM (Appendix A, Table 5;

Figure 7). Specifically, anterior translation was consistently less and posterior translation was consistently greater in C5/C6 arthrodesis subjects in comparison to controls at each non-fused motion segment. The difference in posterior translation was statistically significant at the C6/C7 motion segment (average difference: 0.4 mm, 95%CI 0.0 to 0.8 mm, p = .016), but not at the C4/C5 motion segment after correcting for multiple comparisons (p = .043, N.S.).

2.1.3.3 Clinical Translation Range of Motion

Intervertebral translation in control subjects, as typically measured clinically, ranged from 1.1 mm to 2.3 mm, with no significant differences among levels (Table 1). The only significant difference between control and arthrodesis patients in clinical AP translation occurred at the operated motion segment (p < .001).

Table 1: Clinical anterior-posterior translation range of motion during flexion-extension.

Group	C2/C3	C3/C4	C4/C5	C5/C6	C6/C7
Control	2.0±0.5	2.3±0.6	2.3±0.6	1.7±0.8	1.1±0.6
C56 Fusion	N/A	2.3±0.4	2.8±0.8	0.6±0.3*	1.3±0.3
Difference	N/A	0.0	0.5	-1.0	0.2
95% CI	N/A	-0.4 to 0.4	-0.1 to 1.0	-1.5 to -0.6	-0.2 to 0.6

2.1.3.4 Trial-to-Trial Variability

Average trial-to-trial variability in maximum rotational ROM (defined as the standard deviation of the maximum ROM for all trials for a given subject) was 0.9º or less for all 3 rotational DOF in control subjects during dynamic trials. Variability was consistently greater in flexion-extension rotation (0.4º to 0.9º) than in twist or lateral bend rotation (0.2º to 0.4º) for control subjects. Trial-to-trial variability in rotation ROM was not significantly different between control and fusion groups (all p > .056).

Trial-to-trial variability in maximum translation ROM was .22 mm or less for all 3 translational DOF in control subjects during dynamic trials. Significantly greater variability in C5/C6 fusion subjects in comparison to controls was observed in the medial-lateral direction inferior to the fused segment ($p < .001$).

2.1.3.5 Static versus Dynamic Range of Motion

Intervertebral ROM measured during dynamic, functional movement tended to be larger than intervertebral ROM measured from static full-flexion and full-extension images (Appendix A Table 7, Appendix A Table 8). In control subjects, dynamic ROM was significantly greater than ROM measured from static images in all three rotational and translational DOF in the C2/C3, C3/C4 and C4/C5 motion segments. The effect of measuring ROM using images collected during active motion, as opposed to images collected with the subject stationary, was typically greater in C5/C6 arthrodesis patients than in control subjects (Appendix A Table 7, Appendix A Table 8).

2.1.3.6 Disc Height

Disc height measurements indicated no significant differences between control and arthrodesis groups. No differences in disc height were identified among disc levels in control subjects ($p = .253$), however, significant differences were observed among disc regions (Appendix A, Table 8). Nucleus height was significantly greater than anterior annulus height and posterior annulus height ($p = .001$ and $p < .001$, respectively), while anterior annulus height was significantly greater than posterior annulus height ($p < .001$). Differences between fusion and control subject disc heights were further reduced when corrected for bone size.

2.1.4 Discussion

No significant differences between control subject and C5/C6 arthrodesis patient ROM in non-operated vertebrae were identified in the primary directions of motion during flexion-extension (i.e. flexion-extension rotation and anterior-posterior translation). This result agrees with previous reports that indicated adjacent segment kinematics remained unchanged approximately one year after arthrodesis[13,65], but these results contradict another report of significantly less intersegmental ROM at "almost every level" when arthrodesis subjects were compared to control subjects[66]. The lack of significant in vivo differences between arthrodesis and control group total ROM contradicts in vitro studies that showed excessive motion following arthrodesis on cadaver specimens[12,67-70], suggesting in vitro test protocols may not adequately replicate in vivo loading. The small flexion-extension rotation observed in the C5/C6 arthrodesis subjects at the C5/C6 motion segment consistently followed the flexion-extension patterns of adjacent vertebrae, indicating the flexion-extension ROM calculated in the present study represented actual motion at the operated segment, and was not merely noise in the measurement system.

The results of the current study indicate that the total ROM in secondary components of motion (i.e. twist and bend rotation, medial-lateral and superior-inferior translation), on average, are less than 2.8º in rotation and 0.7 mm in translation in asymptomatic subjects. Single-level anterior arthrodesis does not appear to have a clinically significant affect on ROM in these secondary components of total motion during the flexion-extension movement.

The results indicate single-level anterior arthrodesis appears to affect the distribution of total flexion-extension ROM and total anterior-posterior translation ROM (Table 3 and Table 5). The absence of significant differences between flexion ROM and extension ROM and between

anterior translation and posterior translation ROM in control subjects contradicts a previous study that found significant differences between anterior and posterior translation in control subjects[25]. The current study is the first to compare flexion and extension components of rotation and anterior and posterior components of translation in control and arthrodesis groups. The significant alteration in the balance between flexion and extension ROM and between anterior and posterior translation ROM adjacent to the arthrodesis reveals a kinematic difference between arthrodesis and control subjects and suggests that it may be advantageous to evaluate ROM clinically by measuring ROM from neutral to full-flexion and from neutral to full extension, rather than the current standard of full-extension to full-flexion. It is not clear if the observed kinematic differences in the arthrodesis group modify disc stress and pressure enough to affect disc homeostasis[39-41,71] and lead to disc degeneration.

Clinical AP translation in control subjects was well below the standard of 3.5 mm to indicate excessive translation or pathology[72]. The 3.5 mm standard, determined using cadaver specimens, agrees well with the current in vivo data that shows the upper boundary for the 95% confidence interval for AP translation ROM is 3.45 mm at the motion segments with the greatest AP translation ROM (C3/C4 and C4/C5). However, the present data also suggests the standard AP translation measurement used to identify excessive translation is level dependent, with 2.3 mm being the upper boundary for the 95% confidence interval for AP translation ROM at the C6/C7 motion segment.

When reporting in vivo kinematic data, it is beneficial to be aware of the trial-to-trial variability within subjects. Increased trial-to-trial variability may indicate joint instability or a deficit in neuromuscular control. Furthermore, for research purposes, it is helpful to know how well a single movement trial represents the typical movement being analyzed. The results of the

current study indicate that ROM measurements during flexion-extension are highly repeatable for subjects using the described protocol and measurement techniques. This finding suggests, first, that subjects are capable of performing the flexion-extension movement in a highly repeatable fashion, and second, that the measurement tools used to characterize the motion have high precision. The authors are not aware of any previous studies that collected and analyzed multiple trials from each subject to assess within-subject variability in cervical spine ROM. The variability results presented here provide a standard that potentially can be used to identify cervical spine instability during dynamic, functional movement.

The results of this study indicate ROM measurements that are performed using only static end range-of-motion images significantly underestimate the 6 DOF ROM in the cervical spine (CME2). The present results confirm a previous suggestion that differences may exist between static and dynamic measurements of ROM[30]. Single end-range images obtained during either static positioning or during dynamic movement underestimate ROM because of muscular and inertial force differences between static and dynamic conditions and because all motion segments do not reach their maximal ROM simultaneously. Furthermore, as has been previously demonstrated, static cervical flexion-extension ROM may be increased an average of 2º to 3º per motion segment by manually applying force to the head[22], suggesting the potential exists for additional ROM beyond standard flexion-extension views. The clinical implication of this finding is that range of motion measured from static full-flexion and static full-extension images of arthrodesis patients should be interpreted with the understanding that these measurements may underestimate functional flexion-extension ROM by up to 3º.

There were several limitations associated with this study. First, pre-surgical dynamic, functional movement testing was not performed on the C5/C6 arthrodesis subjects due to pain

and limited movement prior to surgery. As a result, arthrodesis subject data was compared to control subjects of approximately the same age. It is important to note that arthrodesis subjects were tested approximately 7 months after surgery, earlier than adjacent segment disease generally occurs[8]. Therefore, while the present results provide valuable information regarding the short-term effects of arthrodesis, they may not be representative of longer-term effects of arthrodesis. One benefit of this short-term data, however, is that if kinematic differences are observed at longer-term follow-up it will be clear which kinematic changes occurred soon after surgery and which changes developed over a longer time period. An additional limitation is that the age range of the arthrodesis subjects (and therefore the age-matched controls) was relatively narrow for this study. Although this age group is highly relevant from a clinical perspective, the results presented here should be considered representative only for the age group included in this cohort considering the well-known changes that occur in the spine with age[49,71,73,74]. The percentage of smokers in the control and arthrodesis groups were slightly less and slightly more, respectively, than the percentage of smokers in large clinical trials involving anterior arthrodesis/arthroplasty subjects (32% to 45% smokers)[45,49,75] and further study involving a larger number of arthrodesis patients will be necessary to determine if a relationship exists between smoking and cervical kinematics following arthrodesis. Although significant differences in total flexion-extension ROM and total anterior-posterior translation ROM were not identified in this study, other kinematic differences, such as the instant center of rotation[22,30,76] and the sequencing of the intervertebral rotations[24,77] may exist between control and single-level arthrodesis subjects. Furthermore, total ROM measurements may not even be the appropriate parameters to characterize the mechanical effects of arthrodesis on subsequent disc degeneration because end ROM positions are encountered much less frequently during activities of daily

living than mid-range of motion positions. Thus, additional and alternative kinematic measurements may prove more effective in identifying mechanical factors that lead to disc degeneration following arthrodesis. Finally, the ROM results presented here are limited to the flexion-extension movement. The effect of C5/C6 arthrodesis on ROM during twisting and bending rotations may or may not follow the patterns described here.

2.2 CONTINUOUS KINEMATICS

2.2.1 Introduction

Cervical spine kinematics are commonly assessed using static, end-range of motion radiographs collected with the head in full flexion and full extension[16,21-23,51]. Previous studies have demonstrated significant inter-subject variability in intervertebral flexion-extension range of motion (ROM), ranging from 20% to 60% of the overall motion at each motion segment[22,23,25,27,78]. This large variability makes it difficult to identify "abnormal" motion that may develop following injury, degeneration, or surgical intervention. Furthermore, restricting data collection and analysis to static endpoint positions prohibits the characterization of mid-range kinematics that make up the majority of spine motion during activities of daily living[79,80].

While several studies have recorded two-dimensional, continuous cervical motion during dynamic flexion-extension, these studies failed to report intervertebral kinematics throughout the continuous motion[24,25,65,66]. Thus, the high inter-subject variability in flexion-extension ROM, combined with the lack of any quantitative continuous kinematic data throughout the entire movement cycle, precludes the development of a precise and comprehensive definition of "normal" in vivo cervical kinematics during flexion-extension.

The mechanical effects of arthrodesis and disc arthroplasty on adjacent segments are often evaluated by in vitro testing of cervical specimens[12,68-70,81,82] and finite element models derived from in vitro tests[83-87]. The preferred in vitro testing protocol is one that most closely follows the in vivo kinematic pattern for all segments of the cervical spine[88]. Thus, the fidelity of in vitro testing is often evaluated by comparing in vivo and in vitro total range of motion measures over the entire subaxial spine or at each intervertebral motion segment[12,89,90]. The high variability in segmental in vivo range of motion, as well as the lack of data describing mid-range kinematics during in vivo functional loading, make it unclear how accurately the kinematic response of in vitro tests and finite element models represent actual in vivo motion during dynamic functional loading.

The current study was carried out to address the aforementioned limitations to our current knowledge of in vivo cervical spine kinematics during functional loading. The objective of this study was to quantify intervertebral kinematics during continuous, functional flexion-extension in a group of asymptomatic control subjects. As part of this objective, subject-specific disc height and static intervertebral orientation at each cervical level were used to more precisely define "normal" in vivo kinematics. The hypothesis associated with this objective was that static disc height and static orientation would be associated with kinematics at each motion segment

during functional dynamic loading. Finally, in order to demonstrate the benefit of assessing intervertebral kinematics using continuous data, continuous intervertebral kinematics were compared between single-level anterior arthrodesis patients and asymptomatic controls.

2.2.2 Materials and Methods

Following Institutional Review Board approval, data was analyzed from 6 single-level (C5/C6) anterior arthrodesis patients (average age: 48.8 ± 6.9 yrs; 1 M, 5 F; 7.6±1.2 mo. post-surgery) and 18 asymptomatic control subjects of similar age (average age: 45.6 ± 5.8 yrs; 5 M, 13 F) who provided informed consent to participate in this research study. Arthrodesis subjects who were at least 18 years of age and scheduled to undergo (or recently received) single-level ACDF surgery were identified during clinic visits. Pregnant women, patients diagnosed with osteoporosis, and patients with any other injury or disease that interferes with spine function were excluded. Asymptomatic controls who had no history of cervical spine dysfunction or pain were recruited to approximately match the age and gender distribution of the arthrodesis subjects. Control subject recruitment was accomplished through an advertisement in an employee newsletter and word of mouth.

High-resolution CT scans (0.29x0.29x1.25 mm voxels) of the cervical spine (C2-C7) were acquired on each participant (GE Lightspeed 16). Bone tissue was segmented from the CT volume using a combination of commercial software (Mimics software, Materialise, Leuven, Belgium) and manual segmentation[53]. A three-dimensional (3D) model of each vertebra was generated from the segmented bone tissue. Markers were interactively placed on the 3D bone models to define bone-specific anatomic coordinate systems (Figure 8).

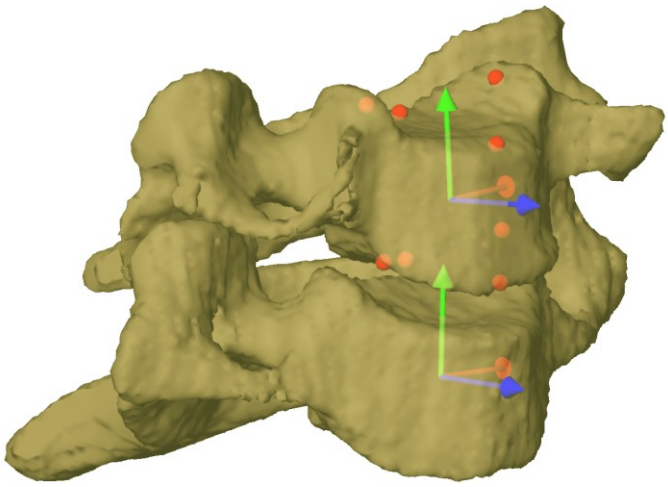

Figure 8: The anatomic coordinate systems in a C6/C7 motion segment.

Subjects were seated within a biplane X-ray system and directed to continuously move their head and neck through their entire range of flexion-extension (Figure 1). A metronome set at 40 to 44 beats per minute was used to ensure the participants moved at a continuous, steady pace to complete each full movement cycle in 3 seconds or less. Radiographs were collected at 30 frames per second for 3 seconds for each trial of continuous flexion-extension (X-ray generator parameters: 70 KV, 160 mA, 2.5 ms X-ray pulses; source-to-subject distance 140 cm). Radiographs were collected for 2 or 3 trials for each subject, resulting in a total of 63 movement trials analyzed for this study. Multiple trials from the same subject were averaged to yield a single average dataset for each subject used for statistical analysis. A static trial with the subject looking forward with the head in the neutral position was also collected for each participant. The effective radiation dose for each dynamic flexion-extension motion trial was estimated to be 0.16 mSv (determined using PCXMC simulation software, STUK, Helsinki, Finland). The effective dose of a cervical spine CT scan has been reported to be between 3.0 mSv and 4.36 mSv[91,92].

A previously validated tracking process determined three-dimensional vertebral position with sub-millimeter accuracy[55] for all static and dynamic trials. Details describing the volumetric model-based tracking process, including hardware and software specifications, calibration and distortion correction procedures, and computational algorithms have been described previously[55-58]. Tracked data was filtered at 1.0 Hz using a fourth-order, low-pass Butterworth filter with the filter frequency determined using residual analysis[59]. Six degree-of-freedom (DOF) kinematics between adjacent vertebrae (3 translations, 3 rotations) were calculated following established standards for reporting spine kinematics[60,61]. Intervertebral position and orientation in each frame of the continuous dynamic trial were normalized to the static neutral trial for each subject. Only the flexion-extension component of vertebral rotation and the anterior-posterior component of vertebral translation were included in the current analysis, as we have previously demonstrated that intervertebral motion out of the flexion-extension plane during in vivo flexion-extension is relatively small (an average 2.1º of rotation ROM and 0.6 mm of translation ROM)[93].

C2 motion relative to C7 (C2/C7) was interpolated to obtain C2/C7 motion at 1% increments of the total cervical ROM for each participant. In this way, the total cervical spine flexion-extension ROM of each participant was standardized to 100%, allowing for comparisons among subjects. Segmental kinematics were then interpolated to obtain relative intervertebral motion for every 1% increment of C2/C7 spine motion. Flexion and extension portions of the overall movement were analyzed separately.

The static neutral trial was used to define intervertebral orientation and disc height of each motion segment for each participant. An automated computer algorithm determined disc height at each level. This algorithm identified the nucleus region of the disc on each bone

surface model according to previous reports[42,94]. Disc height measurements were then acquired within the nucleus region and across the entire central 1/3rd of the disc width. Therefore, the disc height recorded for each disc was the average disc height within the central nucleus region when the head was in a static, upright neutral position.

A regression equation relating range of motion to disc height at each motion segment was determined (Appendix A). A second regression equation relating static orientation to average flexion-extension angle at each motion segment was also determined (Appendix A).

The regression equations developed using control subject data were applied to the continuous kinematic data from arthrodesis subjects to adjust flexion-extension and anterior-posterior translation according to disc height and static orientation at each motion segment.

Analysis of variance (ANOVA) was used to identify statistically significant differences in flexion-extension angle between arthrodesis and control groups at each motion segment at every 10% interval of C2/C7 ROM.

2.2.3 Results

Disc height was significantly correlated to ROM at the C5/C6 and C6/C7 motion segments in control subjects (Table 2). A significant relationship between static orientation and average flexion-extension angle was identified at the C2/C3, C3/C4, C4/C5 and C5/C6 motion segments during flexion and extension in control subjects (Table 3). Similarly, significant correlations between disc height and AP translation were identified at C5/C6 and C6/C7 motion segments (correlation coefficients (r) from 0.650 to 0.690; p-values from .002 to .004) and between static positioning and average AP translation value at all motion segments (correlation coefficients (r) from -0.486 to -0.776; p-values from $\leq$.001 to .041) in control subjects.

Table 2: The relationship between disc height and flexion-extension range of motion.

Motion Segment	Correlations				Regression Equations
	Extension		Flexion		
	r	p-value	r	p-value	
C2/C3	.090	.722	.087	.730	N.A.
C3/C4	.074	.770	.086	.733	N.A.
C4/C5	-.087	.731	-.113	.656	N.A.
C5/C6	.620	.006*	.617	.006*	Ext: $C5/C6_{ROM} = 3.478 + 2.471*C56_{DiscHeight}$ Flex: $C5/C6_{ROM} = 3.487 + 2.470*C56_{DiscHeight}$
C6/C7	.521	.027*	.524	.026*	Ext: $C6/C7_{ROM} = 1.605 + 2.082*C67_{DiscHeight}$ Flex: $C6/C7_{ROM} = 1.566 + 2.037*C67_{DiscHeight}$

Table 3: The relationship between static orientation and average flexion-extension angle.

Motion Segment	Correlations				Regression Equations
	Extension		Flexion		
	r	p-value	r	p-value	
C2/C3	-.555	.017*	-.565	.015*	Ext: $C2/C3_{AVG} = -1.392 - 0.210*C23_{Static}$ Flex: $C2/C3_{AVG} = -0.443 - 0.224*C23_{Static}$
C3/C4	-.695	.001*	-.694	.001*	Ext: $C3/C4_{AVG} = -1.551 - 0.332*C34_{Static}$ Flex: $C3/C4_{AVG} = -1.089 - 0.332*C34_{Static}$
C4/C5	-.622	.006*	-.648	.004*	Ext: $C4/C5_{AVG} = -0.967 - 0.281*C45_{Static}$ Flex: $C4/C5_{AVG} = -1.317 - 0.290*C45_{Static}$
C5/C6	-.610	.007*	-.452	.059*	Ext: $C5/C6_{AVG} = -0.409 - 0.150*C56_{Static}$ Flex: $C5/C6_{AVG} = -0.088 - 0.112*C56_{Static}$
C6/C7	-.333	.176	-.294	.236	N.A.

The average inter-subject variability in flexion-extension angle over the continuous movement path for the control group decreased 15% to 46% after accounting for differences in disc height and static orientation angle (Table 4). Similarly, the average inter-subject variability in AP translation was reduced 14% to 33% after adjusting for disc height and static orientation angle (Table 4).

Table 4: Inter-subject variability in flexion-extension and anterior-posterior translation before and after accounting for disc height and static orientation.

	Inter-Subject Variability					
	Flexion-Extension Rotation			Anterior-Posterior Translation		
Motion Segment	Before Adjustment	After Adjustment	Decrease in Variability	Before Adjustment	After Adjustment	Decrease in Variability
C2/C3	2.1°	1.3°	38%	0.9 mm	0.7 mm	22%
C3/C4	3.5°	2.5°	29%	1.0 mm	0.8 mm	20%
C4/C5	2.9°	1.9°	34%	0.7 mm	0.6 mm	14%
C5/C6	2.6°	1.4°	46%	0.6 mm	0.4 mm	33%
C6/C7	2.9°	2.6°	10%	0.5 mm	0.4 mm	20%

Continuous motion path data revealed nearly identical motion paths in arthrodesis and control groups at the C2/C3 motion segment (Figure 9A, 9B). The motion paths for the two groups diverged when in a flexed orientation (at the C3/C4 motion segment) (Figure 9C, 9D) and when in an extended orientation (at the C6/C7 motion segment) (Figure 9I, 9J). The consistent offset between groups at the C4/C5 motion segment (Figure 9E, 9F) approached significance during flexion from 40% to 90% of the C2/C7 ROM (all $p < .10$) and during extension from 30% to 70% of the C2/C7 ROM (all $p < .10$). As expected, statistically significant differences between groups were identified at the C5/C6 motion segment (0% through 40% and 70% through 100%, all $p < .002$ for flexion and all $p < .009$ for extension). Significant differences were also identified at the C6/C7 motion segment near full extension ($p = .013$ at 0% and 10% of ROM during flexion and $p = .047$ at 100% ROM during extension). Differences between arthrodesis and control in AP translation continuous motion paths were consistent with these flexion-extension differences.

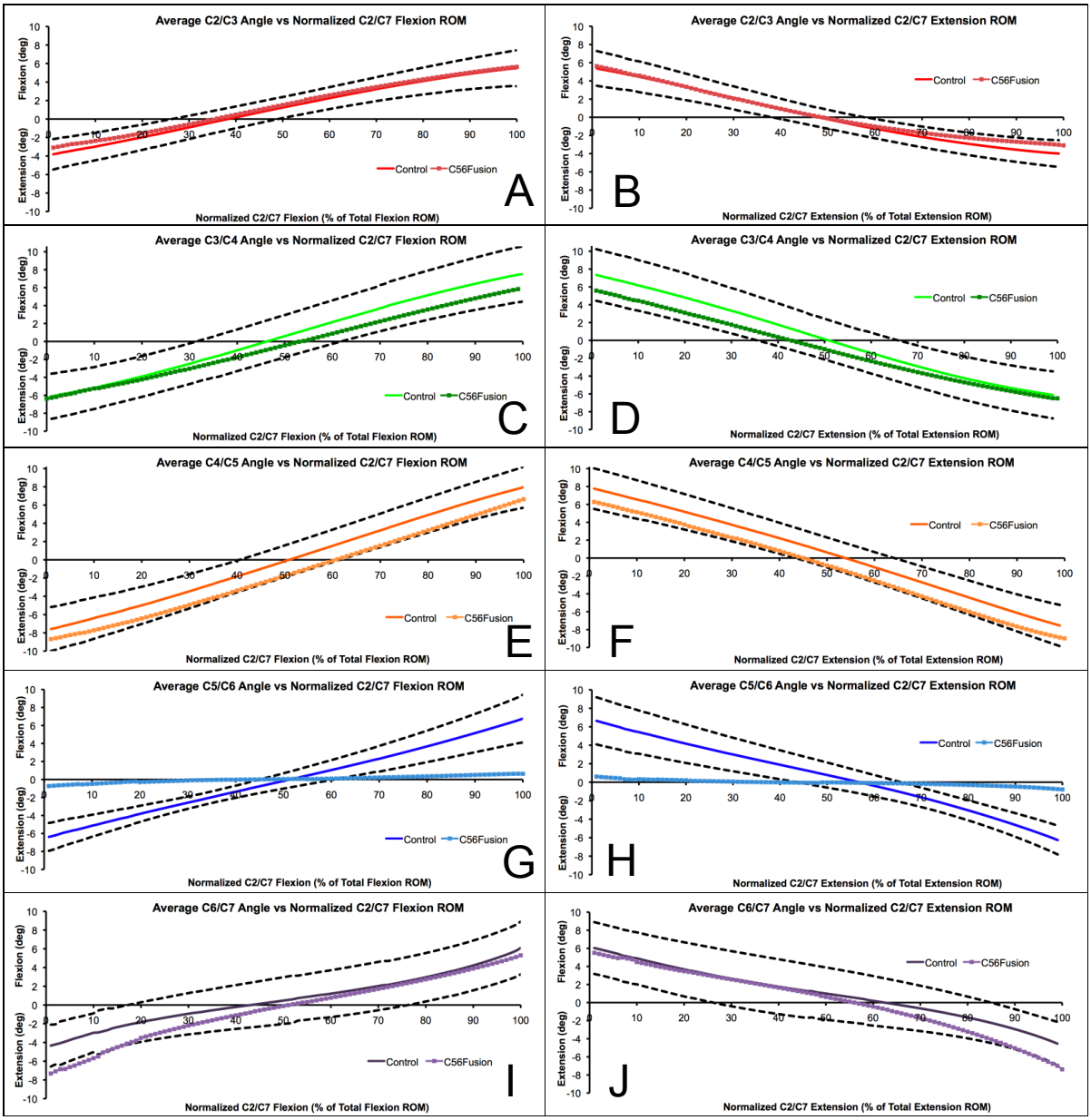

Figure 9: Average intervertebral flexion-extension curves for the control and fusion groups.

2.2.4 Discussion

This is believed to be the initial report of continuous cervical kinematic data during in vivo flexion-extension. The results indicate that disc height and static orientation are parameters that explain a significant portion of the inter-subject variability in cervical kinematics. The logic behind evaluating these two variables was that increased disc height would allow for increased ROM at each motion segment, and that subjects with more extended (or flexed) static orientation angles would tend to be in more extension (or flexion) during their complete active motion cycle after standardizing each subject's ROM to 100%. This study has shown that 27% to 38% of the inter-subject variability in C5/C6 and C6/C7 flexion-extension ROM is associated with differences in disc height at C56 and C67. This finding is in agreement with a previous multivariate analysis study that determined cervical ROM was associated with the severity of disc degeneration[52]. The lack of association between disc height and ROM at more superior disc levels most likely occurred due to little variability in disc height at C23, C34 and C45 in our healthy, asymptomatic subjects. The present study also demonstrated that 31% to 48% of the inter-subject variability in average flexion-extension angle is associated with differences in static orientation at the upper motion segments (C2/C3 through C5/C6). This result indicates static orientation should be taken into account when flexion ROM and extension ROM are measured relative to the static neutral position[25,93].

After accounting for disc height and static orientation, the average inter-subject variability in the continuous flexion-extension motion paths was 1.9º. In contrast, previous studies have reported inter-subject variability from 3.4º to 7.2º in flexion-extension range of motion[22,23,25,27,78]. Adjusting for disc height and static orientation reduced inter-subject variability and helped achieve the primary study objective, to develop a more precise description

of intervertebral kinematics during continuous, functional flexion-extension for asymptomatic control subjects.

As demonstrated in Figure 3, the continuous intervertebral motion paths may provide useful clinical information that cannot be obtained from static flexion-extension radiographs. For example, at the C4/C5 motion segment, if only end ROM data points were selected to measure ROM, the likely conclusion would be there is no difference in kinematics one level above the arthrodesis in comparison to controls. However, the continuous motion data indicates a consistent offset toward more extension in the arthrodesis group relative to control subjects at C4/C5. This preliminary result suggests the mechanical loading applied to the C45 disc may be altered by C5/C6 arthrodesis, providing a potential explanation for the occurrence of adjacent segment degeneration superior to the arthrodesis. Similarly, the continuous motion paths for the C6/C7 motion segment indicate that from full flexion to the neutral orientation, the C6/C7 motion segment kinematics are nearly identical in control subjects and arthrodesis patients. However, as the spine moves into extension, the control group and arthrodesis patient motion paths begin to diverge. This suggests C5/C6 arthrodesis may alter the mechanics of the C6/C7 motion segment in extension, implying a potential explanation for adjacent segment degeneration inferior to the operated motion segment. The continuous kinematic results suggest that studies that report only adjacent segment total range of motion following arthrodesis or arthroplasty[65,95,96] may overlook potential long-term clinically significant effects of these procedures (e.g. an offset toward extension in C4/C5 found in the present study). Furthermore, static, end-range images cannot be used to identify specific ranges of motion where kinematics are altered following surgery (e.g. extreme extension affected C6/C7 kinematics in the present study).

As previously noted, data from cervical arthrodesis patients was included in the current analysis to highlight the advantages of collecting and analyzing in vivo kinematics continuously, throughout the entire flexion-extension movement. Due to the small sample of arthrodesis patients, differences between arthrodesis and control groups should only be viewed as potentially suggesting that anterior cervical arthrodesis may affect adjacent segment kinematics. A larger sample of arthrodesis patients will be necessary to conclusively establish in vivo kinematics in arthrodesis patients. Furthermore, arthrodesis patient testing occurred relatively soon after surgery. Differences between arthrodesis and control groups may become more apparent with longer-term follow-up testing. An additional limitation of the current study is the relatively narrow age range for the asymptomatic control subjects. Although the control subjects in this study were within a clinically relevant age range, continuous kinematics from younger and older asymptomatic cohorts may differ from the current results.

In conclusion, inter-subject variability in cervical flexion-extension kinematics is influenced by disc height and the static orientation of each motion segment. The continuous kinematic technique described may help in the design of the next generation of motion-preserving technology, perhaps allowing for patient-specific implant designs. Continuous kinematic techniques may also detect clinically important differences between arthrodesis and arthroplasty that are not apparent at static, end range of motion positions. Finally, the continuous motion path curves may be used to evaluate and improve the fidelity of in vitro cervical spine mechanical testing protocols.

2.3 CONTRIBUTIONS TO MOTION

2.3.1 Introduction

Degenerative changes adjacent to cervical arthrodesis have been widely reported[5-11]. These degenerative changes occur in 16%[6] to 25%[7] of the patients within 10 years of the operation, and require adjacent level surgery in 6% to 10% of the patients[11,45-48]. The etiology of adjacent segment disease following cervical arthrodesis remains controversial. The disease may progress due to the underlying spondylosis[7,14,50], the arthrodesis may lead to increased motion in adjacent vertebrae, resulting in overload and instability[10,12,15-17], or adjacent segment degeneration may result from a combination of these two factors[9,11]. In an attempt to eliminate the potential overload of adjacent segments following arthrodesis, several motion-preserving disc replacement devices have been recently developed[97-100].

The effects of anterior arthrodesis or disc arthroplasty on adjacent segment kinematics are often evaluated clinically using full flexion and full extension radiographs. These end-range images are not necessarily representative of mid-range cervical kinematics and are characterized by substantial inter-subject variability in range of motion[22,23,25,27,78], potentially due to variable patient effort during imaging. These limitations associated with static end-range imaging make it impossible to determine if cervical motion segment contributions to flexion-extension are constant or if they fluctuate throughout the range of motion. Furthermore, while arthrodesis may not affect overall range of motion in adjacent segments[93], it is not clear if it affects the normal patterns of contributions to motion, which may reflect altered disc loading following arthrodesis. Collecting continuous cervical kinematics over the entire flexion-extension motion and

performing a within-subject analysis of the segmental contributions to overall spine motion may overcome the limitations associated with static, end-range imaging.

The first objective of this study was to characterize segmental percentage contributions to cervical flexion-extension in an asymptomatic control group. The hypothesis tested was that segmental contributions to spine motion would be level dependent and uniform over the entire range of motion. Specifically, contributions from the C4/C5 and C5/C6 motion segments were expected to be the largest and contributions from C2/C3 and C6/C7 were expected to be the smallest throughout the entire range of motion. The second objective of this study was to assess the effect of single-level anterior arthrodesis on adjacent segment contributions to cervical flexion-extension. It was hypothesized that motion segments adjacent to the arthrodesis would disproportionally increase their contribution to cervical flexion-extension over the entire range of motion.

2.3.2 Materials and Methods

2.3.2.1 Subjects

Following Institutional Review Board (IRB) approval, data was collected from 6 single-level (C56) anterior arthrodesis patients (average age: 48.8 ± 6.9 yrs.; 1 M, 5 F; 7.6±1.2 mo. post-surgery) and 18 asymptomatic control subjects of similar age (average age: 45.6 ± 5.8 yrs.; 5 M, 13 F) who provided informed consent to participate in this research study. Pregnant women, patients diagnosed with osteoporosis, and patients with any other injury or disease that interferes with spine function were excluded. Patients were identified during clinic visits.

Control subjects were recruited through an advertisement in an employee newsletter and word of mouth.

2.3.2.2 Data Collection

High-resolution CT scans (0.29x0.29x1.25 mm voxels) of the cervical spine (C2-C7) were acquired on each participant (GE Lightspeed 16). Bone tissue was segmented from the CT volume using a combination of commercial software (Mimics software, Materialise, Leuven, Belgium) and manual segmentation[53]. A three-dimensional (3D) model of each vertebra was generated from the segmented bone tissue. Markers were interactively placed on the 3D bone models to define bone-specific anatomic coordinate systems. The effective dose of a cervical spine CT scan has been reported to be between 3.0 mSv and 4.36 mSv[91,92].

Subjects were seated within a biplane X-ray system and directed to continuously move their head and neck through their entire range of flexion-extension. A metronome set at 40 to 44 beats per minute was used to ensure the participants moved at a continuous, steady pace to complete each full movement cycle in 3 seconds or less. Biplane radiographs were collected at 30 images per second for 3 seconds for each trial of continuous flexion-extension (X-ray parameters: 70 KV, 160 mA, 2.5 ms X-ray pulses, source-to-subject distance 140 cm). Radiographs were recorded for 2 or 3 trials for each subject, resulting in a total of 63 movement trials analyzed for this study. Multiple trials from the same subject were averaged to yield a single average dataset for each subject used for statistical analysis. A static trial with the subject looking forward with the head in the neutral position was also collected for each participant. The effective radiation dose for each 3-second dynamic flexion-extension motion trial was estimated to be 0.16 mSv (determined using PCXMC simulation software, STUK, Helsinki, Finland).

2.3.2.3 Data Processing

A previously validated tracking process determined three-dimensional vertebral position in each pair of radiographs with sub-millimeter accuracy[55] for all static and dynamic trials. Details describing the volumetric model-based tracking process, including hardware and software specifications, calibration and distortion correction procedures, and computational algorithms have been described previously[55-58]. Tracked bone movement data was filtered at 1.0 Hz using a fourth-order, low-pass Butterworth filter with the filter frequency determined using residual analysis[59]. Six degree-of-freedom (DOF) kinematics between adjacent vertebrae (3 translations, 3 rotations) were calculated following established standards for reporting spine kinematics[60,61]. Intervertebral position and orientation in each frame of the continuous dynamic trial were normalized to the static neutral trial for each subject. Only the flexion-extension component of vertebral rotation is presented in the current analysis.

C2 flexion-extension motion relative to C7 (C2/C7) was interpolated to obtain C2/C7 motion at 1% increments of the total cervical ROM for each participant. In this way, the total cervical spine flexion-extension ROM (from C2 to C7) of each participant was standardized to 100%, allowing for comparisons among subjects. Segmental flexion-extension rotation was then interpolated to obtain relative flexion-extension at each intervertebral motion segment for every 1% increment of C2/C7 spine motion. Initial analysis was performed separately for the flexion and extension motions.

2.3.2.4 Statistical Design and Analysis

Statistical analysis was performed by fitting separate mixed-effects models for control and arthrodesis groups, with the random intercept for individual subjects and the cluster variation among motion segments (C2/C3, C3/C4, C4/C5, C5/C6 and C6/C7) to account for the dependency in the data. Each fitted model included motion segment, percent contribution, squared percent contribution, and their interaction terms with the motion segment to capture the curvature in the percentage contribution curves over the ROM. Differences in percent contributions between groups and between motion segments were assessed at given movement percentages by comparing point-wise 95% confidence intervals (CI) from the fitted models.

2.3.3 Results

Percentage contributions to C2/C7 flexion-extension were not significantly different at any motion segment between the flexion and extension movement (all $p \geq .190$ for direction of movement; all $p \geq .571$ for direction by group interaction). Thus, segmental flexion contributions and segmental extension contributions to overall C2/C7 motion were combined at corresponding percentages of ROM for analysis purposes.

Segmental percentage contributions varied substantially within each motion segment over the full range of flexion-extension in control subjects (Figure 10). Two general patterns of contributions to flexion-extension were apparent. The C2/C3, C3/C4 and C4/C5 motion segments, in general, made their maximum contributions during the mid-range of motion, and decreased their percentage contributions near the start and end of the ROM (Figure 10). The C5/C6 and C6/C7 motion segments, on the other hand, made their maximum contributions near the start and end of the ROM, and generally made their smallest contributions over the mid-range

of motion (Figure 10). The lack of overlap between 95% confidence interval boundaries from different motion segments (e.g. C3/C4 and C4/C5 from 70% to 100% of total C2/C7 ROM), indicate the contributions being compared are statistically different at all of the non-overlapping movement percentage points at a significance level of .05. Similarly, within a single motion segment, the 95% confidence intervals may be used to identify portions of the flexion-extension movement cycle where the contributions due to a specific motion segment are statistically different at a significance level of .05 (e.g. the C6/C7 contribution from 40% to 60% of total ROM is less than the C6/C7 contribution from 0%-25% and 75%-100% of total C2/C7 ROM).

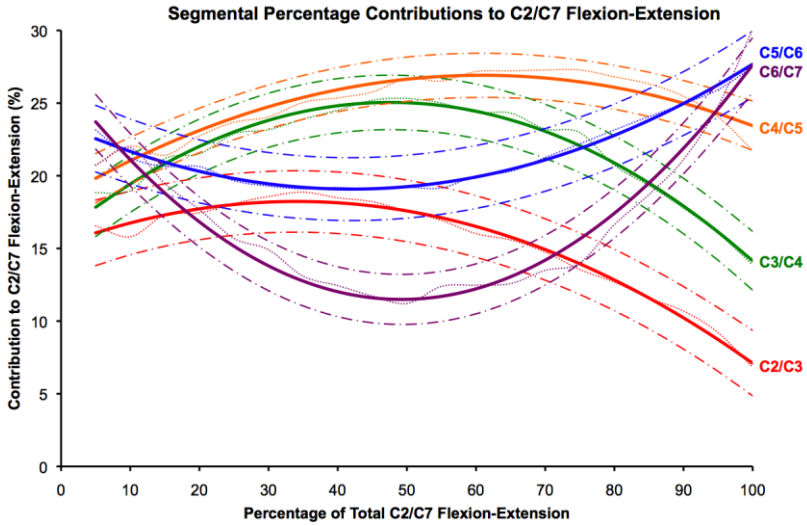

Figure 10: Control group segmental percentage contributions to C2/C7 flexion-extension.

Segmental percentage contributions to C2/C7 flexion-extension in arthrodesis patients followed patterns similar to those in control subjects, with the obvious exception of very little motion attributed to the operated (C5/C6) motion segment (Figure 11). The reduced contribution

from the C5/C6 motion segment in arthrodesis patients was compensated by an increased contribution from the C4/C5 and C6/C7 motion segments. The contribution from the C4/C5 motion segment in arthrodesis patients was significantly increased over the range of motion from 30% to 95% of the total C2/C7 ROM relative to controls (Figure 11C). The contribution from the C6/C7 motion segment in arthrodesis patients was significantly increased over the entire flexion-extension range of motion relative to controls (Figure 11E). The C2/C3 and C3/C4 motion segment contributions were not significantly different between control and arthrodesis groups at any percentage of the C2/C7 flexion-extension movement. The average differences between arthrodesis and control groups in percentage contribution from the C2/C3, C3/C4, C4/C5, C5/C6 and C6/C7 motion segments were 1.7%, 2.5%, 5.1%, -18.2% and 8.9%, respectively, where positive (or negative) values indicate increased (or decreased) percentage contributions in arthrodesis patients relative to controls.

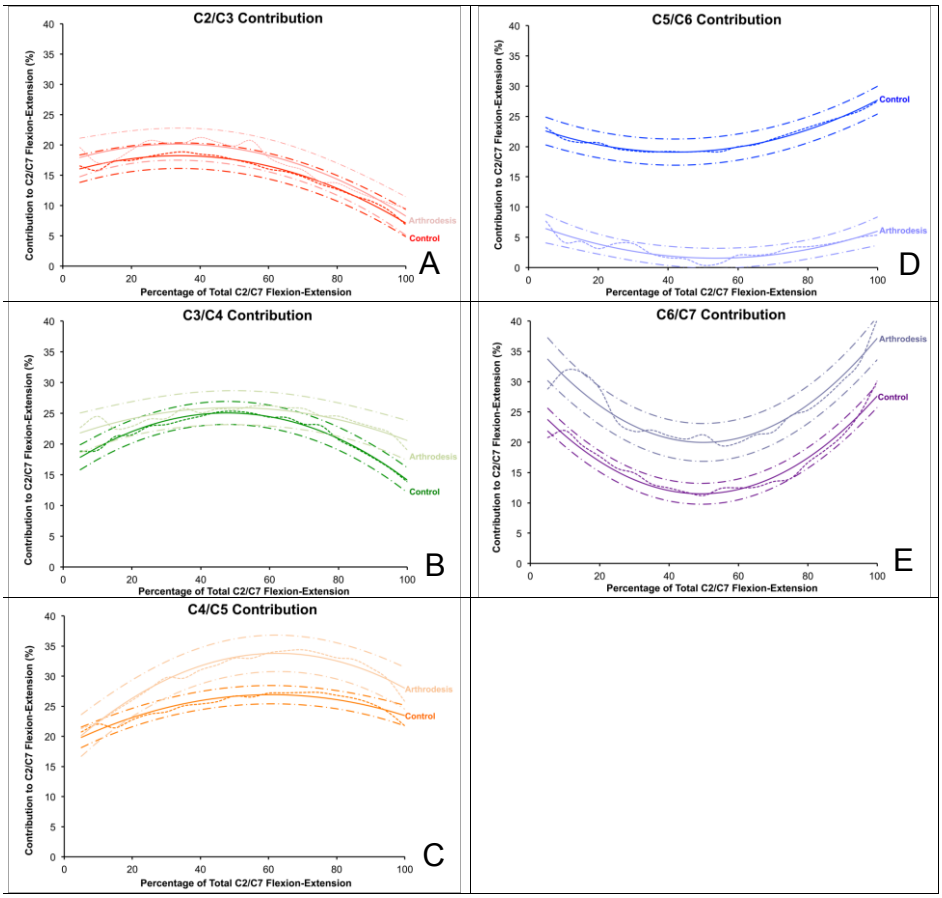

Figure 11: Control and arthrodesis group segmental percentage contributions to C2/C7 flexion-extension.

C2/C7 flexion-extension ROM in the control group (67º±10º) was significantly greater than in the arthrodesis group (57º±7º) ($p = .037$). This difference between groups was primarily due to the reduced ROM at C5/C6 in the arthrodesis group ($p < .001$). No significant differences in total range of motion were observed at any other motion segment (Figure 12).

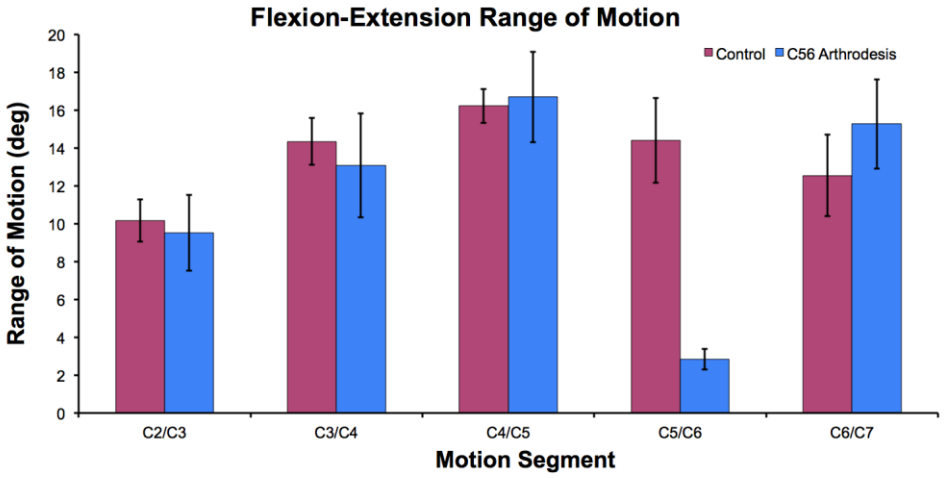

Figure 12: Average range of motion at each motion segment.

2.3.4 Discussion

Segmental percentage contributions to cervical spine flexion-extension have been reported previously using end ROM data (a single full extension and a single full flexion radiograph)[101-103] and images collected from selected midrange positions[77]. These studies found that, in control subjects, segmental contributions were greatest at the C4/C5 motion segment and decreased progressively in the superior and inferior motion segments. The current study provides a more detailed and comprehensive analysis of segmental contributions to flexion-extension. The current study indicates that in asymptomatic subjects, midrange flexion-extension is dominated by C3/C4 and C4/C5 motion, while contributions from C5/C6 and C6/C7 motion segments increase near the start and end of the ROM. Although the C5/C6 and C6/C7 motion segments increase their contributions to spine flexion-extension when loads on the spine are greatest, a clear connection cannot yet be made between these kinematic results and increased disc

degeneration at the C56 and C67 disc levels[104,105]. Further computational modeling of the in vivo cervical spine (e.g. inverse dynamics or finite element modeling) will be necessary to reveal the interaction between kinematics, loading, and disc stress that may lead to degeneration at specific motion segments.

The results indicate that cervical motion segment percentage contributions change significantly through the flexion-extension motion. These fluctuations in segmental contributions suggest that the distribution of compressive and shear loads also fluctuates among the motion segments over the full range of motion. These results make it clear that cervical spine mechanics cannot be fully characterized by static measurements. It is evident that the motion of the vertebrae, and accompanying deformation of the discs, are dependent on the orientation of the head and the muscular loading that occurs with functional motion. This information cannot be obtained from single full-flexion and full-extension radiographs.

As hypothesized, the motion segments adjacent to the arthrodesis significantly increased their contributions to C2/C7 flexion-extension. Care should be taken to avoid misinterpretation of this result. The increased percentage contributions from motion segments adjacent to the arthrodesis do not necessarily indicate an increased total ROM at these motion segments. This is because overall C2/C7 motion was decreased in the arthrodesis groups. As Figure 12 demonstrates, and as we have previously reported for this cohort, there were no significant differences in the total flexion-extension ROM at each non-operated motion segment in arthrodesis and control subjects[93]. A previous clinical study that included 374 cervical arthrodesis patients identified a significantly higher risk of new adjacent segment disease at the C6/C7 motion segment in comparison to the C4/C5 motion segment[7]. The results of the current study suggest a potential mechanical mechanism for this clinical finding. The C6/C7 motion

segment percentage contribution is, on average, 8.9 percentage points higher in arthrodesis patients than in controls, while the C4/C5 motion segment contribution is only 5.1 percentage points higher in arthrodesis patients than controls, on average. Additionally, the increase in percentage contribution from the C6/C7 motion segment is continually greater than the increase from the C4/C5 motion segment over the entire ROM. This implies that even if the arthrodesis patients are advised to limit their ROM following surgery (i.e. avoid full extension and full flexion), the largest change in percentage contribution to motion, relative to controls, will still occur at the C6/C7 motion segment, even over the mid-range of motion.

The results indicate C5/C6 arthrodesis does not drastically alter the pattern of cervical motion segment contributions to flexion-extension. Following arthrodesis, C2/C3, C3/C4 and C4/C5 continue to make their largest contributions to motion through the mid-range, while the C6/C7 motion segment still contributes more near the ends of the range of motion. Although these results suggest the pattern of motion experienced by the discs is not affected by single-level arthrodesis, further research will be required to determine if arthrodesis affects the shear and compressive forces applied to cervical discs following arthrodesis.

One limitation of the current study is that the surgical patients were not tested prior to surgery. Therefore, it is not certain that the observed differences between groups were entirely due to the surgery, as some differences may have existed due to underlying spondylosis. However, pre-surgical testing of surgical patients has indicated substantial variability in range of motion related to pain[65], and therefore pre-surgical data was unlikely to be informative. Second, surgical patient testing occurred relatively soon after surgery. Follow-up testing will be necessary to evaluate the longer-term effects of arthrodesis on segmental contributions to flexion-extension. An additional limitation of the current study is the relatively narrow age

range for the asymptomatic control subjects. Although the control subjects in this study were within a clinically relevant age range, continuous kinematics from younger and older asymptomatic cohorts may differ from the current results given the well-known changes that occur in the spine with age[49,71,73,74].

2.4 RELIABILITY, VARIABILITY AND ACCURACY OF THE INTERVERTEBRAL INSTANT CENTER OF ROTATION

2.4.1 Introduction

Lateral radiographs collected at full-flexion and full-extension have traditionally been used to assess cervical spine kinematics, quantify normal motion, and diagnose abnormalities. These static radiographs are most often used to evaluate intervertebral range of motion (ROM) between adjacent cervical vertebrae. ROM has limited clinical application, however, due to measurement inaccuracy inherent to the manual digitizing of vertebral landmarks and the wide inter-subject variability in "normal" ROM reported for asymptomatic subjects[23,25,78,106].

As an alternative to ROM, the instant center of rotation (ICR) has been proposed for evaluating the quality of movement and exploring abnormalities in the cervical spine[30]. Full-flexion and full-extension radiographs have previously been manually digitized to determine the ICR in asymptomatic subjects[76,106-108] and symptomatic or surgical patients[76,108]. While abnormalities in the ICR may correspond to specific pathologies[109], the clinical utility of measurements obtained from images collected only at the ends of the ROM remains limited. The dynamic function of muscles and ligaments cannot be assessed from static end ROM

measurements, and end ROM data points are not necessarily representative of mid-range motion where the majority of our activities of daily living occur[79,80]. In addition, the ICR will change location during dynamic motion and may not be fully described by a single point[110].

In an attempt to fully characterize joint motion, the path of the ICR through a full range of motion, i.e. the centrode [111], may be calculated. The centrode has been determined for various joints including the wrist[112], knee[113-115], lumbar spine[116], and foot/ankle[117,118]. Centrode information may be particularly valuable to clinicians, as the centrode indicates *how* motion occurs between adjacent bones during continuous motion (i.e. motion quality), not simply *how much* motion occurs between adjacent bones (i.e. ROM). Furthermore, characterizing the centrode during cervical spine motion is currently of particular interest due to the recent FDA approval of several cervical disc replacement devices in the United States[97,119,120]. These disc replacements have either fixed or variable centers of rotation, and it is not clear how well these designs mimic in vivo cervical spine function.

ICR calculations are notoriously sensitive to factors such as tracking error, marker placement, and rotation step size. Therefore, it is important that the experimental methods are thoroughly validated and expected errors are quantified prior to implementing these calculations in a new application[121]. Although parametric sensitivity analyses using simulated data may be used to identify factors influential to determining the ICR[121-124], assessing the accuracy of ICR calculations obtained from in vivo data proves to be more difficult. In vivo, during dynamic motion, a "known" center of rotation is not available to use as a gold standard for comparison in parametric evaluations. In this situation, the accuracy of ICR calculations may be assessed through a simulation experiment designed to characterize the computational accuracy given the expected in vivo tracking error and marker distribution. Furthermore, the in vivo reliability may

be assessed by analyzing multiple trials from the same subject, while the in vivo sensitivity may be assessed by a parametric evaluation of factors affecting the ICR calculation.

The purpose of the present study was to assess the sensitivity, reliability and accuracy of in vivo dynamic cervical spine ICR path calculations obtained using biplane radiographs and a volumetric model-based tracking algorithm. The in vivo sensitivity and reliability were evaluated with respect to movement direction (flexion versus extension), rotation step-size, filter frequency, and tracking error using a large cohort of asymptomatic subjects. The experimental accuracy was determined by a simulation experiment using parameters appropriate for the in vivo protocol (i.e. tracking noise, distance from bone to ICR, filter frequency, rotation step size).

2.4.2 Materials and Methods

2.4.2.1 In Vivo Data

Following Institutional Review Board (IRB) approval, data was collected from 20 asymptomatic subjects (13 F, 7 M; average age: 45.6 ± 5.7 yrs.) who provided informed consent to participate in this research study. Subjects were seated within a biplane X-ray system and, for each trial, directed to continuously move their head and neck through their entire range of flexion-extension. A metronome set at 40 to 44 beats per minute was used to ensure the participants moved at a continuous, steady pace to complete each full movement cycle in approximately 3 seconds. Radiographs were collected at 30 frames per second for 3 seconds for each trial of flexion-extension (X-ray parameters: 70 KV, 160 mA, 2.5 ms X-ray pulses, source-to-subject distance 140 cm). Radiographs were recorded for 2 or 3 separate trials for each subject (allowing for a rest period between trials), resulting in a total of 50 trials included in the present in vivo analysis. In addition, high-resolution CT scans (0.29x0.29x1.25 mm voxels) of the cervical

spine (C2-C7) were acquired from each participant (GE Lightspeed 16). The effective radiation dose for each dynamic flexion-extension motion trial was estimated to be 0.16 mSv (determined using PCXMC simulation software, STUK, Helsinki, Finland). The effective dose of a cervical spine CT scan has been reported to be between 3.0 mSv and 4.36 mSv[91,92].

Bone tissue was segmented from the CT volume using a combination of commercial software (Mimics software, Materialise, Leuven, Belgium) and manual segmentation[53]. A three-dimensional (3D) model of each vertebra was generated from the segmented bone tissue. Markers were interactively placed on the 3D bone models to define bone-specific anatomic coordinate systems. In vivo bone motion of C2 through C7 vertebrae was tracked using a volumetric model-based tracking technique previously described in detail (Figure 2)[55,56,58]. This model-based tracking technique has been previously validated in vivo to have a precision of 0.33 mm or better for intervertebral translations and 1.1° for intervertebral rotations of the cervical spine[55]. Cervical spine intervertebral kinematics were determined following established standards for reporting spine kinematics[60,61]. Intervertebral flexion-extension angle during dynamic movement trials was normalized to a trial collected with the participant in the static neutral position.

A series of ICR locations was calculated between each pair of adjacent vertebrae over the subject's full range of motion using the finite helical axis (FHA) method [125]. Each ICR was defined as the intersection point of the computed FHA and the sagittal anatomical plane of the inferior vertebra. The anterior-posterior (AP) and superior-inferior (SI) location of each ICR was defined with respect to the inferior bone anatomic coordinate system and expressed as a percentage of the inferior bone size. The path of ICR positions during flexion-extension was interpolated at 1° increments of intervertebral flexion-extension to allow for comparison among

trials, movement direction, and participants. ICR locations calculated to be more than 200% of inferior bone width or height (for AP ICR and SI ICR, respectively) from the inferior bone origin were excluded from analysis. Due to inter-subject variability in flexion and extension range of motion at each motion segment, and the fact that the ROM was not centered about the neutral position for all subjects, ICR data were available at different ranges of intervertebral flexion-extension for each participant (Figure 13). Therefore, analysis was restricted to ICR values at 1º intervals that contained data from at least 6 participants (Figure 13 and Table 5) as has been previously done for evaluating ICR repeatability[115].

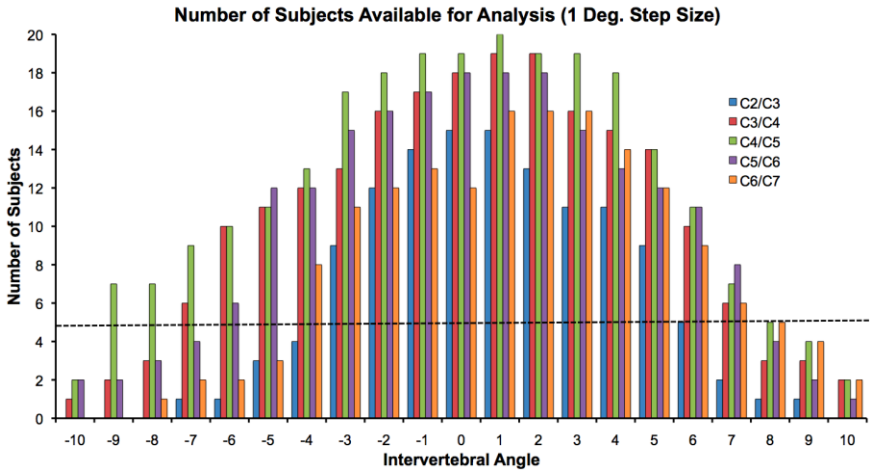

Figure 13: The number of subjects with available data at each intervertebral flexion-extension angle for each cervical motion segment.

Table 5: Intervertebral flexion-extension range of motion included in the analysis.

		Step Size		
		0.5 Deg.	1.0 Deg.	2.0 Deg.
Motion Segment	C2/C3	-4° to +6°	-3° to +5°	-3° to +5°
	C3/C4	-7° to +7°	-7° to +7°	-5° to +6°
	C4/C5	-9° to +8°	-9° to +7°	-8° to +7°
	C5/C6	-6° to +8°	-6° to +7°	-5° to +6°
	C6/C7	-5° to +8°	-4° to +7°	-4° to +7°

The effects of movement direction (flexion versus extension), intervertebral rotation step-size (0.5°, 1.0°, and 2.0°), filter frequency (1.0 Hz, 2.0 Hz, 4.0 Hz) and in vivo tracking errors (±0.5°, ±1.0° rotation; ±0.25 mm, ±0.5 mm translation) on ICR location were evaluated. These filter frequencies were selected because a previous analysis of this in vivo kinematic data[93] indicated an optimal cutoff frequency of 1.7 Hz using residual analysis[59]. A low-pass, 4th-order Butterworth filter was used to smooth the 6 DOF motion path of each bone (3 translations and 3 rotations). Differences in ICR location during the flexion and extension movements were calculated at each 1° increment of intervertebral flexion-extension for each motion segment. The average of these differences was then calculated across all intervertebral flexion-extension angles for each subject for analysis purposes (Figure 14).

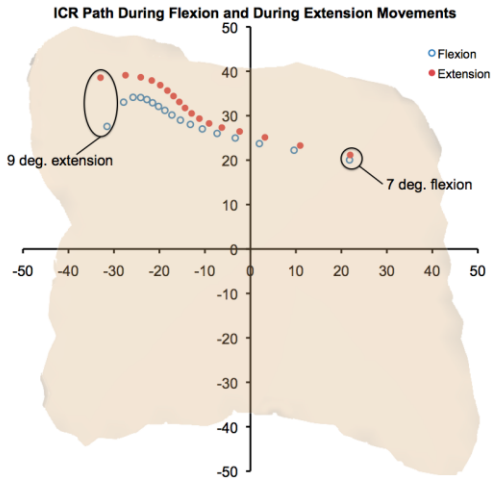

Figure 14: Flexion versus extension ICR comparison from a representative trial.

Within-subject trial-to-trial variability (i.e. reliability) in ICR locations was determined in a similar fashion by calculating differences among trials in ICR location at each corresponding 1° increment of intervertebral flexion-extension (after averaging corresponding flexion and extension ICRs for each trial) and then averaging across all intervertebral flexion-extension angles for each subject (Figure 15).

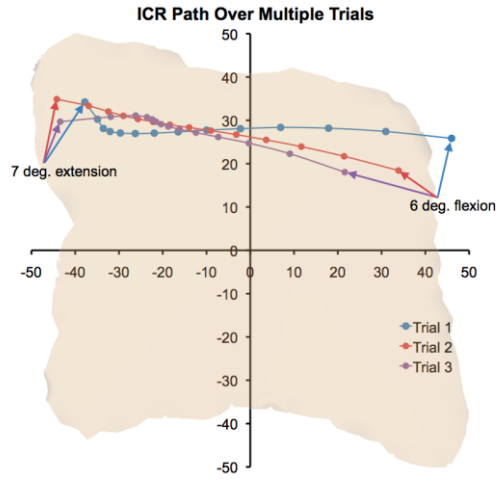

Figure 15: The path of the ICR over three flexion-extension trials.

Inter and intra-subject sensitivity to filter frequency and step size were determined by processing each trial for each individual at each level of filter frequency and step size (50 trials by 3 filter frequencies by 3 step sizes). The sensitivity to in vivo tracking error was assessed by systematically modifying the tracking results in each of the six degrees of freedom for one motion segment of one subject. Rotation tracking errors of ±0.5º and ±1.0º were introduced independently in each rotational degree of freedom, and tracking errors of ±0.25 mm and ±0.5 mm were introduced independently in each translational degree of freedom.

2.4.2.2 Simulated Data

Simulated bone motion data was created to assess the effects of tracking error, distance from the moving bone to the ICR, filter frequency, and rotation step size on ICR accuracy. Values included in the parametric evaluation were selected to span the range of potential values encountered during in vivo cervical spine motion using the previously described in vivo testing conditions and equipment. An initial dataset of "perfect" 3D bone motion was generated to simulate intervertebral flexion-extension about a fixed center of rotation. The "moving bone" rotated through 15º of flexion-extension (from 8º extension to 7º flexion back to 8º extension) over 3.0 seconds, with data sampled at 30 Hz to replicate in vivo ROM and testing conditions. The "perfect" simulated bone motion followed a circular path about the ICR, with angular velocity varying in a sinusoidal pattern (highest at the center of motion, lowest at the ends) to replicate in vivo flexion-extension angular velocity. At its peak, the moving bone was rotating about the fixed bone at 40º/s, also representative of our in vivo recorded motion. The effect of tracking error was assessed by adding random, uniformly distributed 3D noise to the ideal

dataset. Random 3D noise in the translation of the center of the moving bone (mean = 0) was introduced at two levels: standard deviation = 0.2 mm and standard deviation = 0.3 mm. Random rotation noise about each axis of the moving bone (mean = 0) was introduced at one level: standard deviation = 1.0º. These noise values were representative of the previously reported in vivo tracking precision using the model-based tracking technique for the cervical spine[55]. It should be noted that the noise was added to the bone model motion, thus all "points" on the bone remained in the same location relative to each other after the noise was added. This replicated our model-based tracking technique. A low-pass, 4th-order Butterworth filter was used to smooth the 3D bone motion using filter frequencies of 1.0 Hz, 2.0 Hz and 4.0 Hz as part of the parametric evaluation. Three distances from the known center of rotation to the center of the bone model were evaluated: 14 mm, 18 mm and 22 mm. These ICR-to-bone center distances were selected to span the potential range of distances between the geometric center of each cervical vertebra and its center of rotation. Rotation step sizes of 1.0º and 2.0º were selected for evaluation of the simulated data. As in the in vivo experiment, the ICR paths were interpolated at 1º increments of rotation and flexion ICR values were averaged with extension ICR values at corresponding flexion-extension angles, yielding 16 ICR values for each flexion-extension cycle. The average error in these ICR values was determined by the distance from the known ICR on the sagittal plane of the "fixed" bone (a point at 0,0) to the calculated ICR: $AverageError = \frac{\sum \sqrt{(X_{calculated})^2 + (Y_{calculated})^2}}{n}$ where n = the number of ICR values calculated. The simulation was repeated 20 times for each combination of parameters investigated (noise, filter frequency, step size, and distance between bone and ICR), resulting in 320 ICRs for each combination of parameters (16 ICRs X 20 repeated simulations).

2.4.3 Results

2.4.3.1 In Vivo Data

The total number of ICR locations included in the analysis varied by vertebral level and rotation step size (Table 6). The number of outliers excluded from analysis was greatest at the C2/C3 motion segment (1.6% of the total ICRs calculated after interpolation at C2/C3) and 0.5º step size (0.6% of the total ICRs calculated after interpolation using 0.5º step size).

Table 6: The number of ICR locations included in the in vivo analysis at each vertebral level and flexion-extension rotation step size after interpolating all ICR data to 1 degree intervals.

		Step Size			
		0.5 Deg.	1.0 Deg.	2.0 Deg.	Total
Motion Segment	C2/C3	564 (13)	512 (8)	425 (3)	1501 (24)
	C3/C4	927 (4)	889 (2)	781 (0)	2597 (6)
	C4/C5	1077 (1)	1031 (0)	926 (1)	3034 (2)
	C5/C6	931 (0)	873 (0)	763 (0)	2567 (0)
	C6/C7	753 (7)	687 (3)	581 (3)	2021 (13)
Total		4252 (25)	3992 (13)	3476 (7)	

Average bone height and bone depth were 13.5 mm and 14.7 mm, respectively. Inter-subject variability (defined as the 95% confidence interval (CI)) in bone height and depth was ±0.7 mm and ±1.1 mm, respectively. ICR results were calculated as a percentage of bone size for each individual. Therefore, on average, a one percent increment in bone height represented 0.135 mm and a one percent increment in bone depth represented 0.147 mm (Table 7).

Table 7: Bone height and depth.

	Bone Height			Bone Depth		
	Lower 95% CI	*Mean*	*Upper 95% CI*	*Lower 95% CI*	*Mean*	*Upper 95% CI*
C3	13.1	13.8	14.5	13.0	13.7	14.5
C4	12.7	13.3	13.8	13.4	14.3	15.2
C5	12.4	12.9	13.4	14.0	15.1	16.3
C6	12.6	13.0	13.4	14.4	15.5	16.7
C7	14.0	14.5	15.0	13.8	14.8	15.8

Average differences between flexion and extension motion ICR locations were always less than 5% of bone size and the 95% confidence intervals included zero for each vertebral level, each rotation step size, and each filter frequency (Figure 16). This indicates ICR locations calculated during the flexion motion were not different from those calculated at corresponding intervertebral angle during the extension motion. The 2 Hz filter frequency and 2º step size produced the minimum combination of intra-subject differences (the size of the bars in Figure 16) and inter-subject variability (the size of the 95% CIs in Figure 16) in flexion versus extension differences.

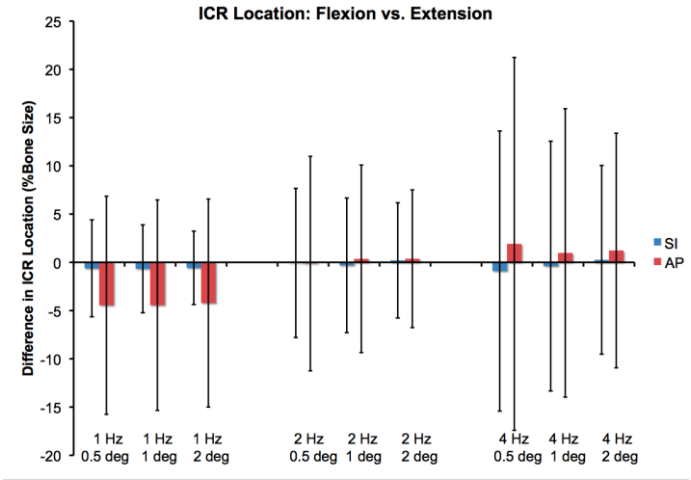

Figure 16: Average differences in ICR location during the flexion and the extension movement at corresponding angles of intervertebral rotation.

Trial-to-trial variability increased at the 4 Hz filter frequency and consistently decreased with increasing step size (Figure 17). Within-subject trial-to-trial variability in the SI direction was minimized by using the 1 Hz filter and 2º step size (3.7% bone height, which corresponds to 0.5 mm), while variability in the AP direction was minimized by using the 2 Hz filter frequency and a 2º step size (6.7% bone depth, which corresponds to 1.0 mm). Inter-subject differences in trial-to-trial variability, represented by the size of the 95% CI bars in Figure 17, consistently decreased with increasing step size.

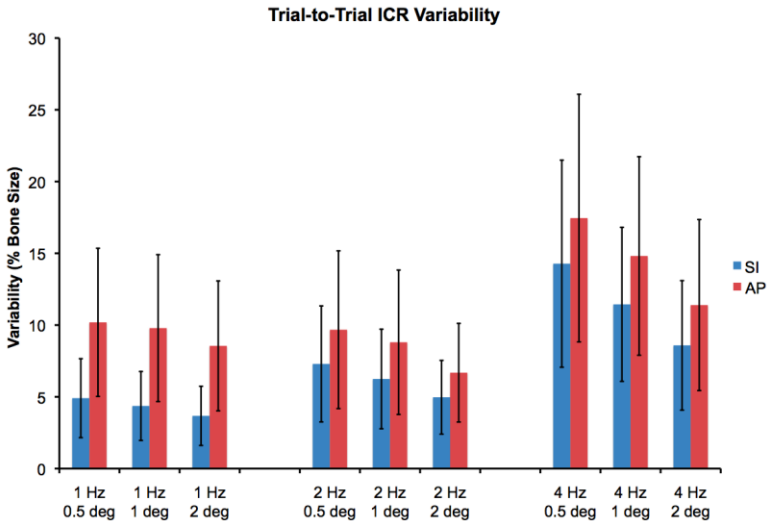

Figure 17: Trial-to-trial variability in the ICR at corresponding angles of intervertebral flexion-extension as a function of frequency and step size

The inter-subject variability in ICR location, characterized by the 95% CI of the mean ICR location at each intervertebral flexion-extension angle, averaged ±1.2 mm in the SI direction and ±2.2 mm in the AP direction across all intervertebral flexion-extension angles and all motion segments.

ICR location was most sensitive to translation tracking errors within the flexion-extension plane (Table 8). Small errors in AP and SI tracking (±0.25 mm) led to substantial alterations in ICR location (86% and 80% bone size), while small errors in FE tracking (±0.5 deg) led to smaller, yet substantial changes in ICR location (46% bone size).

Table 8: Sensitivity to model-based tracking errors.

	Sensitivity to Translation Tracking Errors		
	Tracking Error	+/-0.25 mm	+/-0.50 mm
Translation Direction	AP	86%	172%
	ML	8%	15%
	SI	80%	159%
	Sensitivity to Rotation Tracking Errors		
	Tracking Error	+/-0.5 deg	+/-1.0 deg
Rotation Direction	LB	4%	11%
	TW	16%	44%
	FE	46%	85%

2.4.3.2 Simulated Data

Filtering the simulated data at 1 Hz, 2 Hz and 4 Hz resulted in average ICR location errors of 1.1 mm, 3.1 mm and 6.8 mm, respectively, after applying noise levels appropriate for the given tracking system (Figure 18). The evaluated step size and noise parameters had little effect on ICR error at lower cutoff frequencies of 1 Hz and 2 Hz. The average ICR errors in the 18 mm and 22 mm bone-to-ICR configurations were different from 14 mm bone-to-ICR errors by only 0.1 mm and 0.02 mm, respectively, across all combinations of filter frequency and step size.

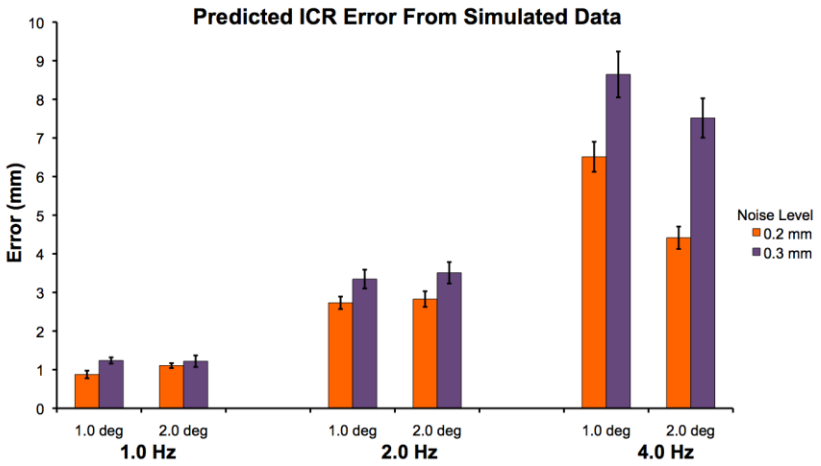

Figure 18: Average ICR error using simulated data with 3D noise added.

2.4.4 Discussion

The in vivo results indicate that ICR locations are not different between the flexion movement and the extension movement at corresponding intervertebral flexion-extension angles. This finding was consistent across all filter frequencies and all step sizes. This suggests that differences in loading during the flexion motion versus the extension motion do not appreciably affect the motion path between adjacent vertebrae, at least in this group of asymptomatic subjects. The small average difference between flexion and extension ICR for the 2 Hz filter and 2º step size, in combination with the narrow 95% CI of the difference in flexion versus extension ICR path (±0.8 mm in the SI direction and ±1.0 mm in the AP direction), suggests the ICR path may be a sensitive indication of dysfunction during the flexion-extension movement. This information may be used to evaluate a clinical cohort, such as whiplash patients, who have soft tissue injury that may preferentially affect movement in flexion or extension. It is typically difficult to identify tissue damage in whiplash patients[126], and differences between flexion and extension ICR paths may address this clinical challenge. The consistent ICR path during flexion

and during extension implies that for a motion-preserving disc replacement to replicate in vivo motion, the disc replacement should allow a single path of the ICR for flexion and extension movements (i.e. there is no "hysteresis" in the flexion-extension ICR path).

In vivo, the path of the ICR can reliably be characterized within 0.5 mm in the SI and 1.0 mm in the AP direction, on average. This trial-to-trial variability in the ICR path, at least when restricted to midrange motion of healthy controls, is comparable to the trial-to-trial variability in total ROM (0.1 mm in translation and 0.4º in rotation)[93]. Given these trial-to-trial variability results, it appears that collecting 2 to 3 trials of flexion-extension movement is sufficient to reliably estimate the path of the center of rotation in vivo with a precision of 1.0 mm or better. It should be noted that these trial-to-trial variability measures include variability due to tracking errors each trial and variability due to differences in movement by the subject from one trial to the next. We have previously demonstrated that inter-operator variability in running the automated software to track individual bone models is 0.02 mm in translation and 0.06º in rotation[55]

Although analytical models have been developed to estimate ICR calculation error due to marker cluster design (i.e. the number of markers and their locations relative to the ICR)[127], the current application is unique in that entire bone models are tracked, not individual points on the bone. Therefore, the errors in tracking marker locations (if there were markers placed on each bone) would not be independent. The computational experiment using "ideal" simulated data with added noise suggests that the expected in vivo accuracy in the ICR calculation is between 1.1 mm and 3.1 mm at filter frequencies of 1 Hz and 2 Hz, respectively. It should be noted that the noise values applied for the simulation study were obtained from a previous in vivo validation study that required placing fiducial markers closely together in the cervical

vertebrae[55]. Close placement of fiducial markers may have limited the accuracy of the "gold standard" reference values used to evaluate the model-based tracking accuracy. For example, in practice, the trial-to-trial variability in intervertebral ROM[93] was approximately one half of the variability expected given the previously reported accuracy of the model-based tracking system. Therefore, it is possible the noise added in the simulated experiment was approximately 2 times higher than the tracking error achieved in practice.

The tracking errors estimated from simulated data are lower than several previous reports of ICR accuracy simulation experiments[121,128] due to three factors: 1) the small distance between the bone and the ICR, 2) the tracking of the entire bone model rather than individual points on the bone, and 3) the filtering of tracked data. Collecting continuous data at a high sample rate, then filtering the tracked data, clearly reduces the error associated with calculating the ICR. Additionally, a previous study has concluded that the small-step-size sensitivity of the ICR no longer applies following low-pass smoothing of data acquired at a relatively high sample rate, and the ICR may be accurately calculated for even small rotations[129].

The current study was designed to assess the sensitivity, reliability and accuracy of a model-based tracking system for determining the ICR at each cervical motion segment during in vivo flexion-extension. Potential clinical applications for this information include assessing the effects of surgery (e.g. arthrodesis, disc replacement) on the ICR path of motion segments adjacent to the surgery and identifying mechanical alterations following injury (e.g. whiplash). A limitation of the current study is that the ICR analysis was limited to the mid-range of motion common to many subjects and the ICR at the ends of the ROM were generally not included in the analysis. Additionally, this study only reported variability within a single test session; inter-session reliability in ICR calculations remains to be determined.

2.5 MOTION PATH OF THE INSTANT CENTER OF ROTATION

2.5.1 Introduction

Cervical spine kinematics are most often assessed through static lateral radiographs collected in the full-flexion and full-extension positions[22,23,130]. Intervertebral range of motion (ROM) is the most common measurement acquired from these static end-range images. However, ROM is highly variable among subjects[22,23,25,27,78] and ROM measurements fail to characterize mid-range motion where the majority of our activities of daily living occur[79,80]. Furthermore, ROM only provides information about the *quantity* of intervertebral motion (i.e. total translation and total rotation), while failing to characterize the *quality* of motion (i.e. how the motion occurs).

The instant center of rotation (ICR) has been proposed as an alternative to ROM for evaluating the quality of spine movement and for identifying abnormal cervical spine kinematics[30]. The location of the ICR between two adjacent cervical vertebrae reflects the combined relative translation and rotation that occur during flexion-extension (Figure 19). It has been proposed that the location of the ICR has clinical significance, as specific abnormalities in the ICR may correspond to specific pathologies[109]. Additionally, ICRs may be useful in diagnosing deviations of normal segmental motion in the sagittal plane[26] and in diagnosing whiplash injuries[129]. The ICR has recently been used to evaluate cervical adjacent segment motion quality following arthrodesis and arthroplasty[108,131,132].

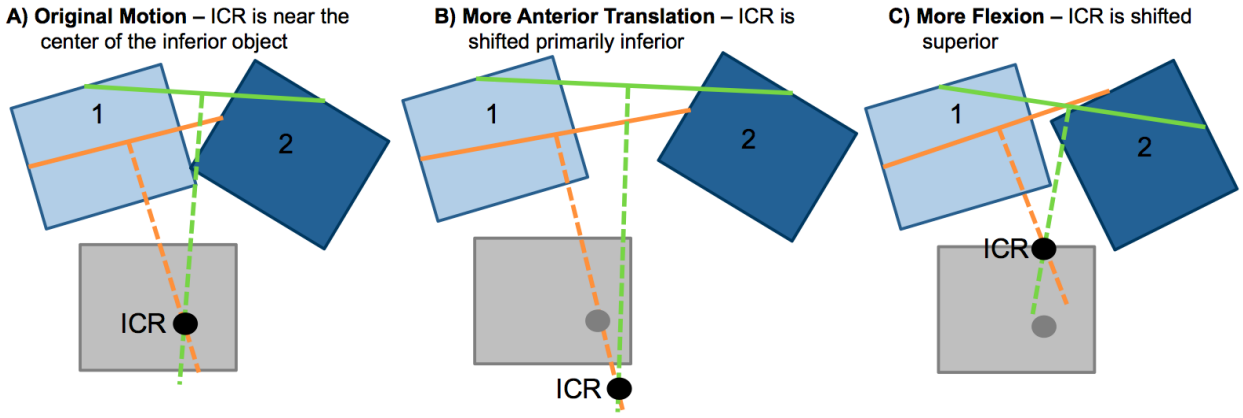

Figure 19: The effects of relative translation and rotation on the location of the instant center of rotation (ICR).

The location of the center of rotation for each cervical motion segment has traditionally been measured using radiographs collected at the ends of the ROM[76,106-108,131], although one study reported an average center of rotation by using a sequence of radiographs collected during the flexion-extension motion[26]. These single locations for the center of rotation, calculated from end-range radiographs or from averaged data, fail to account for the fact that the ICR may change location during dynamic motion and may not be fully described by a single point[110].

Correctly identifying the in vivo path of the center of rotation between adjacent cervical vertebrae is clinically significant due to the recent FDA approval of several cervical disc replacement devices in the United States[97,119,120]. These disc replacements have either fixed or variable centers of rotation, and it is not clear how well these designs mimic in vivo cervical spine movement. Additionally, an abnormal motion path of the ICR in motion segments

adjacent to arthrodesis may reflect altered adjacent segment loading, potentially leading to adjacent segment degeneration.

The first objective of this study was to characterize the movement path of the ICR at each cervical motion segment from C2 to C7 during dynamic in vivo flexion-extension in asymptomatic subjects. It was hypothesized that the ICR location would undergo significant translation in the anterior-posterior direction, but not in the superior-inferior direction, during flexion-extension. It was also hypothesized that the path of the ICR would be unique for each motion segment in asymptomatic spines. The second objective of this study was to perform a preliminary comparison of ICR paths in asymptomatic subjects and single-level arthrodesis patients during flexion-extension. It was hypothesized that the ICR path in motion segments adjacent to the arthrodesis would be significantly different in arthrodesis patients when compared to corresponding motion segments in asymptomatic subjects.

2.5.2 Materials and Methods

All subjects provided informed consent prior to participating in this Institutional Review Board-approved study. Participants included 20 asymptomatic subjects (7 M, 13 F, average age 46±6 yrs.), 12 C5/C6 single-level anterior arthrodesis patients (2 M, 10 F, average age 47±10 yrs., 7±1 months post surgery, 9 autograft, 3 allograft) and 5 C6/C7 single-level anterior arthrodesis patients (2 M, 3 F, average age 43±8 yrs., 7±1 months post surgery, 1 autograft, 4 allograft). Surgical indications were spondylotic radiculopathy due to disc herniation or stenosis. All surgeries included fusion instrumentation, and patients were placed in a cervical collar for 3 weeks post-surgery. Radiographic union was confirmed prior to dynamic movement testing.

Pregnant women, patients diagnosed with osteoporosis, and patients with any other injury or disease that interferes with spine function were excluded. Healthy asymptomatic subjects were recruited through an employee newsletter to approximately match the age and sex distribution of the arthrodesis patients.

High-resolution CT scans (GE Lightspeed 16) (0.29 mm x 0.29 mm x 1.25 mm voxels) of the cervical spine (C2-C7) were acquired on each participant. Bone tissue was segmented from the CT volume using a combination of commercial software (Mimics software, Materialise, Leuven, Belgium) and manual segmentation[53]. A three-dimensional (3D) model of each vertebra was generated from the segmented bone tissue. Eight markers were interactively placed on the 3D bone models to define bone-specific anatomic coordinate systems (4 on each endplate: most anterior, most posterior, left edge and right edge). The origin of the anatomic coordinate system for each bone was defined as the average of the most anterior and most posterior points on the superior and inferior endplates.

Subjects were seated within a biplane X-ray system and directed to continuously move their head and neck through their entire range of flexion-extension. A metronome set at 40 to 44 beats per minute was used to ensure the participants moved at a continuous, steady pace to complete each full movement cycle in 3 seconds or less. Biplane radiographs were collected simultaneously at 30 images per second for 3 seconds for each trial of continuous flexion-extension (X-ray parameters: 70 KV, 160 mA, 2.5 ms X-ray pulses, source-to-subject distance 140 cm). Radiographs were recorded for 2 or 3 trials for each subject, resulting in a total of 96 movement trials analyzed for this study. A static trial with the subject looking forward with the head in the neutral position was also collected for each participant. The effective radiation dose for each dynamic flexion-extension motion trial was estimated to be 0.16 mSv (determined using

PCXMC simulation software, STUK, Helsinki, Finland). In comparison, the effective dose of a cervical spine CT scan has been reported to be between 3.0 mSv and 4.36 mSv[91,92].

A previously validated model-based tracking process was used to determine three-dimensional vertebral position with sub-millimeter accuracy[55] for all static and dynamic trials. The model-based tracking algorithm involved recreating the geometry of the biplane imaging system within the computer and passing simulated X-rays through the three-dimensional subject-specific bone models to create digitally reconstructed radiographs (DRRs) (Figure 2). A computer algorithm translated and rotated the 3D bone models in lab-based 3D space until the DRRs were matched to edge-enhanced versions of the original radiographs. Details describing the volumetric model-based tracking process, including hardware and software specifications, calibration and distortion correction procedures, and computational algorithms have been described previously[55-58].

Tracked data was smoothed using a 1.0 Hz fourth-order, low-pass Butterworth filter[59]. The intervertebral flexion-extension angle in each frame of the continuous dynamic trial was normalized to the static neutral trial for each subject. The C2 vertebra was not sufficiently captured in the CT scan and/or in the biplane radiographs for several arthrodesis patients. Therefore, ICR data at the C2/C3 motion segment was not included in the analysis for arthrodesis patients.

The finite helical axis method[125] was used to calculate the three-dimensional axis of rotation between adjacent vertebrae for each 2º change in intervertebral flexion-extension. The ICR was defined as the point at which this three-dimensional axis of rotation vector intersected the sagittal anatomical plane of the inferior vertebra. The anterior-posterior (AP) and superior-inferior (SI) location of each ICR was defined with respect to the inferior bone anatomic

coordinate system and expressed as a percentage of the inferior bone size. The path of ICR positions during flexion-extension was interpolated at 1º increments of intervertebral flexion-extension to allow for comparison among trials and participants. Multiple trials from the same subject were averaged to yield a single average dataset for each subject used for statistical analysis. The instant center of rotation was not calculated for the motion segment included in the arthrodesis.

The ICR calculation is highly sensitive to a number of factors, including the amount of rotation that occurs between start and end images (i.e. the step size), tracking (or digitizing) error, and the distance from the moving body to its center of rotation[121-124]. We previously completed a parametric analysis of factors affecting ICR accuracy and precision during in vivo flexion-extension[133]. Processing the data as described above, the within-subject reliability in ICR path location was 0.5 mm in the SI direction and 1.0 mm in the AP direction. A computational experiment demonstrated the in vivo accuracy in ICR location was between 1.1 mm and 3.1 mm[133]. This parametric analysis also indicated there was no significant difference between ICR locations calculated during the flexion and extension movement. Therefore, ICRs calculated during the flexion movement were averaged with ICRs calculated at corresponding angles during the extension movement for the present analysis.

A previous study that calculated cervical motion segment ICRs indicated inter-subject variability in the ICR location would range between 1.0 mm and 2.2 mm[132]. Setting power to 80%, with an estimated inter-subject variability of 1.0 to 2.2 mm, the sample size calculation[134] indicated that between 6 and 21 subjects would be required per group (for inter-subject variability of 1.0 and 2.2 mm, respectively) in order to identify a difference between groups of 2 mm in ICR location.

A linear mixed-model analysis was performed to characterize differences in the path of the center of rotation according to motion segment in control subjects. Additionally, the length of the ICR path in the SI and AP directions was quantified. In order to normalize the path lengths among motion segments with different amounts of flexion-extension, the change in location of the ICR per degree of intervertebral flexion-extension was determined by fitting a line through the ICR location versus intervertebral angle paths for each motion segment of each subject. The change in ICR location per degree of flexion-extension was compared across motion segments using repeated measures analysis of variance. Differences in ICR paths between control subjects and arthrodesis groups were identified using linear mixed-model analysis. Significance was set at $p < .05$ for all tests, and the Bonferroni correction was applied to adjust for multiple comparisons in all cases.

2.5.3 Results

ICR data were available over different ranges of intervertebral flexion-extension for each participant due to inter-subject variability in flexion and extension range of motion at each motion segment. Therefore, analysis was restricted to flexion-extension angles that contained a sufficient number of participants in each group (n = at least 6 in the control group, at least 4 in the C5/C6 arthrodesis group and at least 3 in the C6/C7 arthrodesis group) (Table 9). For example, for the C4/C5 motion segment in the control group, the number of subjects available for each 1º increment of flexion from neutral to 10º of flexion was 19, 20, 19, 19, 18, 14, 11, 7, 5, 4, 2. Therefore, ICR values were included in the analysis up to +7º of flexion (7 participants) at the C4/C5 motion segment for the controls (Table 9).

Table 9: Flexion-extension range of motion included in the ICR analysis for each group and each motion segment.

		Group		
		Control	C5/C6 Arthrodesis	C6/C7 Arthrodesis
Motion Segment	C2/C3	-3° to +5°	N/A	N/A
	C3/C4	-5° to +6°	-5° to +5°	-2° to +4°
	C4/C5	-8° to +7°	-9° to +2°	-4° to +4°
	C5/C6	-5° to +6°	N/A	-6° to +4°
	C6/C7	-4° to +7°	-4° to +5°	N/A

2.5.3.1 Control Group

The mean SI location of the ICR became progressively more superior from the C2/C3 motion segment to the C6/C7 motion segment (Figure 20, Figure 21, Table 10). Significant differences in the mean SI location of the ICR were found between all motion segments (all $p < .001$ after correction for multiple comparisons) except the C3/C4 and C4/C5 levels ($p = 1.000$). The average SI location of the ICR did not change significantly with intervertebral flexion-extension angle ($p = .747$). The interaction between flexion-extension angle and motion segment level also was not significant ($p = .844$), indicating the effect of flexion-extension angle on SI ICR location was not significantly different among motion segments.

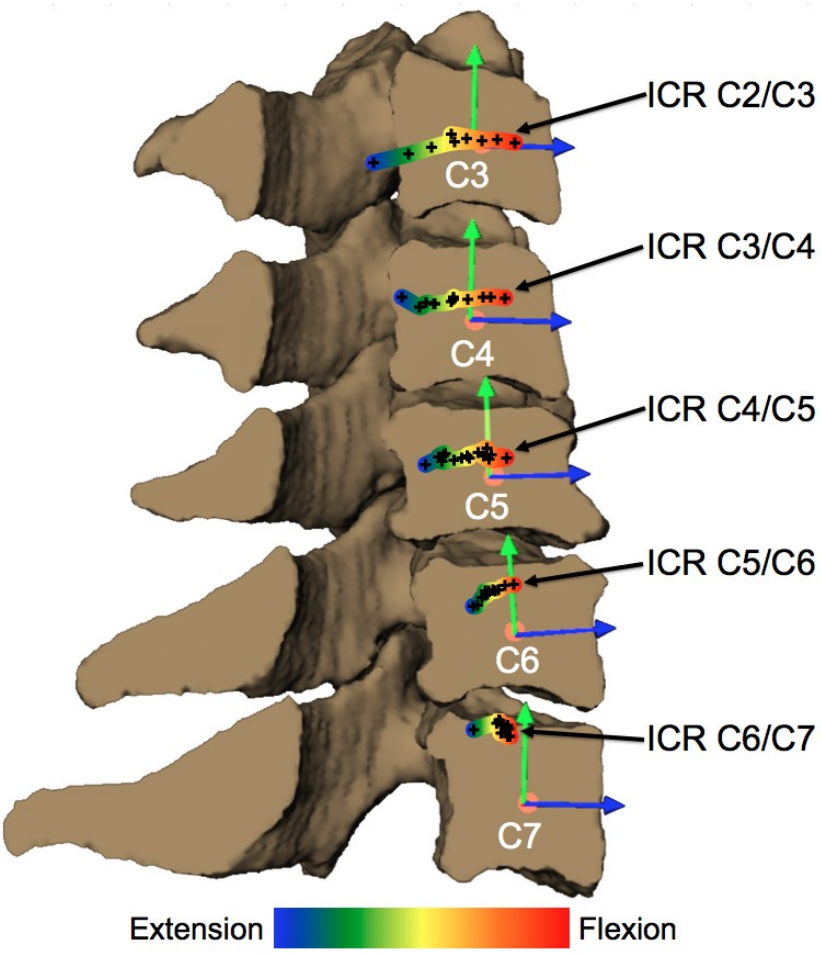

Figure 20: ICR path during flexion-extension in the asymptomatic cervical spine.

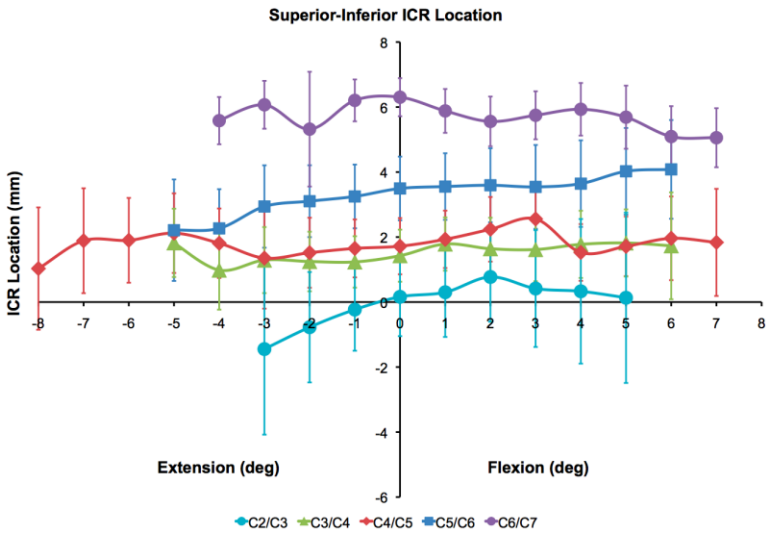

Figure 21: The mean superior-inferior motion path of the ICR at each motion segment in asymptomatic controls at 1° increments of flexion-extension.

Table 10: Mean ICR location in the superior-inferior and anterior-posterior directions.

Motion Segment	Lower 95% CI (mm)	Mean Superior-Inferior ICR Location (mm)	Upper 95% CI (mm)	Lower 95% CI (mm)	Mean Anterior-Posterior ICR Location (mm)	Upper 95% CI (mm)
C2/C3	-1.1	-0.3	0.5	-3.9	-2.8	-1.8
C3/C4	0.7	1.5	2.2	-2.7	-1.8	-0.8
C4/C5	0.9	1.6	2.3	-2.9	-1.9	-0.9
C5/C6	2.5	3.2	3.9	-3.1	-2.0	-1.0
C6/C7	5.1	5.9	6.7	-3.1	-2.0	-1.0

The average AP location of the ICR path was posterior to the geometric center of the inferior vertebral body and not significantly different among levels (Figure 20, Figure 22, Table 10). The AP ICR location was significantly affected by the angle of intervertebral flexion-extension, indicating significant translation of the ICR in the AP direction during flexion-extension ($p < .001$). Furthermore, there was a significant interaction between intervertebral flexion-extension angle and motion segment level ($p < .001$), indicating differences among

motion segments in the relationship between AP location of the ICR and intervertebral flexion-extension angle.

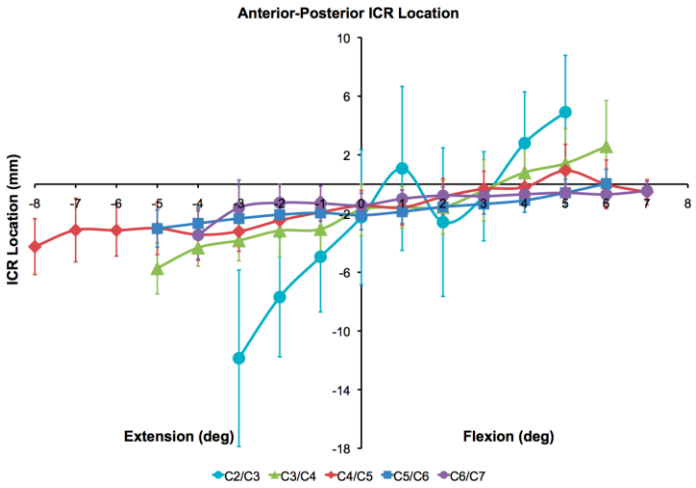

Figure 22: The mean anterior-posterior motion path of the ICR at each motion segment in asymptomatic controls at 1° increments of flexion-extension.

The change in ICR location in the AP direction per degree of flexion-extension generally decreased from the C2/C3 motion segment to the C6/C7 motion segment (Table 11). The change in ICR location in the AP direction per degree of flexion-extension was significantly different among all motion segments (all $p \leq .021$), with the exception of the C6/C7 motion segment, which was not different from the C4/C5 and C5/C6 motion segments (both $p = 1.000$) (Table 11).

Table 11: Mean change in the AP location of the ICR per degree of intervertebral flexion-extension.

Motion Segment	Lower 95% CI (mm/deg)	Change in AP ICR Location Per Degree of Flexion-Extension (mm/deg)	Upper 95% CI (mm/deg)
C2/C3	3.2	3.9	4.7
C3/C4	1.0	1.4	1.7
C4/C5	0.5	0.7	0.9
C5/C6	0.1	0.3	0.5
C6/C7	0.1	0.5	0.8

The inter-subject variability in the ICR location in asymptomatic subjects, defined by the 95% CI of the mean at each intervertebral flexion-extension angle, averaged ±1.2 mm in the SI direction and ±1.9 mm in the AP direction across all intervertebral flexion-extension angles and all motion segments (Figure 21, Figure 22). While inter-subject variability in the SI direction was fairly consistent among motion segments (the 95% CI of the mean was 1.8 mm, 1.0 mm, 1.2 mm, 1.2 mm and 0.9 mm for the C2/C3 through the C6/C7 motion segments, respectively) (Figure 21), inter-subject variability in the AP direction was by far the highest in the C2/C3 motion segment (the 95% CI of the mean was 4.4 mm, 1.9 mm, 1.4 mm, 0.9 mm and 0.9 mm for the C2/C3 through the C6/C7 motion segments, respectively) (Figure 22).

2.5.3.2 Asymptomatic versus Arthrodesis

No significant differences between the control and arthrodesis groups were identified when comparing the average location of the ICR paths in the SI (all $p \geq .528$) or AP direction (all $p \geq .579$) (Table 12). The average 95% confidence interval of the difference in ICR location between asymptomatic and C5/C6 or C6/C7 arthrodesis patients was ±1.4 mm and ±2.0 mm, respectively. No significant differences were observed when comparing the control and arthrodesis groups in terms of the change in ICR location in the AP direction per degree of flexion-extension (all $p \geq .249$) (Table 13). The average 95% confidence intervals for the

differences in the change in the AP ICR location per degree of flexion-extension between asymptomatic and arthrodesis groups was ±0.6 mm/deg.

Table 12: Difference between groups in mean ICR location.

Motion Segment ICR		Asymptomatic vs. C56 Arthrodesis			Asymptomatic vs. C67 Arthrodesis		
		Lower 95% CI	Mean Difference	Upper 95% CI	Lower 95% CI	Mean Difference	Upper 95% CI
C3/C4	SI	-1.8	-0.3	1.1	-0.9	1.1	3.1
	AP	-1.5	0.2	1.9	-4.1	-1.5	1.2
C4/C5	SI	-2.4	-1.0	0.5	-1.5	0.2	2.0
	AP	-1.2	0.2	1.6	-3.5	-1.4	0.7
C5/C6	SI	N/A	N/A	N/A	-1.9	0.2	2.3
	AP	N/A	N/A	N/A	-1.3	0.2	1.8
C6/C7	SI	-1.0	0.4	1.8	N/A	N/A	N/A
	AP	-0.6	0.7	2.0	N/A	N/A	N/A

Table 13: Difference between groups in the change in anterior-posterior ICR location per degree of intervertebral flexion-extension.

Motion Segment ICR	Asymptomatic vs. C56 Arthrodesis			Asymptomatic vs. C67 Arthrodesis		
	Lower 95% CI	Mean Difference	Upper 95% CI	Lower 95% CI	Mean Difference	Upper 95% CI
C3/C4	-1.4	-0.5	0.4	-0.1	0.7	1.5
C4/C5	-0.5	-0.1	0.2	-0.5	0.0	0.5
C5/C6	N/A	N/A	N/A	-0.3	0.1	0.5
C6/C7	-0.9	-0.3	0.3	N/A	N/A	N/A

2.5.4 Discussion

This is believed to be the first report of the motion path of the ICR in the cervical spine during in vivo functional movement. This study has revealed important kinematic differences among motion segments during functional mid-range motion in asymptomatic subjects. These level-dependent differences include the average location of the ICR in the SI direction and the amount of AP translation in the ICR per degree of intervertebral flexion-extension. These findings clearly illustrate that if the goal of cervical disc replacements is to replicate in vivo motion, they

should be designed to account for level-specific differences in the location and motion path of ICR. For example, although the average ICR in the AP direction was located posterior to the geometric center of each inferior vertebra, it is clear that the ICR translates significantly in the AP direction with flexion-extension, and that the amount of this translation varies by motion segment. Furthermore, although the SI position of the ICR did not change significantly within motion segments during flexion-extension, there were clear differences among motion segments in the average SI location of the ICR. The average center of rotation was located posterior to the geometric center of the inferior vertebral body in the AP direction. The center of rotation in the SI direction was located near the center of C3 for C2/C3 and moved progressively closer to the disc for each motion segment until C6/C7, where the ICR was located near the top endplate of C7 (Figure 20). This variation in the SI location of the ICR with respect to motion segment is in agreement with previous studies that have reported single ICR locations for each cervical motion segment[26,76,106,107].

Previous studies have demonstrated significant inter-subject variability in intervertebral flexion-extension range of motion (ROM) in asymptomatic subjects, ranging from 20% to 60% of the overall motion at each motion segment[22,23,25,27,78], which corresponds to standard deviations of 4º or more. This large variability makes it difficult to identify abnormal motion that may develop following injury, degeneration, or surgical intervention. In fact, if inter-subject variability is only 4º (a "best-case" scenario given previous results[22,23,25,27,78]), in order to detect a 2º difference in ROM between groups, 64 subjects would be required per group[134]. In comparison, the inter-subject variability in ICR location for asymptomatic subjects in this study, represented by the 95% CI of the mean, ranged between ±0.9 mm to ±1.4 mm in the lower cervical spine motion segments where the vast majority of degeneration requiring surgery occurs

(C4/C5, C5/C6 and C6/C7). Future studies that evaluate ICR motion paths in arthrodesis and arthroplasty patients in comparison to control subjects will most likely focus on these motion segments. Using the data collection and processing tools described in the current study, it is estimated that with power set at 80%, between 13 and 26 subjects per group will be required to identify ICR path differences as small as 2 mm[134] for ±0.9 mm and ±1.4 mm 95% CIs, respectively. Given the lack of correspondence between ROM (in degrees) and ICR (in mm), it is difficult to definitively state that one measurement is more sensitive than the other, especially when the amount of change necessary to reach clinical significance it not well defined for either parameter.

In the current study, the inability to detect significant differences between the asymptomatic and arthrodesis groups was influenced by the sample size and by the effect size of the treatment. First, the relatively small sample sizes of the arthrodesis groups limited the statistical power of the study. However, the 95% confidence intervals of the differences between groups were quite small, indicating the ICR motion paths were consistent between control and surgical groups. Second, the effect size of the treatment (i.e. the differences between asymptomatic and arthrodesis groups) was small. For example, the mean difference between asymptomatic and arthrodesis groups was 0.6 mm for average ICR location and 0.2 mm/deg for ICR translation per degree of flexion-extension. The combination of narrow confidence intervals and small effect size provides preliminary evidence to suggest that single-level anterior arthrodesis does not appear to affect cervical motion quality during flexion-extension.

While the current results suggest that single-level arthrodesis does not affect the quality of motion in adjacent segments, the effects of single-level disc arthroplasty on adjacent segment motion quality remain unknown. Previous results investigating adjacent segment ICR following

arthroplasty or fusion have been contradictory. While two studies have indicated arthroplasty[108] and arthroplasty or fusion[132] do not affect adjacent segment center of rotation, another study found arthroplasty shifted the center of rotation in the superior motion segment in comparison to fusion[131]. These studies, however, were performed using only full-flexion and full-extension radiographs to calculate a single, stationary center of rotation. Further investigation will be necessary to compare adjacent segment effects on the motion path of the ICR following arthroplasty or fusion. It is possible a poorly designed disc replacement could lead to significant alterations in adjacent segment motion quality. This may be the case with current disc replacement designs that have a fixed center of rotation and/or fail to allow for vertebral level differences in motion. The mechanical benefits of increased ROM associated with total disc replacements may be negated by poor motion quality, leading to no significant reduction in adjacent segment degeneration in comparison to arthrodesis[98,135].

A limitation of the current study was the relatively narrow, yet clinically important, age range of the subjects. ICR motion paths may differ in young and older spines, given the degenerative changes that occur with age[49,71,73,74]. A second limitation was the fact that the arthrodesis subjects were tested approximately 7 months after surgery. This time frame is earlier than adjacent segment disease generally occurs[8]. Therefore, while the present results provide valuable information regarding the short-term effects of arthrodesis, the results may not be representative of longer-term effects. Furthermore, the current data only assesses adjacent segment motion quality in single-level arthrodesis patients. The effects of multi-level arthrodesis on the quality of adjacent segment motion remain unknown.

3.0 INTERVERTEBRAL ARTHROKINEMATICS

3.1 DISC DEFORMATION

3.1.1 Introduction

Degenerative changes adjacent to fused cervical vertebrae are well documented[5-11], and lead to recurrent pain[5] and ultimately adjacent level surgery in 6% to 16% of patients[5,11,45-48]. The etiology of adjacent segment disease following cervical arthrodesis remains controversial. The disease may progress due to the underlying spondylosis[7,14,136], the arthrodesis may lead to increased motion in adjacent vertebrae, resulting in overload and instability[10,12,15,16], or adjacent segment degeneration may result from a combination of these two factors[11,9].

Previous kinematic studies investigating adjacent segment disease have focused on vertebral range of motion (most often flexion-extension and anterior translation) when assessing spine mechanics in asymptomatic subjects and arthrodesis patients[65-66]. One limitation of these kinematic studies is that they only take into account bone position at the end of the range of motion, typically under static loading conditions. Relative motion between adjacent vertebrae in the middle range of motion (which is most often encountered in activities of daily living[79,80]) and during dynamic, functional loading is not assessed. A second limitation is that kinematic reports that focus solely on bone range of motion fail to reveal how the coupled translation and rotation

between adjacent vertebrae combine to deform the intervertebral disc throughout the movement. These are critical limitations because intervertebral disc deformation during dynamic, functional movement can reflect the magnitude and direction of the loads applied to the disc and the material properties of the disc. Therefore, disc deformation patterns may be beneficial in identifying altered mechanical loading and modified disc material properties following cervical arthrodesis.

Techniques to evaluate *in vitro* disc strain have progressed from adhering optical targets to the disc surface[137] to using high-resolution MRI images and image correlation techniques[138]. *In vitro* testing, however, has limitations in replicating subject-specific *in vivo* dynamic loading and kinematics. *In vivo* disc deformation during functional loading remains poorly defined due to limitations of previous studies, including the large error associated with manual identification of vertebral edges on radiographs[17,139] and data collection restricted to static postures[17].

The primary aim of this study was to characterize cervical disc deformation in asymptomatic control subjects during *in vivo* dynamic flexion-extension. It was hypothesized that each disc level would exhibit a unique shear and compression/distraction deformation pattern during dynamic loading. A secondary aim was to assess disc deformation in single-level arthrodesis subjects. It was hypothesized that discs adjacent to the arthrodesis would undergo increased shear and compressive deformation when compared to corresponding discs in asymptomatic control subjects.

3.1.2 Materials and Methods

3.1.2.1 Subjects

Twenty asymptomatic control subjects (46±9 yrs.; 7 M, 13 F) and 15 single-level anterior arthrodesis patients (10 C5-C6 arthrodesis: 45±6 yrs.; 2 M, 8 F; 7±1 mo. post surgery; 5 C6-C7 arthrodesis: 2 M, 3 F, average age 43±8 yrs.; 7±1 months post surgery) provided informed consent to participate in this Institutional Review Board-approved study. Asymptomatic controls that reported no previous neck disability were recruited to approximately match the age and gender distribution of the arthrodesis patients. Control subject recruitment was accomplished through an advertisement in an employee newsletter and word of mouth. Arthrodesis subjects who were at least 18 years of age and scheduled to undergo (or recently received) single-level anterior cervical discectomy and fusion (ACDF) surgery were identified during clinic visits. Pregnant women, subjects diagnosed with osteoporosis, and subjects with any other injury or disease that interferes with spine function were excluded.

3.1.2.2 Data Collection

Subjects were seated within a biplane X-ray system (Figure 1) and, for each trial, directed to continuously move their head and neck through their entire range of flexion-extension. A metronome set at 40 to 44 beats per minute was used to ensure the participants moved at a continuous, steady pace to complete each full movement cycle in approximately 3 seconds. Radiographs were collected at 30 frames per second for 3 seconds for each trial of flexion-extension (X-ray parameters: 70 KV, 160 mA, 2.5 ms X-ray pulses, source-to-subject distance 140 cm). Radiographs were recorded for 2 or 3 separate trials for each subject (allowing for a rest period between trials). A total of 92 dynamic flexion-extension trials were included in this

analysis, however, multiple trials for each subject were averaged to obtain a single trial for each participant for statistical analysis. An additional 0.1 s static trial was collected for each subject with the head in the neutral position. The effective radiation dose for each 3-second dynamic flexion-extension motion trial was estimated to be 0.16 mSv (determined using PCXMC simulation software, STUK, Helsinki, Finland).

High-resolution CT scans (0.29x0.29x1.25 mm voxels) of the cervical spine (C2-C7) were acquired on each participant (GE Lightspeed 16). The effective dose of a cervical spine CT scan has been reported to be between 3.0 mSv and 4.36 mSv[91,92]. Bone tissue was segmented from the CT volume using a combination of commercial software (Mimics software, Materialise, Leuven, Belgium) and manual segmentation[53]. A three-dimensional (3D) model of each vertebra was generated from the segmented bone tissue. Eight markers were placed on the 3D bone models to define bone-specific anatomic coordinate systems (4 on each endplate: most anterior, most posterior, left edge and right edge).

3.1.2.3 Data Processing

A previously validated bone-model-based tracking process was used to determine three-dimensional vertebral motion with sub-millimeter accuracy for all static and dynamic trials[55]. The bone-model-based tracking algorithm involved recreating the geometry of the biplane imaging system within the computer and passing simulated X-rays through the three-dimensional subject-specific bone models to create digitally reconstructed radiographs (DRRs) (Figure 2). A computer algorithm translated and rotated the 3D bone model in lab-based 3D space until the DRRs were matched to edge-enhanced versions of the original radiographs. Details describing the volumetric model-based tracking process, including hardware and software specifications,

calibration and distortion correction procedures, and computational algorithms have been extensively described[55-58]. Tracked bone movement data was filtered at 1.0 Hz using a fourth-order, low-pass Butterworth filter with the filter frequency determined using residual analysis[59]. The tracked data was used to determine intervertebral flexion-extension using the bone-specific anatomic coordinate systems.

Nucleus and annulus regions were defined on the vertebral endplate surfaces according to previous reports[42,94], and all disc height and dynamic disc deformation measurements were acquired within the central 1/3rd of the disc width (Figure 5). Average disc height within the nucleus (N), anterior annulus (AA) and posterior annulus (PA) regions was determined from the static trial using an automated computer algorithm that measured disc height over the entire central 1/3rd of the disc width (Figure 23A and Figure 23B). Average disc deformation was calculated every frame of dynamic movement within each disc region to determine shear and compression-distraction deformation (Figure 23C). Disc deformations were normalized to disc height in the static neutral position to determine the average percent deformation within each anatomic region of the disc (Figure 24). The disc deformation versus intervertebral flexion-extension curves generated from the continuous motion data were interpolated at 1º increments of flexion-extension to facilitate statistical analysis.

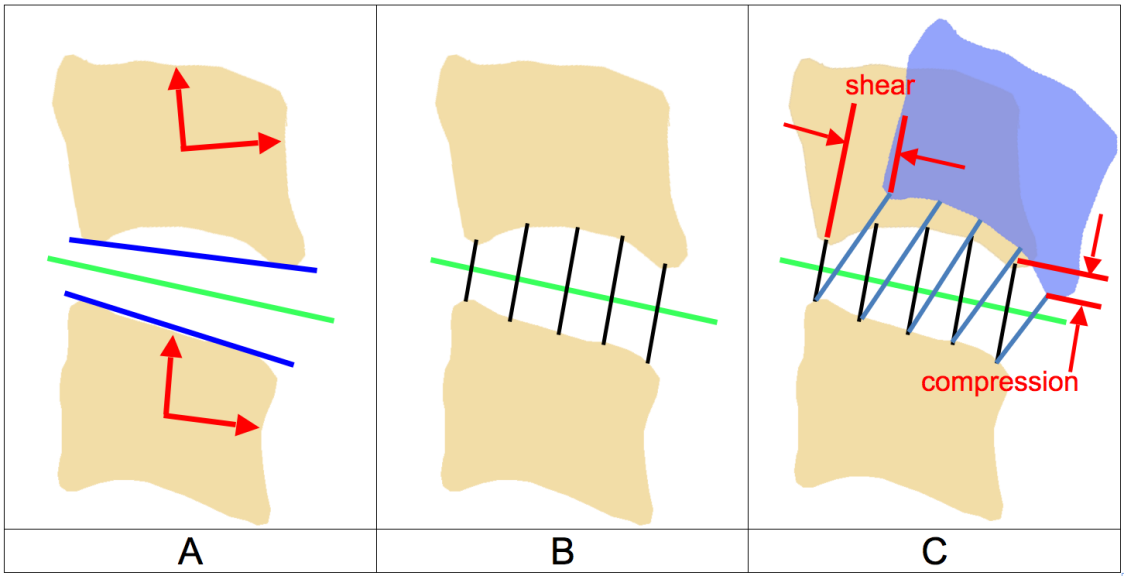

Figure 23: Calculating disc height and disc deformation.

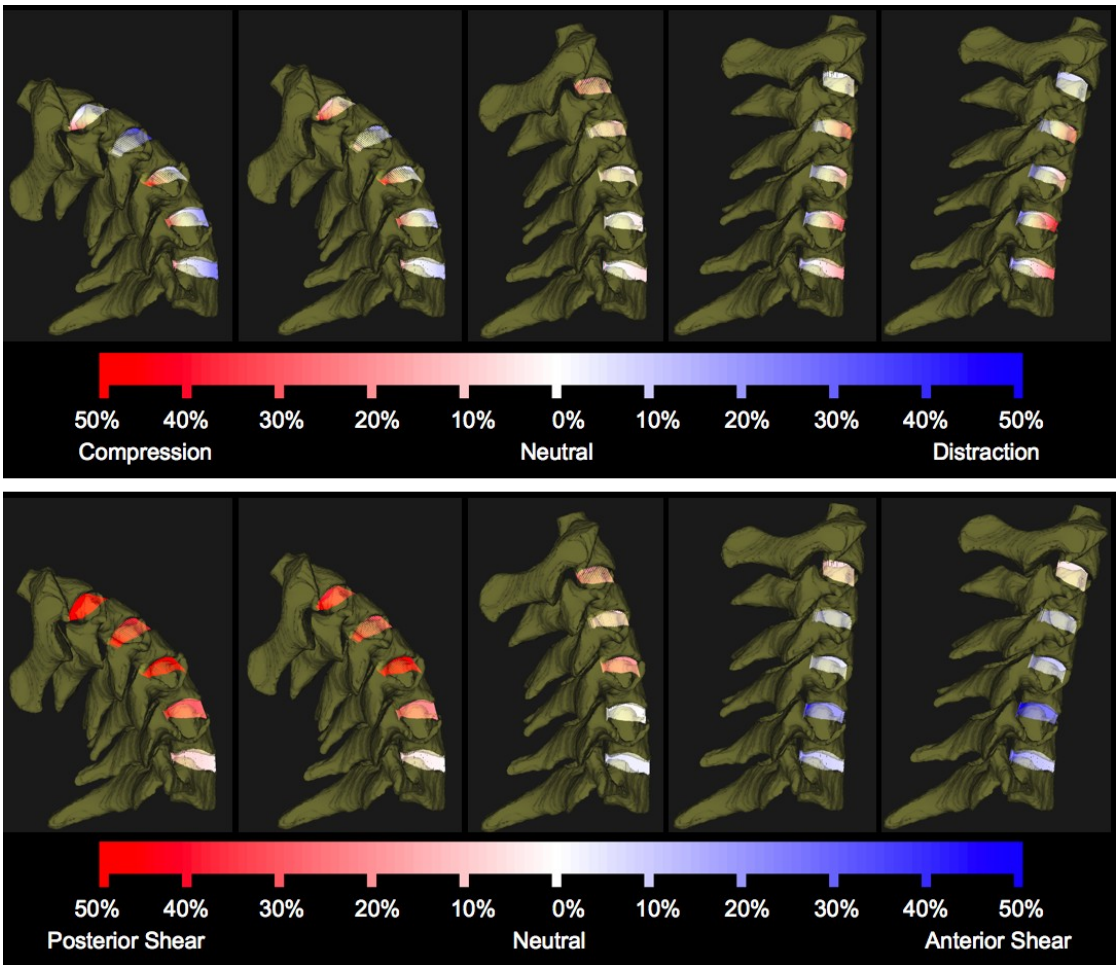

Figure 24: C23 to C67 disc compression-distraction deformation (above) and shear deformation (below) during dynamic flexion-extension.

The average disc height across all three disc regions of all discs between C2 and C7[140] and the precision of the tracking system in measuring flexion-extension rotation and anterior-posterior translation[55] were used to estimate that the tracking system can determine disc deformation (shear and compression-distraction) with a precision of 3.6% or better. A power calculation was performed to estimate the number of subjects necessary to identify differences between groups that were in excess of our tracking system variability (i.e. greater than 3.6%).

This power analysis indicated that 17 subjects would be necessary per group, with power set at 0.80 and alpha equal to 0.05[134].

3.1.2.4 Data Analysis

Within-subject differences in disc deformation during the flexion and extension movement directions were assessed within each disc region (posterior annulus, nucleus, anterior annulus) and disc level (C23 through C67) in control subjects. These flexion versus extension differences were used to determine if disc deformation was dependent upon movement direction. The within-subject trial-to-trial variability in disc deformation was also determined within each disc region and disc level in control subjects in order to assess within-subject repeatability in disc deformation during functional loading.

A linear mixed-model analysis was performed to identify differences in disc compression-distraction and shear deformation curves at each disc level (C23 through C67) for each of the three disc regions (posterior annulus, nucleus, anterior annulus) in control subjects. Arthrodesis and control subject comparisons were also performed using linear mixed model analysis to identify differences in compression-distraction deformation curves at discs adjacent to the arthrodesis (C45 and C67 for the C5-C6 arthrodesis group, and C56 for the C6-C7 arthrodesis group) for each of the three disc regions (posterior annulus, nucleus, anterior annulus). In order to statistically compare shear deformation in control and arthrodesis groups, the slope of the line formed by the shear deformation versus flexion-extension angle plot was determined (i.e. the rate of shear deformation). T-tests were used to identify differences between arthrodesis and control subjects in terms of the rate of shear deformation (calculated by the slope of the shear deformation versus flexion-extension angle for each motion segment). Significance

was set at $p < .05$ for all tests, with the Bonferroni correction applied in cases of multiple comparisons.

3.1.3 Results

3.1.3.1 Flexion versus Extension Differences

The average difference in disc deformation between the flexion motion and the extension motion at identical angles of intervertebral flexion-extension was 0.9% and 0.1% for disc compression-distraction and disc shear, respectively, across all disc levels (C23 through C67) and all disc regions (anterior annulus, nucleus, posterior annulus) in the control subject group. Therefore, disc deformation values during flexion were averaged with deformation values during extension at each corresponding intervertebral angle for all subsequent analysis.

3.1.3.2 Repeatability

Within-subject trial-to-trial variability (i.e. standard deviation) in compression-distraction deformation at identical angles of intervertebral flexion-extension averaged 2.4% across all disc levels, with greatest variability in the C23 disc (3.8%) and smallest variability in the C56 disc (1.4%) in control subjects. Within-subject trial-to-trial variability in shear deformation at identical angles of intervertebral flexion-extension was consistent across disc levels and averaged 1.1%.

3.1.3.3 Control Subject Disc Deformation

A consistent pattern in control subject disc compression-distraction was evident across disc levels in each disc region. Disc compression was greatest in the C23 disc, and compression decreased with each successive inferior disc (Figure 25). In the control group in the anterior annulus region, the C23 disc was significantly more compressed than all other discs (all $p < 0.001$). Similarly, the C34 anterior annulus was significantly more compressed than the C45, C56 and C67 anterior annulus regions (all $p \leq 0.002$) (Figure 25A). C45, C56 and C67 compression-distraction patterns in the anterior annulus were not significantly different (all $p = 1.000$) (Figure 25A). In the nucleus region, the C23 disc was significantly more compressed than all other discs (all $p < 0.001$) (Figure 25B). The C34 nucleus region was more compressed than the C56 and C67 nucleus regions ($p < 0.001$). The C45 nucleus was more compressed than the C56 ($p = 0.029$) and C67 nucleus regions ($p < 0.001$). Compression in the C56 and C67 nucleus was not significantly different ($p = 0.193$) (Figure 25B). In the posterior annulus region, the C23 disc was significantly more compressed than all other discs (all $p \leq 0.002$) (Figure 25C). No significant differences were identified among the C34, C45 and C56 posterior annulus regions (all $p \geq 0.514$); however, the C67 posterior annulus was significantly less compressed than all other disc levels (all $p < 0.001$) (Figure 25C).

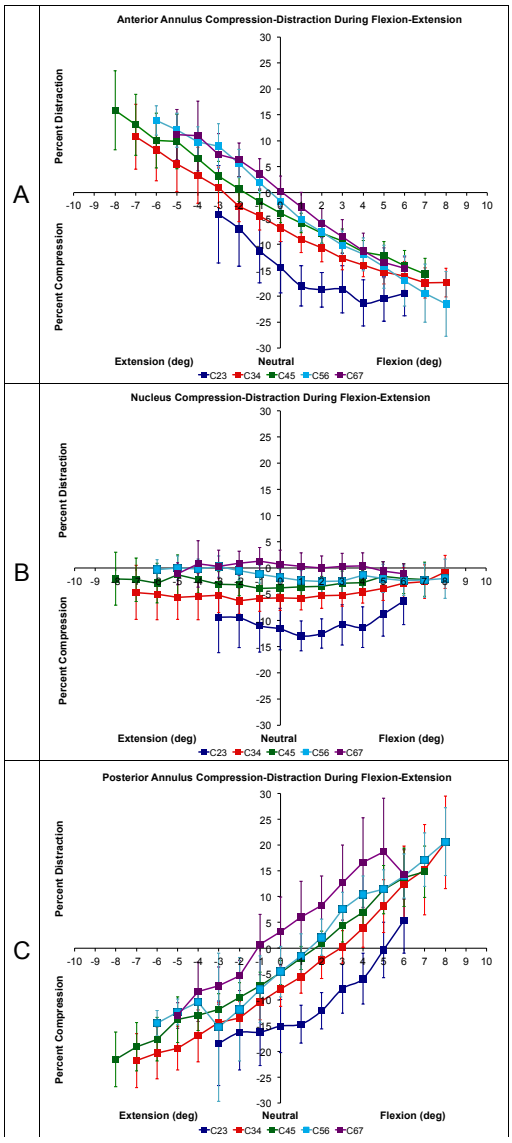

Figure 25: Mean disc compression-distraction deformation in the anterior annulus (A), nucleus (B), and posterior annulus (C) during flexion-extension in asymptomatic control subjects.

The rate of disc shear deformation progressively decreased from the C23 disc to the C67 disc (Figure 26). The only significant difference in the rate of shear deformation occurred

between the C67 level and the C23, C34, C45 levels (all $p < 0.001$). Static disc height within each disc region was not significantly different among disc levels (Figure 27).

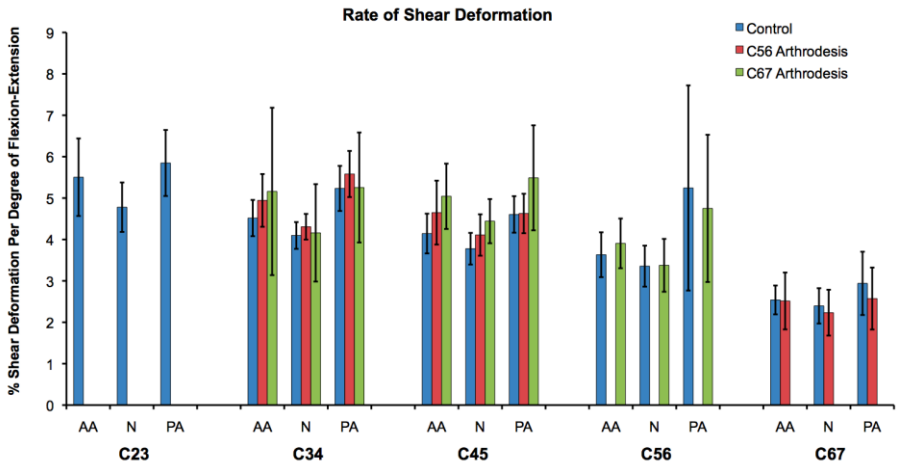

Figure 26: Average rate of shear deformation in the anterior annulus (AA), nucleus (N) and posterior annulus (PA) for each cervical disc.

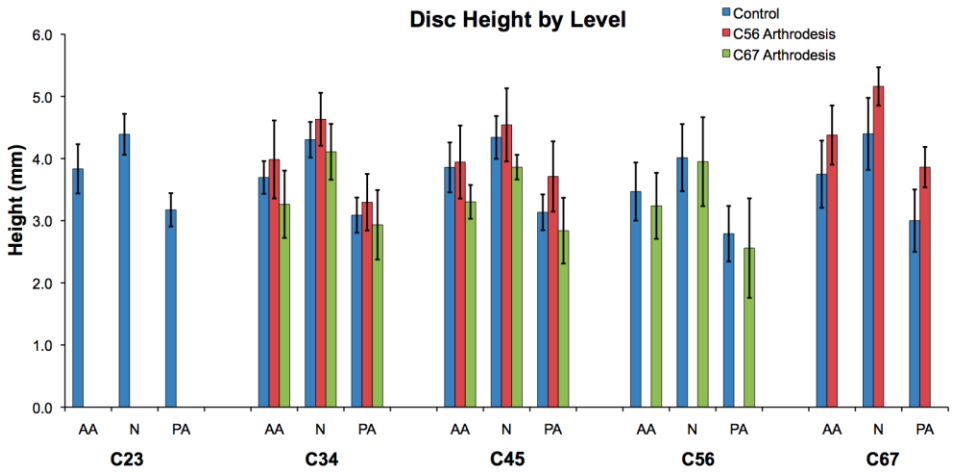

Figure 27: Disc height in the anterior annulus (AA), nucleus (N) and posterior annulus (PA) in the static neutral position.

3.1.3.4 Control versus Arthrodesis Adjacent Segment Deformation

In the C5-C6 arthrodesis group, the C45 discs were significantly less compressed than in the control group in all disc regions ($p = 0.003$, $p = 0.022$ and $p = 0.026$ in the anterior annulus, nucleus and posterior annulus, respectively) (Figure 28). No significant differences between the C5-C6 arthrodesis group and the control group were identified in the C67 disc compression-distraction curves for any disc region ($p = 0.759$, $p = 0.743$, $p = 0.398$ in the anterior annulus, nucleus and posterior annulus, respectively). In the C6-C7 arthrodesis group, the C56 discs were significantly less compressed than the control group in the nucleus ($p = 0.023$) and posterior annulus ($p = 0.014$) regions, but not the anterior annulus region ($p = 0.137$).

No significant differences in the rate of shear deformation were identified at any disc level adjacent to the arthrodesis region when comparing the control and arthrodesis groups (all $p \geq 0.264$ and all $p \geq 0.105$ for the C5-C6 and C6-C7 arthrodesis groups, respectively) (Figure 26).

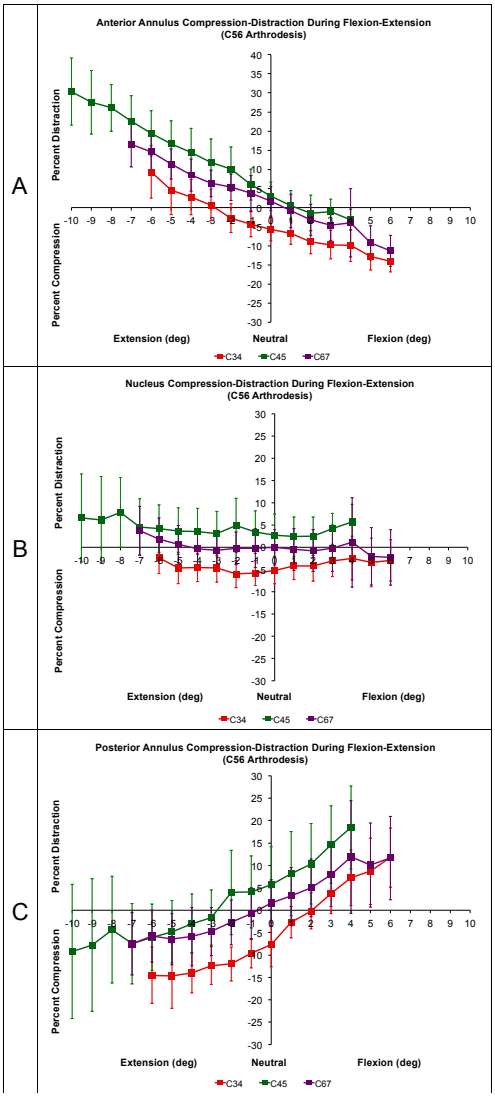

Figure 28: Mean disc compression-distraction deformation in the anterior annulus (A), nucleus (B), and posterior annulus (C) during flexion-extension in C56 arthrodesis patients.

3.1.4 Discussion

The control subject data provides new insights into disc deformation during *in vivo* functional loading and provides a standard for comparison when evaluating the effects of surgery on adjacent cervical discs. The mean control subject compression-distraction curves were "shifted" toward compression during *in vivo* functional loading (with the exception being the C67 disc). As an example, during the dynamic movement trial, when the intervertebral angle was identical to the neutral position angle, all three disc regions (anterior annulus, nucleus and posterior annulus) were compressed (with the exception being the C67 disc). Similarly, at equivalent magnitudes of flexion or extension, the compression deformation was much greater than the distraction deformation (with the exception being the C67 disc) (Figure 25). This shift toward compression likely reflects the effects of increased muscular forces necessary to produce the dynamic flexion-extension.

Few reports of disc deformation are available to compare with the present results. In one study, pre-operative flexion/extension radiographs of cervical fusion patients indicated that pre-operative shear strain averaged 5% to 7% in segments adjacent to the surgical site[17]. However, the magnitude of the pre-surgical adjacent segment range of motion was not provided, making it difficult to interpret this finding. Another study used cineradiography to estimate lumbar disc deformation during standing flexion and extension[139]. This study estimated maximum compressive and shear strains of 35% and 60%, respectively, at full flexion[139]. In vitro studies of lumbar motion segments have reported strains averaging between 5% and 8%[137,141].

The disc deformation curves presented here may be used to improve *in vitro* organ level or explant mechanobiology dynamic loading regimens and *in vivo* controlled loading via external fixation devices[142-146]. As previous studies have demonstrated, certain dynamic loading

conditions are beneficial to maintaining matrix homeostasis[147,148] and improving various biological therapies[149,150]. However, the loads applied to the disc during *in vivo* physiologic loading are currently unknown, so it is not clear how well these *in vitro* tests replicate *in vivo* loading. The control subject disc deformation curves presented here provide valuable information regarding the *in vivo* deformation experienced by disc tissues during functional loading. For example, the current results indicate that during dynamic flexion-extension, the anterior and posterior annulus regions of cervical discs undergo compression-distraction deformation of up to 20%, while the nucleus region is continuously compressed between 0% and 15%, depending on disc level. Similarly, the results indicate that during *in vivo* flexion-extension, the peak shear deformation ranges from 16% (at C67) to 33% (at C45), given the average flexion-extension range of motion at each motion segment[140]. This information may be used to guide *in vitro* and *in vivo* studies that investigate cell and tissue responses to stress and strain. As noted previously, reproducing *in vivo* conditions is important because the wrong type or magnitude of loading will lead to very different cell responses, and potentially misleading results[39].

There are two potential explanations for the significant level-dependent differences in compression-distraction observed in this study. First, the results may be explained by variation in disc material properties from the C23 disc to the C67 disc. The present data indicate that the C23 disc compresses the most, and compression decreases with each successive inferior disc. This suggests the C23 disc is the most compliant, and compressive stiffness increases with each successive inferior disc. This idea is supported by *in vitro* material testing that demonstrated compressive stiffness progressively increases from the C23 disc (637.5 N/mm) to the C67 disc (829.7 N/mm)[151]. An alternative explanation for the observed level-dependent differences in

disc compression-tension is that in the static neutral position, which was used as a reference to normalize all disc deformation measurements, compressive loading on the C23 disc was relatively small (compared to the load applied during functional motion) and the static compressive loading on the C67 disc was nearly equivalent to the load applied during functional motion.

The trend toward decreasing shear deformation per degree of flexion-extension, from the superior to inferior discs, indicates the translation between endplates decreases successively from C23 to C67 for a given amount of intervertebral flexion-extension. As a result, even though the flexion-extension range of motion in the C2-C3 motion segment is slightly less than in the C6-C7 motion segment[140], the C23 disc undergoes considerably more shear deformation. The significant decrease in C67 shear deformation, in comparison to superior discs, corresponds to a relatively fixed center of rotation in the C6-C7 motion segment in comparison to cranial levels during flexion-extension[152].

This study provides evidence to suggest that single-level anterior arthrodesis alters the compression-distraction patterns in the disc immediately superior to the arthrodesis while not affecting compression-distraction inferior to the fused site. While it is not clear why this difference exists superior to the arthrodesis, potential explanations include a change in disc material properties, altered compression-distraction loads following arthrodesis, or there may be an iatrogenic cause. The current shear deformation results agree with a previous study that reported no increase in the shear strain in discs adjacent to fusion using measurements obtained from static full-flexion and full-extension radiographs[17].

The relatively short time between surgery and testing for arthrodesis subjects is one limitation of this study. Fusion may not have occurred in the arthrodesis group at 7 months post-

surgery. Fusion status was evaluated using total flexion-extension ROM during dynamic movement in a subgroup of 8 C5-C6 arthrodesis patients who have returned for follow-up testing 2-years post surgery. In this sample of 8, total ROM at the operated site decreased from 3.6° at 7 months post-surgery to 2.4° at 24 months post-surgery. Differences in disc deformation adjacent to the arthrodesis may be amplified as motion decreases in the operated segment. Therefore, 2-year follow-up testing is being completed for the remainder of the arthrodesis group. Another limitation is that the results are specific to single-level anterior arthrodesis and it would be inappropriate to extrapolate the results to different single-level or multiple-level anterior surgeries. The asymptomatic control subjects, who were selected to approximately match the age of the arthrodesis patients, exhibited varying amounts of age-related spondylosis. Considering the well-known changes that occur in the spine with age[49,71,74,153], the disc deformation patterns presented for the control group are likely representative only of subjects within their age-range. We are currently collecting data on a cohort of young (20-35 years) asymptomatic subjects to assess the effect of age on spine kinematics. Finally, the deformation values reported in this study were obtained using bone-to-bone measurements that represent *in vivo* tissue-level deformation. The reported deformations do not necessarily represent localized or cell-level deformation.

3.2 FACET JOINT CAPSULE DEFORMATION

3.2.1 Introduction

The cervical facet joint has been identified as the most common source of neck pain[154,155] and it is thought to play a role in chronic neck pain related to whiplash injury[156,157-159]. Long-term symptoms are common following whiplash, with approximately half of those affected remaining symptomatic one year after the injury[160]. The precise site of injury within the facet joint capsule (FJC) has yet to be identified, however, facet joint injury mechanisms may include excessive compression of the facet joint[161,162] and/or capsular ligament strain beyond physiological limits[162,163].

Our current knowledge of cervical facet joint kinematics is based on mechanical testing of cadaver specimens subjected to loading conditions designed to simulate "physiologic"[156,162,164], "whiplash"[162-164], and "catastrophic"[156,163] conditions. Given our inability to accurately estimate *in vivo* cervical spine loads during dynamic movement, it is not clear how well these *in vitro* tests, performed under "physiologic loading", replicate *in vivo* spine loading and kinematics. As a result, our current perception of *in vivo* facet kinematics may be mistaken.

The primary aim of the current study was to characterize subaxial cervical facet joint kinematics and FJC deformation during *in vivo*, dynamic flexion-extension in a group of asymptomatic control subjects. It was hypothesized that FJC deformation is significantly different among motion segments and that FJC deformation is dependent upon anatomic region of the facet joint (e.g. anterior vs. lateral vs. posterior facet). A secondary objective was to assess the effect of single-level anterior arthrodesis on FJC deformation during the flexion-

extension motion. It was hypothesized that FJC deformation adjacent to the arthrodesis would be significantly greater than in corresponding facet joints of age-matched control subjects.

3.2.2 Materials and Methods

3.2.2.1 Subjects

Data from 14 asymptomatic control subjects (average age 43.4 ± 5.2 yrs, 5 M, 9 F) and 9 single-level (C5-C6) anterior arthrodesis patients (average age 45.9 ± 9.5 yrs.; 2 M, 7 F; 6.9 ± 1.3 mo. post-surgery) was included in the present analysis. Surgical indications were spondylotic radiculopathy due to disc herniation or stenosis. The surgeon's preferred approach to this problem was anterior fusion. Exclusion criteria included pregnant females, previous diagnosis of osteoporosis, and any other injury or disease that interferes with spine function. Patients were identified during clinic visits. Control subjects were recruited through an advertisement in an employee newsletter and word of mouth.

3.2.2.2 Data Collection

High-resolution CT scans (0.29 x 0.29 x 1.25 mm voxels) of the cervical spine (C2 through C7) were acquired on each participant (GE Lightspeed 16, GE Medical Systems, Waukesha, WI). Three-dimensional (3D) bone models were generated from the CT volume using a combination of commercial software (Mimics software, Materialise, Leuven, Belgium) and manual segmentation[53]. Markers were interactively placed on the 3D bone models to define bone-specific anatomic coordinate systems.

Participants were seated within a biplane X-ray system and directed to continuously move their head and neck through their full range of flexion-extension. A metronome set at 40

to 44 beats per minute was used to assist the participants in moving at a continuous, steady pace to complete each full movement cycle in 3 seconds or less. Biplane radiographs were collected at 30 images per second for 3 seconds for each trial of continuous flexion-extension (X-ray parameters: 70 KV, 160 mA, 2.5 ms X-ray pulses, source-to-subject distance 140 cm). Radiographs were recorded for 2 or 3 trials for each subject, resulting in a total of 59 movement trials analyzed for this study. Multiple trials from the same subject were averaged to yield a single average dataset for each subject used for statistical analysis. A static trial with the subject looking forward with the head in the neutral position was also collected for each participant. The effective radiation dose for each 3-second dynamic flexion-extension motion trial was estimated to be 0.16 mSv (determined using PCXMC simulation software, STUK, Helsinki, Finland). For comparison, the effective dose of a cervical spine CT scan has been reported to be between 3.0 mSv and 4.36 mSv[91,92].

3.2.2.3 Data Processing

A previously validated tracking process determined 3D vertebral position with sub-millimeter accuracy[55] by matching bone models from the CT scan to the biplane radiographs for all static and dynamic trials. The volumetric model-based tracking process[55-58] and data processing techniques[55,140,152,165] have been detailed previously. Intervertebral position and orientation in each frame of the continuous dynamic trial were normalized to the static neutral trial for each subject. Only the flexion-extension component of vertebral rotation is presented in the current analysis.

Four markers defining a facet-specific plane parallel to the facet surface were placed on each superior facet of the 3D bone model (Figure 29). An automated computer algorithm identified attachment sites for fibers forming each FJC (Figure 30) using average FJC

dimensions from the literature[166]. FJC fibers, lying on the surface of each bone model and oriented perpendicular to the plane of the facet joint in the neutral position[166], were represented by points connecting corresponding upper and lower FJC attachment sites (Figure 30). In order to facilitate the analysis, the FJC fibers were grouped into fibers representing the anterior, lateral, posterior-lateral, posterior, and posterior-medial FJC (Figure 30). While the fiber attachment sites remained fixed to the respective bone models, the points that represented the rest of the fiber were allowed to slide across the surface of the bone during the flexion-extension movement (Figure 31). The total length of each FJC fiber (determined by adding the lengths between consecutive points representing the fibers), and the length of each fiber parallel and perpendicular to the facet joint surface were determined in the static neutral position. Intervertebral flexion-extension angles and FJC fiber deformations (total, shear and compression-distraction) relative to the static position were determined for each cervical motion segment (C2-C3 through C6-C7) over the entire flexion-extension motion. This resulted in a continuous curve relating fiber deformation to intervertebral angle at each motion segment. For analysis purposes, data at each motion segment was divided according to the intervertebral orientation relative to the neutral position (flexion or extension). The rate of fiber deformation per degree of flexion-extension was then determined for each fiber group within each cervical motion segment.

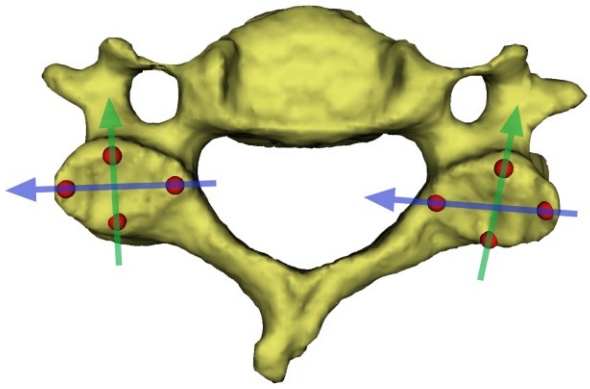

Figure 29: Defining the plane of the facet.

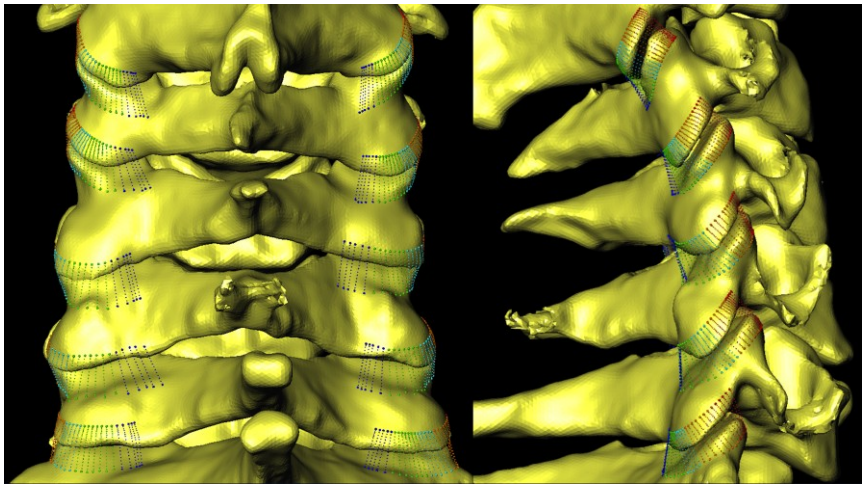

Figure 30: Posterior and lateral views of the facet joint capsule attachment sites and fibers.

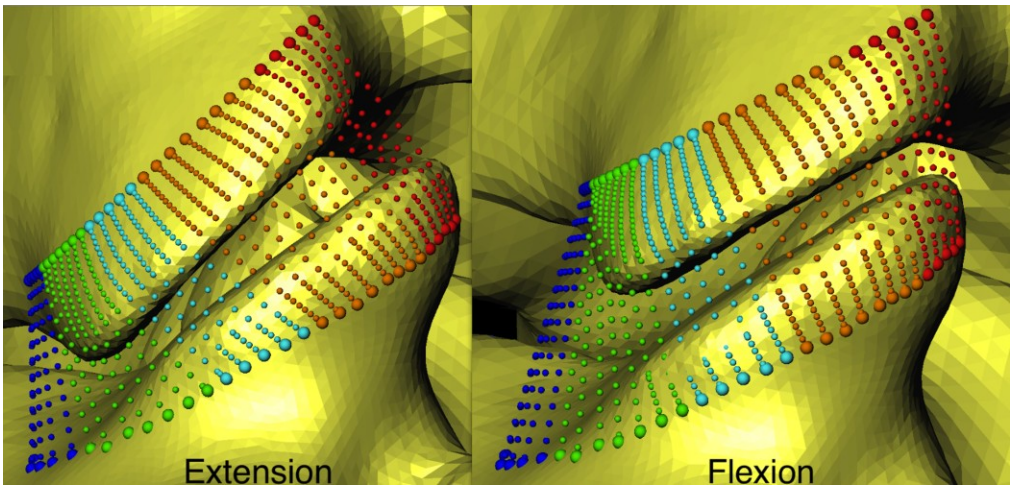

Figure 31: A close-up view of the facet joint capsule demonstrating that the attachment sites remained fixed but the fibers were allowed to slide across the bone surfaces.

3.2.2.4 Statistical Analysis

FJC deformation values for the corresponding left and right facets of each subject were averaged to yield a single FJC length value at each motion segment for each instant of the flexion-extension movement. Repeated measures analysis of variance was used to identify differences in the rate of facet joint capsule fiber deformation among motion segments and among fiber regions for the control group (IBM SPSS Statistics, version 21). Analysis of variance was used to identify differences between the control group and the C5-C6 arthrodesis group at the C4-C5 and C6-C7 motion segments. The Bonferroni correction for multiple comparisons was used when significant main effects were identified, with significance set at $p < .05$ for all tests.

3.2.3 Results

The primary mechanism driving facet joint capsule fiber deformation varied depending on fiber location and vertebral orientation. In some cases increased deformation due to shear was countered by decreased deformation due to compression (e.g. Figure 32A and 32B, flexion ROM). In other cases, shear and compression/distraction deformation combined to increase (e.g. Figure 32C-E Flexion ROM) or decrease (Figure 32D and 32E- extension ROM) fiber lengths.

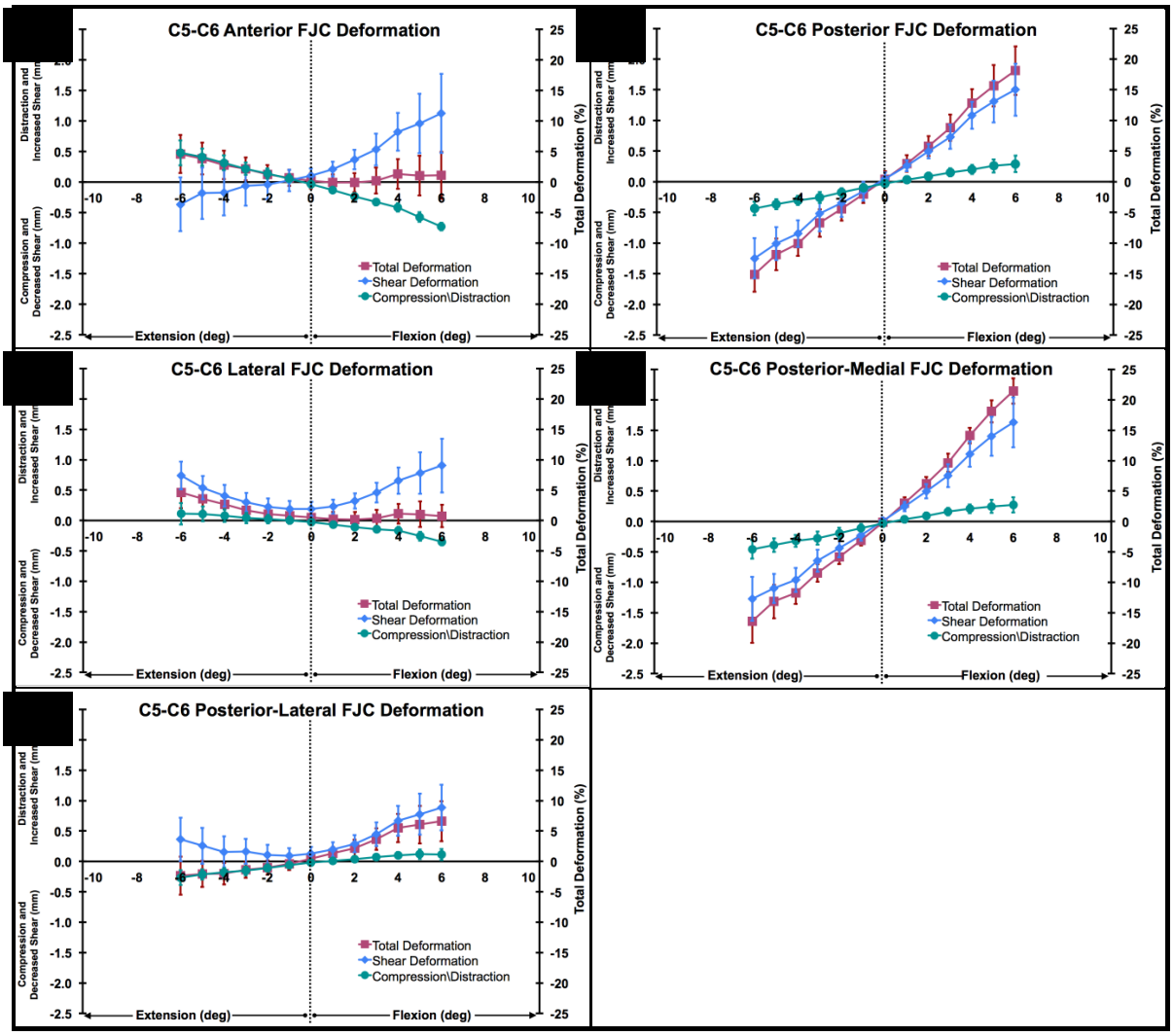

Figure 32: Facet joint capsule deformation during flexion-extension.

Fibers within all regions of the FJC increased in length as the motion segments moved from the neutral position into increased flexion (Figure 33). The rate of fiber deformation in flexion was not different among motion segments (main effect of motion segment: $p = .159$). However, the rate of fiber deformation was different among fiber regions (main effect of fiber region: $p < .001$). Post-hoc tests indicated fiber deformation rates in the anterior and lateral fiber regions were not different ($p = .198$), however, every other region was different from all others (all $p < .001$).

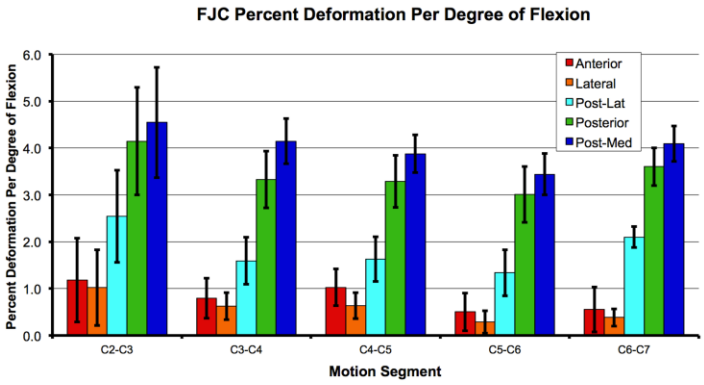

Figure 33: Rate of facet joint capsule deformation in a flexed orientation.

As the cervical motion segments increased their flexed orientation, the anterior and lateral fibers increased length due to the shear deformation rate (0.17 mm/deg.) being greater than the compressive deformation rate (0.04 mm/deg.). Simultaneously, the posterior-lateral, posterior and posterior-medial fibers increased length due to the combined effects of shear (0.26 mm/deg.) and distraction (0.07 mm/deg.) deformation.

As the motion segments moved from neutral orientation into more extension, only the anterior and lateral fiber regions consistently increased in length (Figure 34). Therefore, only anterior and lateral fiber regions were included in the statistical analysis of the extension range of the movement. The rate of fiber deformation during extension was different among motion segments (main effect of motion segment: $p < .001$). Post-hoc tests indicated the rate of fiber deformation in the C3-C4 motion segment was greater than in C5-C6 and C6-C7 ($p = .003$ and $p = .042$, respectively). The rate of deformation in the anterior region was also greater than in the lateral region ($p = .001$).

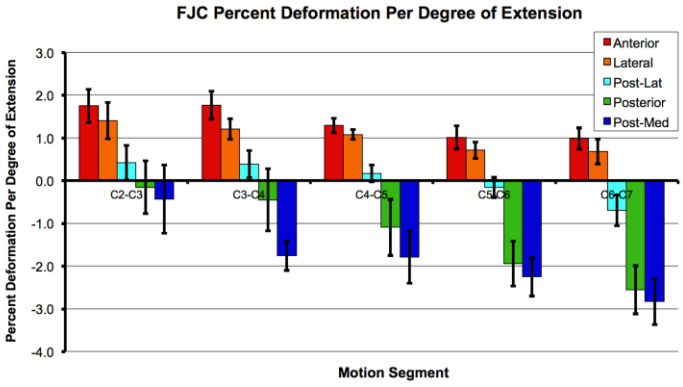

Figure 34: Facet joint capsule deformation in an extended orientation.

When the cervical motion segments were in an extended orientation relative to the neutral position, the mechanism for increasing length was different for the anterior and lateral FJC fibers. The anterior fibers were distracted more than the lateral fibers ($p < .001$), while the lateral fibers experienced more shear than the anterior fibers ($p = .008$).

In an extended orientation, the rate of FJC deformation adjacent to the arthrodesis (0.434%/deg) was less than in corresponding FJCs in asymptomatic subjects (0.969%/deg) ($p = .001$) (Figure 35). In the flexed orientation, the groups were not different ($p = .284$).

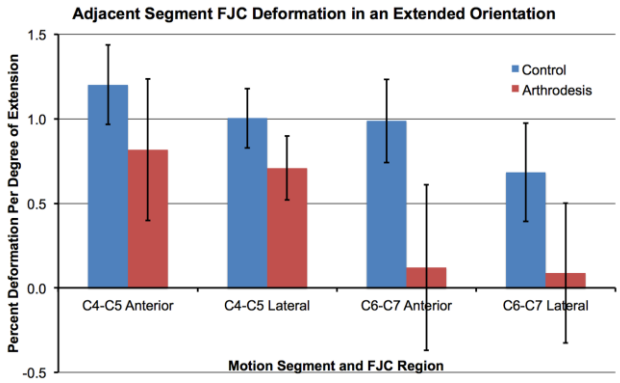

Figure 35: Rate of FJC deformation in an extended orientation for control and arthrodesis groups.

Although differences in the rate of FJC deformation were observed adjacent to the arthrodesis, control and arthrodesis groups were not different with respect to static neutral orientation (Table 14), total range of motion (Table 15) and flexion and extension components of total range of motion (Table 16). Additionally, FJC fiber lengths in the static neutral position (Figure 36) were not different between control and arthrodesis groups at any fiber region or vertebral level (all $p > .093$).

Table 14: Mean sagittal plane intervertebral orientation in the static neutral position.

	C2-C3	C3-C4	C4-C5	C5-C6	C6-C7
Control	-6.8 ± 4.8	-5.1 ± 7.0	-2.8 ± 5.3	-0.3 ± 7.6	-3.7 ± 6.9
Arthrodesis	N/A	-2.7 ± 6.2	1.7 ± 7.8	-2.8 ± 6.7	-4.1 ± 7.5

Table 15: Total intervertebral flexion-extension range of motion.

	C2-C3	C3-C4	C4-C5	C5-C6	C6-C7
Control	9.7 ± 2.5	14.9 ± 2.8	16.3 ± 2.2	15.3 ± 5.2	12.8 ± 5.2
Arthrodesis	N/A	13.4 ± 3.4	16.4 ± 3.5	2.8 ± 0.7	12.8 ± 4.3

Table 16: Flexion and extension components of total range of motion.

	C2-C3		C3-C4		C4-C5		C5-C6		C6-C7	
	Flexion	Extension	Flexion	Extension	Flexion	Extension	Flexion	Extension	Flexion	Extension
Control	5.1±1.9	-4.6±2.3	7.9±4.2	-7.0±3.5	7.8±2.5	-8.5±3.1	7.1±3.2	-8.2±3.9	7.0±4.6	-5.8±2.5
Arthrodesis	N/A	N/A	6.6±3.2	-6.8±2.3	5.6±3.6	-10.8±3.9	1.8±1.0	-1.0±1.1	5.8±3.4	-7.0±2.5

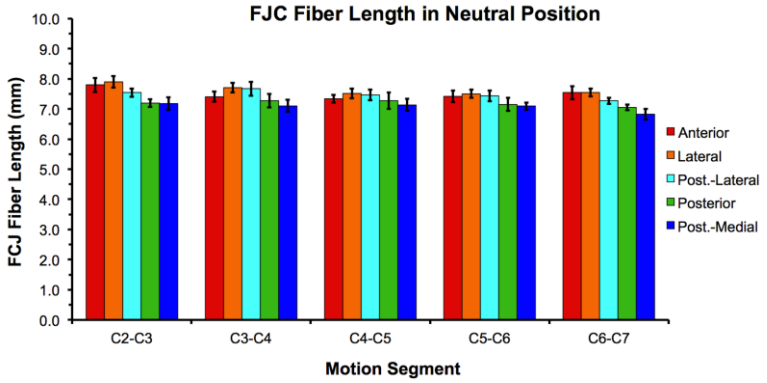

Figure 36: Facet joint capsule fiber length in the static neutral position.

3.2.4 Discussion

The first goal of this study was to determine if facet joint capsule deformation in control subjects varies significantly among motion segments and anatomic regions of the facet joint. The second goal was to assess the effect of single-level anterior arthrodesis on FJC deformation during the flexion-extension motion.

The experimental results indicate that FJC deformation is different among motion segments and among FJC regions during flexion-extension in asymptomatic control subjects. These motion segment-specific and FJC region-specific deformations in controls suggest to the basic scientist that strain data acquired from a single motion segment or from a single region of the FJC is not representative of all motion segments and all regions of the facet joint capsule. The experimental design of *in vitro* research should take these differences into consideration.

Additionally, in this study, control subjects and arthrodesis patients demonstrated different rates of FJC deformation in the extended orientation. This finding suggests that arthrodesis may affect adjacent segment facet joint mechanics.

The current results contradict several previous *in vitro* reports of FCJ strain. Some of these differences may have been associated with the high variability associated with spine mechanical testing (7.1% to 17.9% variability in strain[162] versus 3% to 5% inter-subject variability in the current study). Also, capsular strain distributions have been reported to be "highly non-uniform" across the surface of the facet capsule[156]. In contrast, the current results indicate a highly organized and repeatable pattern of strain distribution among the five capsular regions when in flexion and when in extension. One explanation for these differences may lie in the initial positioning of cadaver specimens prior to loading (the "neutral position"). As the current study demonstrates, the neutral orientation is highly variable *in vivo* (Table 14). It may

not be advantageous to position all specimens in the same "neutral" orientation for *in vitro* testing[156]. Additional explanations for discrepancies between *in vivo* and *in vitro* results include differences in range of motion (e.g. only 2.6°±1.5° ROM in extension at C4-C5 under "physiologic loading"[164]), differences in loading, the age of the participants/specimens, and the techniques used to estimate capsular strain. Overall, the current data indicate that FJC deformations calculated from *in vitro* "physiological loading" experiments differ substantially from *in vivo* results. This also calls into question how well *in vitro* experiments designed to replicate "whiplash loading"[162-164] reflect true *in vivo* facet kinematics during actual whiplash loading.

Considering the well-known changes that occur in the spine with age[49,71,74,153], the FJC deformation results presented for the control group are likely representative only of subjects within their age-range. Also, arthrodesis patient data was collected approximately 7 months post-surgery, and significant changes in adjacent segment FCJ deformation may occur at a later date. An additional limitation is that FJC dimensions were determined from mean values provided in the literature and not on a subject-specific basis. Furthermore, changes in FJC lengths were presented as "deformation", rather than "strain", as the true zero strain length of the fibers is unknown. Finally, the etiology of chronic neck pain following whiplash may be multifactorial[167] and not solely related to FJC kinematics.

Previous reports of *in vivo* spine kinematics have neglected to assess kinematics of the facet joints, instead focusing on the motion between adjacent vertebral bodies. The current study is believed to be the first to characterize the facet joint capsule *in vivo* during dynamic, functional loading. These novel results indicate that in asymptomatic controls, FJC deformation is dependent upon motion segment and upon FJC region. Additionally, single-level arthrodesis

affects adjacent segment FJC deformation, suggesting a potential mechanical etiology for adjacent segment degeneration.

4.0 COMPUTATIONAL MODELING

4.1 INVERSE DYNAMICS

4.1.1 Introduction

The most common surgical treatment for cervical spine disorders is anterior arthrodesis[2], a surgery that involves replacing the degenerated intervertebral disc with a bone graft and attaching a rigid plate to the adjacent vertebrae to help stabilize the joint. It is believed arthrodesis may lead to increased motion in adjacent vertebrae, resulting in overload[10,12,15-17] that leads to degeneration[5-11] and potentially additional surgery[11,45-48]. In an attempt to eliminate or minimize adjacent segment overload, several motion-preserving disc replacement devices have been recently developed[97-100].

The effects of degeneration and surgery on cervical spine mechanics are commonly evaluated through in vitro testing[12,68-70,81,82] and finite element models derived from in vitro tests[83-87]. Due to the fact that cervical spine specimens will buckle under a compressive load of approximately 10 N[168], in vitro test protocols often apply only a moment to the specimen to simulate in vivo kinematics[85,90,169]. However, pure-moment loading methods do not replicate the physiological response and are poorly suited for evaluating certain surgical procedures and instrumentation[88]. More recently, "follower load" protocols have been developed to increase the

compressive force applied to spine and avoid bucking[87,170,171]. However, it is not clear how well these protocols replicate in vivo dynamic, functional loading.

An estimate of cervical spine loading may be obtained through inverse dynamics models. Previous inverse dynamics models of the cervical spine have primarily focused on the response of the head and neck to impacts[172-175]. The biofidelity of these models may be increased by including muscular activation in the model[176]. However, it is difficult to accurately and reliably obtain muscular activation parameters for deep neck muscles during dynamic movement[177].

The objectives of the current study were to estimate the load applied to the C2 vertebra during in vivo functional flexion-extension and to evaluate the effects of anterior cervical arthrodesis on spine loads. The load applied to the superior cervical spine (C2) was estimated using subject-specific kinematic motion data obtained from conventional motion analysis (for head motion) and biplane radiography (for vertebral motion), in combination with muscular attachment and maximal muscle force parameters obtained from the literature. The first hypothesis tested was that spinal loads would not be significantly different in asymptomatic control subjects and single-level anterior arthrodesis patients. The second hypothesis tested was that the load applied to C2 would change significantly throughout the range of head flexion-extension.

4.1.2 Materials and Methods

Following Institutional Review Board (IRB) approval, data were analyzed from 6 single-level anterior arthrodesis patients (average age: 43.2 ± 8.8 yrs; 2 M, 4 F; 3 C56 arthrodesis, 3 C67 arthrodesis; 7.0 ± 0.6 mo. post-surgery) and 10 asymptomatic control subjects of similar age

(average age: 44.7 ± 6.6 yrs; 3 M, 7 F) who provided informed consent to participate in this research study. High-resolution CT scans (0.29x0.29x1.25 mm voxels) of the cervical spine (C2-C7) were acquired on each participant (GE Lightspeed 16, GE Medical Systems, Waukesha, WI). Bone tissue was segmented from the CT volume using a combination of commercial software (Mimics software, Materialise, Leuven, Belgium) and manual segmentation[53]. A three-dimensional (3D) model of each vertebra was generated from the segmented bone tissue. Three-dimensional male and female skull models were generated using male and female data from the Visible Human dataset[178] and scaled for each subject according to subject-specific anterior to posterior skull dimensions obtained from the sagittal scout view prior to the CT scan.

Participants were seated within a biplane X-ray system (Figure 1) and, for each trial, directed to continuously move their head and neck through their entire range of flexion-extension. A metronome set at 40 to 44 beats per minute ensured the participants moved at a continuous, steady pace to complete each full movement cycle in 3 seconds or less. Biplane radiographs were collected simultaneously, at 30 frames per second for 3 seconds, as the subject performed continuous flexion-extension. Radiographs were recorded for 2 or 3 separate trials for each subject (allowing for a rest period between trials), resulting in a total of 42 movement trials analyzed for this study (25 control trials and 17 arthrodesis trials). A trial with the subject stationary, looking forward with the head in the neutral position, was also collected for each participant. Reflective markers were placed on the head and torso to determine head motion using conventional motion analysis techniques (sample rate 60 Hz; Vicon-MX, Oxford, UK).

A previously validated volumetric model-based tracking process determined three-dimensional vertebral position with sub-millimeter accuracy[55] for all static and dynamic trials. Details describing the tracking process, including hardware and software specifications,

calibration and distortion correction procedures, and computational algorithms have been described previously[55-58]. Three-dimensional bone positions and reflective marker data were filtered at 1.0 Hz and 10.0 Hz, respectively, using a fourth-order, low-pass Butterworth filter with the filter frequency determined using residual analysis[59]. A calibration object containing radiopaque and reflective markers was used to co-register tracked vertebrae and head motion.

The skull orientation relative to the head reflective markers was determined from the static neutral trial by manually aligning the foramen magnum to the spinal canal. Correct alignment between the skull and C2 was verified using three-dimensional animations of the flexion-extension movement. For each trial, it was visually confirmed that the foramen magnum remained aligned with the spinal canal passing through C2 as the skull and cervical spine moved through the entire range of flexion-extension.

The musculoskeletal model included three flexor muscles that were active only when the head was in an extended orientation relative to the neutral position (sternocleidomastoid (SCM), longus capitis (LGC), infrahyoid), and four extensor muscles that were active only when the head was in a flexed orientation relative to the neutral position (trapezius (Trap), splenius capitis (SPL), semispinalis capitis (SSP) and rectus capitis posterior major (RCP)). Attachment sites[179-181] and maximal force output[179,181] for each muscle were obtained from the literature (Table 17). The longus capitis muscle was required to wrap around C2 and C3 when the vector from its origin to insertion intersected these bones, while all other muscles were modeled using straight line paths. The infrahyoid attachment was defined as 35 mm anterior and 3 mm inferior to the C3 vertebra[182], and its location remained constant relative to C3[183]. Muscle insertion sites were identified on the 3D skull models (and therefore did not vary among males nor among females, although they were scaled along with the size of the skull), while muscle origin sites were

determined from subject-specific reflective marker data (in the case of trapezius, infrahyoid and sternocleidomastoid) and subject-specific vertebral anatomy (for the remaining four muscles) (Figure 37). Head mass (male = 4.2 kg; female = 3.4 kg), center of mass (59 mm superior and 18 mm anterior to the occipital condyle) and moment of inertia about the skull anatomical axes values were obtained from the literature[169].

Table 17: Muscle attachments and peak forces.

Muscle	Origin	Insertion	Peak Force (N)
Sternocleidomastoid	Sternum	Mastoid process	344
Longus Capitis	C4 anterior tubercle	Basilar part of occipital bone	96
Infrahyoid (Omohyoid, Sternohyoid, Sternothyroid)	Sternum	Hyoid bone	138
Trapezius	Clavicle	Superior nuchal line of occipital bone	264
Splenius Capitis	C7 spineous process	Mastoid process of temporal bone/superior nuchal line of occipital bone	216
Semispinalis Capitis	C6 articular process	Between superior and inferior nuchal line of occipital bone	386
Rectus Capitis Posterior Major	C2 spineous process	Anterior to inferior nuchal line of occipital bone	181

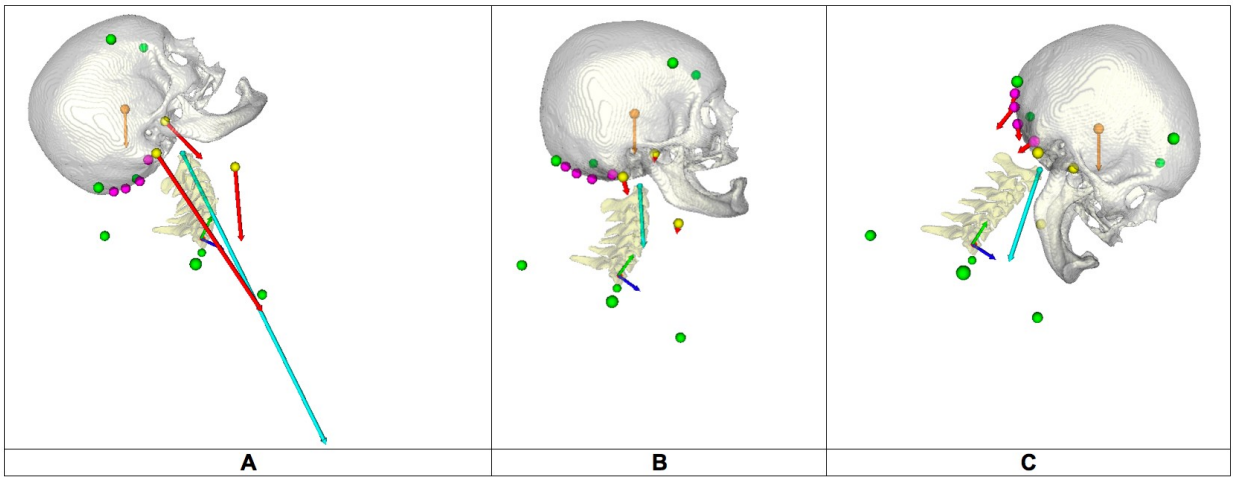

Figure 37: The skull and cervical spine model in an extended orientation (A), in the neutral position (B), and in a flexed orientation (C).

Two assumptions were made to determine the force applied by the skull on C2. The first was to require equal activation in all active muscles (i.e. the same percentage of maximum muscle force). Second, zero co-contraction was assumed in antagonistic muscles. With these assumptions in place, the force applied by the skull on C2 was determined by solving the equations of dynamic equilibrium as follows: The midpoint of the superior facets on C2 was used to represent the single point on C2 where the head applied force to the cervical spine. The muscle moment arms for each frame of data were determined for each muscle given the head, torso and spine position obtained from the tracked reflective and radiographic data. This was accomplished by calculating the perpendicular distance from the midpoint of the C2 superior facets to the line of action of the muscle. The maximum torque that could be generated (T_{max}) was then determined using the muscle moment arms and corresponding maximal muscle forces (Table 17). Next, the torque required by the muscles to counter the torque generated by the skull

angular acceleration and the weight of the head was determined: $\sum T_m = I_{skull_{C2PT}} \cdot \alpha_{skull} - T_{WH}$, where T_m is the total muscle torque, $I_{skull_{C2PT}}$ is the moment of inertia of the skull about the midpoint of the superior facets on C2, α_{skull} is the angular acceleration of the skull (obtained from head reflective markers) and T_{WH} is the torque due to the weight of the head. The torque required by the muscles was expressed as a percentage of maximum torque: $T_{Percent} = \frac{\sum T_m}{T_{\max}}$. The magnitude of each muscle force was then calculated by multiplying each maximum muscle force by $T_{Percent}$. The components of each muscle force were calculated from the muscle magnitudes and lines of action (from muscle attachments). Then the total force applied to C2 was calculated: $F_{C2} = m_H a_H - F_{WH} - \sum F_m$ where F_{C2} was the force applied to C2, $m_H a_H$ was the mass and acceleration of the head, F_{WH} was the force due to the weight of the head, and $\sum F_m$ was the sum of the muscle forces. Two-dimensional motion was assumed and muscular attachment sites and activation levels were assumed to be symmetric about the sagittal plane.

Cervical spine kinetics were characterized by the following parameters: the total force applied to C2 due to muscular and inertial forces, and the moment arm of each muscle throughout the range of flexion-extension.

Head flexion-extension angle, normalized to the static neutral trial, was calculated for each tracked data frame and interpolated at 1º intervals for each trial. Forces and moment arm values that were calculated at each tracked radiographic frame were then interpolated to correspond to each 1º increment in head flexion-extension angle. Multiple trials from the same subject were averaged to yield a single average dataset for each subject used for statistical analysis.

Statistical analysis was carried out using data corresponding to 10º increments in head flexion-extension, from 40º of extension (-40º) to 40º of flexion. An independent-samples t-test was used to test for differences between asymptomatic and arthrodesis groups in the total force applied to C2. A paired-samples t-test was used to identify differences in the force applied to C2 at identical angles of head flexion-extension during the flexion and extension movement directions. Repeated measures analysis of variance was used to identify significant differences in muscle moment arms at each 10º increment of head flexion-extension. Significance was set at $p < .05$ for all tests. P-values were adjusted for multiple comparisons using the False Discovery Rate[64].

The sensitivity of the model to muscle attachment sites was evaluated by adjusting the SCM and SSP attachments to the skull and the infrahyoid attachment to the hyoid by ±8 mm, ±4 mm, ±2 mm and ±1 mm in the anterior (+) and posterior (-) directions of the skull coordinate system. The model was run with each of these independently altered attachment sites for the SCM, SSP and infrahyoid. The percent change in total force applied to C2 was calculated for each altered attachment site at 10º increments of head flexion-extension.

4.1.3 Results

4.1.3.1 Total Force Applied to C2

The total force applied to C2 was not different between asymptomatic and arthrodesis groups at any 10º interval of head flexion-extension, from 40º of extension to 40º of flexion (average absolute difference: 8.2 N; range of differences between groups: -32 N to +21 N; all p-values ≥ 0.937). Therefore, data from asymptomatic and arthrodesis subjects were combined to determine if the force applied to C2 differed during the flexion and extension movements.

The total force applied to C2 followed a consistent pattern within subjects. In the flexed orientation (relative to the static neutral position), the force applied to C2 was slightly higher when the head was moving in the direction of flexion than in the direction of extension. When the head was in an extended orientation, the force applied to C2 was higher when the head was moving in the direction of extension. These differences in total force applied to C2 during the flexion and extension motions were statistically significant at all head orientations except for the neutral position (Figure 38). The average within-subject trial-to-trial variability (i.e. standard deviation) in the total force applied to C2 averaged 8.6% of the total force applied to C2 over the range of motion from 40º of extension to 40º of flexion.

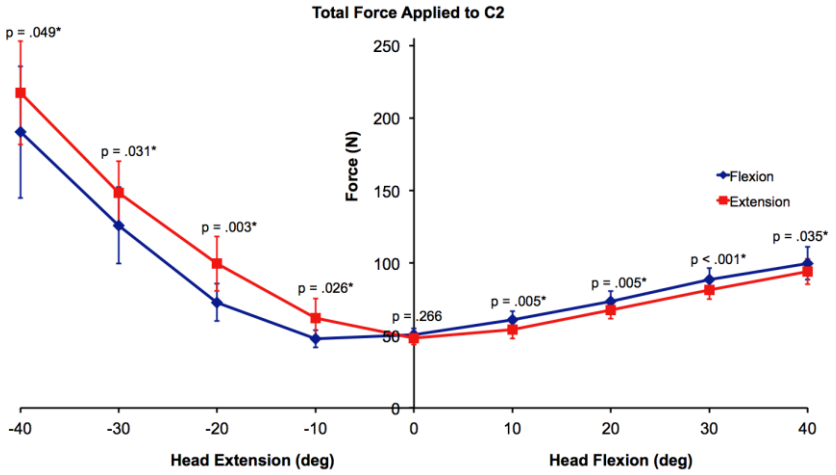

Figure 38: The total force made by the skull on C2 as the head moved in flexion (blue) and extension (red).

4.1.3.2 Flexor Muscle Moment Arms

Flexor muscle moment arms were not significantly different between asymptomatic and arthrodesis groups at any 10º increment of head extension from neutral to 40º extension (SCM: average absolute difference between groups: 1.3 mm, range of differences between groups: 0.2

mm to 2.2 mm, all $p \geq .850$; LGC: average absolute difference between groups: 0.6 mm, range of differences between groups: -0.5 mm to 0.9 mm, all $p \geq .828$; infrahyoid: average absolute difference between groups: 5.9 mm, range of differences between groups: 2.9 mm to 9.5 mm, all $p \geq .197$). Therefore, asymptomatic and arthrodesis subjects were grouped for further statistical analysis.

Flexor muscle moment arms were consistently greater when the head was moving in flexion versus extension (Figure 39). These differences in muscle moment arms when moving in flexion versus extension were significant at each 10º increment of head motion for the LGC and infrahyoid muscles (all $p \leq .003$ and all $p \leq .002$, respectively), but only at 0°, 10° and 20° of extension for the SCM moment arm ($p \leq .033$) (Fig. 39).

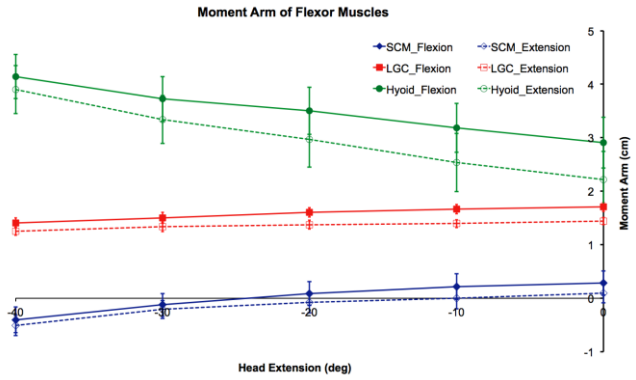

Figure 39: Flexor muscle moment arms during flexion and extension.

The SCM moment arm changed significantly each 10º of head flexion-extension from neutral to 40º of extension (all $p \leq .020$). On average, the sternocleidomastoid muscle functioned as a head flexor when the head was within 25º of the neutral position, and as the head orientation progressed beyond 25º of extension, the sternocleidomastoid muscle began to function as a head extensor. The LGC moment arm significantly decreased each 10º of head flexion-extension

from neutral to 40º of extension (all $p \leq .001$), while the infrahyoid moment arm significantly increased each 10º of head flexion-extension from neutral to 40º of extension (all $p \leq .001$) (Fig. 39).

4.1.3.3 Extensor Muscle Moment Arms

Extensor muscle moment arms were not significantly different between asymptomatic and arthrodesis groups at any 10º increment of head flexion from neutral to 40º flexion (Trap: average absolute difference between groups: 1.8 mm, range of differences between groups: 0.8 mm to 3.5 mm, all $p \geq .832$; SPL: average absolute difference between groups: 3.2 mm, range of differences between groups: -4.2 mm to -2.2 mm, all $p \geq .373$; SSP: average absolute difference between groups: 0.5 mm, range of differences between groups: -0.9 mm to 0.8 mm, all $p \geq .875$; RCP: average absolute difference between groups: 0.4 mm, range of differences between groups: -1.1 mm to 0.0 mm, all $p \geq .961$). Therefore, asymptomatic and arthrodesis subjects were grouped for further statistical analysis.

Trapezius, splenius capitis and semispinalis muscle moment arms significantly increased at each successive 10º increment of head motion when the head was moving in extension (all $p \leq .001$ for trapezius and semispinalis, all $p \leq .002$ for splenius capitis) (Figure 40). The rectus capitis posterior muscle moment arm was significantly greater when the head was moving in extension from 10º to 40º of head flexion (all $p \leq .022$).

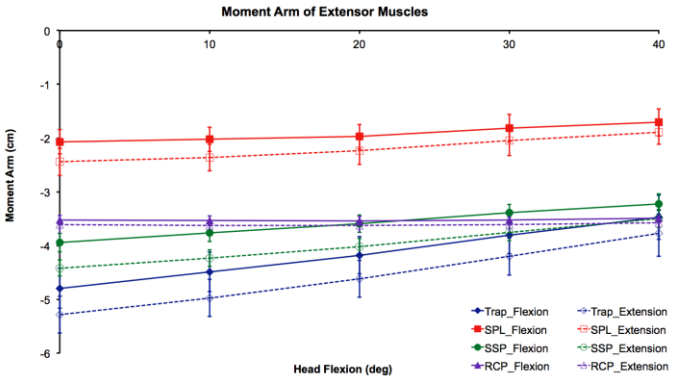

Figure 40: Extensor muscle moment arms during flexion and extension.

Trapezius and splenius moment arms decreased significantly each 10º of head flexion from neutral to 40º of flexion (all $p \leq .016$ and all $p \leq .038$, respectively). Similarly, the semispinalis moment arm decreased significantly each 10º of head flexion from neutral to 30º of flexion (all $p \leq .015$). The rectus capitis posterior major moment arm significantly decreased from 30º to 40º of head flexion ($p = .019$) (Figure 40).

4.1.3.4 Sensitivity Analysis

The model was relatively insensitive to changes in the semispinalis attachment location. The maximum change in total force applied to C2 was less than 5%, and occurred at 40º of flexion with a +8 mm adjustment to the semispinalis attachment site. The model was more sensitive to changes in the infrahyoid attachment site, estimating up to a 24% increase in the total force applied to C2 when the head was at 40º of extension. The model was most sensitive to changes in the sternocleidomastoid attachment site, estimating a 59% increase in the total force applied to C2 with a -8 mm adjustment to the sternocleidomastoid attachment site and the head at 40º of extension (Figure 41).

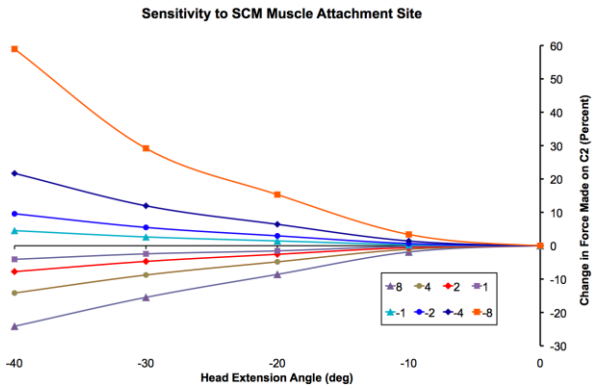

Figure 41: Sensitivity of the model to changes in the sternocleidomastoid attachment site on the skull.

4.1.4 Discussion

The current in vivo data indicate that inertial and muscular forces combine to exert force on the upper cervical spine in a predictable pattern related to head orientation during flexion-extension. The model estimated the force applied by the head to C2 is smallest in the neutral position and increased slowly with head flexion and increased rapidly with head extension. The statistically significant differences in force applied to C2 at corresponding head angles when moving in flexion and in extension have not been reported or discussed previously. The differences in force stem from differences in muscle moment arms in flexion and extension for identical head angles (Figure 39 and Figure 40). As we have reported previously, during flexion-extension, the head leads the motion and the vertebrae follow the head[184]. Therefore, the spine orientation relative to the head is not identical when moving in flexion and in extension for any given head angle. From this, it follows that the muscle moment arms are different when moving in flexion and in extension for any given head angle.

The present model suggests the force applied to the top of C2 reaches maximum values of approximately 200 N (or about 5 times head weight) at 40º of head extension and 100 N (or about 2.5 times head weight) at 40º of head flexion. In comparison, the literature contains wide-ranging estimates of cervical spine loads. It has been suggested that the compressive force applied to the cervical spine approaches three times the weight of the head (approximately 120 N) due to muscle co-activation forces balancing the head in the neutral, relaxed posture, and that minimal to moderate isometric muscle effort increases this compressive force to 250 N, however, no experimental or modeling data were provided to support this assertion[170]. A previous computational model predicted cervical spine forces from isometric contraction data and suggested that the compressive load is estimated to reach 1200N in activities involving maximal isometric muscle efforts[176]. In agreement with the current results, this previous model estimated the compressive force at C2 in the neutral position, due to forces from muscles attached to the skull and head weight totaled approximately 53 N[176]. The current results are also in agreement with Hattori who measured in vivo disc pressure in various head orientations and found the highest disc pressure in extension (approximately equivalent to a compression force of 155 N) and lowest disc pressure in the neutral position (approximately equivalent to a compression force of 63 N)[87,170,185].

The change in the force applied to C2 that occurred with head flexion-extension and the differences in force applied to C2 with movement direction suggest that cervical spine testing protocols that apply a constant follower load to the specimen may not accurately represent in vivo kinetics. It is possible the biofidelity of in vitro tests may be improved by reproducing the shape of the force curves presented in Figure 38.

The current study is believed to be the first to estimate changes in muscle moment arm during active in vivo flexion-extension. The results indicate that muscle moment arms change significantly during flexion-extension, and the magnitude of muscle moment arms are significantly different during flexion and extension movements. These results suggest computational models of spine loading should account for head orientation and direction of movement when determining moment arms for muscles attached to the skull. This in vivo data confirms a previous computational model that concluded that variations in muscle moment arms throughout the range of motion can alter muscle moment-generating capacities[186]. The moment arms of the muscles attached to the hyoid appear to be the most dependent on head flexion angle. The importance of including muscles attached to the hyoid in cervical spine models has been noted previously[177,179,181]. Results from the current study suggest the infrahyoid muscles may be particularly important when the head approaches full extension, as this is the orientation in which infrahyoid moment arm is largest (thus permitting the generation of a large flexor moment) and simultaneously the sternocleidomastoid muscles are exerting an extensor moment about the upper cervical spine. This interpretation of the results suggests that when the head is near full extension, the required flexion torque may be generated, and forces on the cervical spine minimized, if sternocleidomastoid activation is decreased and infrahyoid activation is increased. There are currently no in vivo data to suggest infrahyoid muscles increase their activation and sternocleidomastoid muscles decrease activation in order to minimize forces on the spine at large head extension angles.

The muscle moment arms determined in the current study, calculated geometrically (perpendicular distance method), are in general agreement with a recent cadaver-based study of neck muscle moment arms at C0-C1 measured by the tendon excursion method (SCM: 0.1 cm;

Trap: 4.6 cm; SPL: 1.3 cm; SSP: 4.9 cm; RCP: 1.9 cm)[180]). A previous computational model of the neck included some muscle moment arms in the neutral position that were in agreement with values determined in the current study (SCM: 1 cm; LCG: 1 cm; Trap 5 cm) and some muscle moment arms that were substantially larger than in the current study (SPL: 5 cm; SSP: 6.2 cm)[186]. The current study, in agreement with previous cadaveric studies[180,181], indicates that the sternocleidomastoid acts as a head flexor and extensor.

One simplifying assumption of the model was that each muscle attachment site could be represented by a single point. The model sensitivity to the location of this point varied by muscle (low sensitivity to SSP attachment site, high sensitivity to SCM attachment site), head flexion-extension angle (sensitivity increased as the head moved from the neutral position) and distance from the original attachment site (the model was relatively insensitive to moving the muscle attachment 4 mm or less from the original position, but highly sensitive to an 8 mm change in muscle attachment site). These results suggest that if subject-specific attachment sites are included in the model (perhaps from MRI images), the model results will be substantially affected by errors in muscle attachment site in excess of ±4 mm. The sensitivity analysis of the hyoid and sternocleidomastoid are particularly informative, as they indicate model sensitivity to hyoid kinematics (the hyoid was assumed fixed relative to C3) and model sensitivity to the broad attachment between the sternocleidomastoid and the skull.

As with any computational model, there are assumptions and limitations associated with the model and results. The muscles that were selected for inclusion in the model have been established as the major force generating muscles responsible for flexion-extension of the skull[177,179,181]. However, the muscle models do not include characteristics such as the force-length-velocity relationship, active and passive stiffness parameters, muscle fiber length and

pennation angle. While these muscle parameters could be included in future model development, it is not clear that a more complex model would yield additional functional or clinically significant information. The assumption that co-contraction is minimal in the neck muscles has been supported by EMG data[177] and this assumption has been made previously[176]. It is extremely difficult to acquire muscle activation patterns (let alone muscle force estimates) from deep muscles of the neck. Therefore, there are no reliable data available to provide a basis for the magnitude and timing of muscle co-contraction during dynamic, functional movement. Previous fine-wire EMG data for the anterior neck muscles[177] support the common modeling assumption of uniform activation used in the current model. The relatively small sample size limited the power of the study to detect significant differences between groups if they did, in fact, exist. An additional limitation is that the current study only estimated forces applied to the C2 vertebra. Forces applied to inferior vertebrae are affected by muscles that attach these vertebrae to more inferior bones. More accurate estimates of the effects of arthrodesis on tissue-level cervical disc mechanics may be determined by increasing the complexity of the model by adding muscles that attach the vertebrae to the torso. Additionally, subject-specific finite element models that are subjected to loads that change in magnitude as the head moves through flexion-extension may reveal important tissue-level differences between asymptomatic and arthrodesis patients.

4.2 FINITE ELEMENT MODEL

4.2.1 Introduction

Mechanical loading of the spine is one of the primary factors believed to influence intervertebral disc health [187,188]. Due to ethical and technical limitations, our knowledge of intervertebral in vivo disc loading is extremely limited [185,189,190]. Consequently, finite element models, based on cadaveric specimens, have been created to estimate disc loads [191,192].

A limitation of the traditional finite element model development and validation paradigm is that it is not clear how well in vitro loading conditions replicate in vivo dynamic, functional loading. For example, under axial compression, the cervical spine specimens buckle under as little as 10 N of compression load [168]. Therefore, in vitro tests used to validate cervical spine finite element models are often performed by applying pure bending moments to load spine specimens [85]. Using the "follower load" technique, compressive loads of up to 250 N may be applied to the cervical spine during mechanical loading tests [170]. Still, it is not clear how well these loading paradigms replicate in vivo loading. There is no consensus in the literature regarding the magnitude of in vivo loads on the spine, with cervical spine loading estimates ranging from 120 N to 1200 N [170,176,193]. The inability to estimate in vivo loads applied to the

cervical spine is a critical limitation to estimating intervertebral disc stresses during functional loading.

Subject-specific validation is essential to developing accurate computational models of the cervical spine. The high inter-subject variability in cervical kinematics has been well documented [22,23,27,78,194] and suggests that validating the kinematic output of a single model with group means [84,195,196] may be inappropriate.

The aim of the current study was to develop and demonstrate a novel computational modeling approach to estimate the in vivo load applied to a cervical motion segment during flexion-extension. In this technique, highly accurate kinematic data obtained from a biplane radiography system was used as the validation criteria. A sensitivity analysis was performed to determine the kinematic response of the computational model to material properties and applied loads. An optimization process, applied to the finite element model, was then implemented to determine the applied load necessary to replicate the in vivo kinematics. The change in disc stress during the in vivo flexion-extension movement was then determined.

4.2.2 Materials and Methods

4.2.2.1 In Vivo Data

The kinematic and anatomic data for this study was obtained from a 39 year-old female who consented to serve as a healthy control in an IRB-approved protocol to assess the effects of single-level anterior fusion on cervical spine kinematics. Details on the collection and processing of biplane radiographs for this study have been provided previously [197]. To summarize, the participant was seated within a biplane X-ray system and radiographs were collected with the head in the static neutral position. Next, the participant was directed to

continuously move her head and neck through its entire range of flexion-extension. Radiographs were collected at 30 images per second for 3 seconds of continuous flexion-extension. A high-resolution CT scan (0.29x0.29x1.25 mm voxels) of the cervical spine (C2-C7) was acquired (GE Lightspeed 16, GE Medical Systems, Waukesha, WI). A three-dimensional (3D) model of each vertebra was generated from the segmented bone tissue. In vivo bone motion of C2 through C7 vertebrae was tracked in each pair of radiographs using a previously validated volumetric model-based tracking technique with sub-millimeter accuracy [55]. Six degree-of-freedom (DOF) intervertebral translations and rotations were determined for the static trial and during the flexion-extension movement. These intervertebral translations and rotations, recorded in vivo during dynamic, functional loading, served as the "gold standard" criteria for the optimization process described below.

4.2.2.2 Finite Element Model

The computational model consisted of the C5 and C6 vertebrae, cartilage endplates, the intervertebral disc (annulus, lamella, and nucleus), facet cartilage, and ligaments (anterior longitudinal ligament (ALL), posterior longitudinal ligament (PLL), ligamentum flavum (LF), interspinous ligament (ISL) and capsular ligaments (CL)). TrueGrid was used to create 8-noded hexahedral elements for the bones, endplates, cartilage and intervertebral disc. The vertebrae were modeled as rigid bodies, with the C6 vertebrae fixed in place. Material properties for the disc and cartilage were assigned according to the literature (Table 18). Lamellae were modeled using five concentric rings of tension-only rebar, with their orientation alternating between adjacent rings from +30° to -30°. Articular cartilage was modeled using a three-element thick cartilage model, with thickness ranging from 0.5 mm to 1.0 mm from the edges to the center of

the facet, respectively [198]. Ligaments were modeled as tension-only springs, with resting lengths [199] and stiffness values [200] obtained from the literature. Force applied to the model was distributed over the top surface of the C5 vertebral body.

Table 18: Material properties used in the finite element model.

Tissue	Properties
Cartilage Endplates	E = 600 MPa; *v = 0.35*
Disc Annulus	E = 4.0 MPa; *v = 0.4*
Disc Lamella	Tension only rebar E = 300 MPa; *v = 0.3*
Disc Nucleus	E = 1.5 MPa; *v = 0.499*
Facet Cartilage	E = 10.4 MPa; *v = 0.4*
Anterior Longitudinal Ligament (ALL)	17.9 N/mm
Posterior Longitudinal Ligament (PLL)	23.0 N/mm
Ligamentum Flavum (LF)	21.6 N/mm
Interspinous Ligament (ISL)	6.36 N/mm
Capsular Ligament (CL)	36.9 N/mm

Custom software was used to interactively place 8 fiducial markers on each vertebral body to define anatomic coordin8ate systems used to calculate intervertebral translation and rotation. The location of these 8 fiducial markers, and the anatomic coordinate systems created from them, were identical in the in vivo kinematic data and the computational model run in Abaqus.

4.2.2.3 Convergence Study

A convergence study was performed on the vertebral body-disc-vertebral body portion of the model to assess the effect of mesh resolution on model predictions. Sufficient resolution was attained when the evaluation criteria (in this case kinematic response and regional disc stress) changed by less than 5% [201] as mesh resolution of the intervertebral disc increased (96, 864, 1800 and 4164 elements). Nine separate forces were applied to the superior endplate of C5 as part of the convergence study: 3 magnitudes (22.5 N, 45 N and 76.5 N) of an anterior-compressive force

(+45° from vertical), 4 magnitudes (45 N, 90 N, 135N and 180 N) of a purely compressive force (0° from vertical), and 2 magnitudes (22.5 N, 45 N) of posterior-compressive force (-45° from vertical). These force magnitudes were selected based on typical head weight of approximately 45 N [169]. The parameters evaluated in the convergence study included the anterior-posterior and inferior-superior translations, the flexion-extension rotation, and the regional disc stress (average von Mises stress) within the anterior annulus, posterior annulus, posterior-lateral annulus and nucleus (average pressure).

4.2.2.4 Sensitivity Analysis

A sensitivity analysis was performed on the finite element model of the complete motion segment after adding posterior bone elements (facets, lamina, spinous process), facet cartilage, and all ligaments to the bone-disc bone model used in the convergence study. The sensitivity analysis was designed to assess sensitivity of the model to material properties (modulus for disc and cartilage, and stiffness for ligaments) and applied load (magnitude and direction). The motion segment was oriented in the static neutral position for this subject (7.1° of extension), and material properties were assigned values within the range commonly reported in the literature (Table 18) to create a "base" model. Two load values were applied independently to the model: an anterior-compressive load of 90 N (+45° from the vertical) and a posterior-compressive load of 90 N (-45° from the vertical). Each material property and load (both magnitude and direction) was systematically adjusted from the base model value by ±10% and ±25% (load directions were varied by ±4.5° and ±11.25°, corresponding to 10% and 25% changes in load direction). Model sensitivity was assessed by calculating the change in anterior-posterior translation and flexion-

extension rotation relative to the base model for the anterior-compressive and posterior-compressive loads.

4.2.2.5 Optimization

The finite element analysis was iteratively run within a genetic algorithm optimization routine in Matlab. The optimized parameters were the three components of the total force applied to the C5 vertebra (Fx_{lab}, Fy_{lab} and Fz_{lab}). After each iteration of the optimization routine, the kinematic output of the model (relative rotations and translations between bones) was calculated by a Python program that read fiducial landmark locations from the Abaqus output file. The optimization function (equation 1) weighted errors in translation (in mm) by a factor of 4 in comparison to errors in rotation (in degrees) in agreement with our previous in vivo validation study results [55]. Considering the primary motions were flexion-extension rotation and anterior-posterior translation, errors in these components were weighted by an additional factor of 2.

$$Total\ Error = 2 \times flexion\_extension\_error + bend\_error + twist\_error + 8 \times anterior\_posterior\_error + 4 \times medial\_lateral\_error + 4 \times superior\_inferior\_error$$

Each kinematic error value was the squared difference between the Abaqus output and the tracked in vivo data.

The in vivo kinematic data for the C5-C6 motion segment included in the optimization process covered a range of motion of 20.3° in flexion-extension, 4.5° mm in anterior-posterior translation, and small out-of-plane motions (Figure 42).

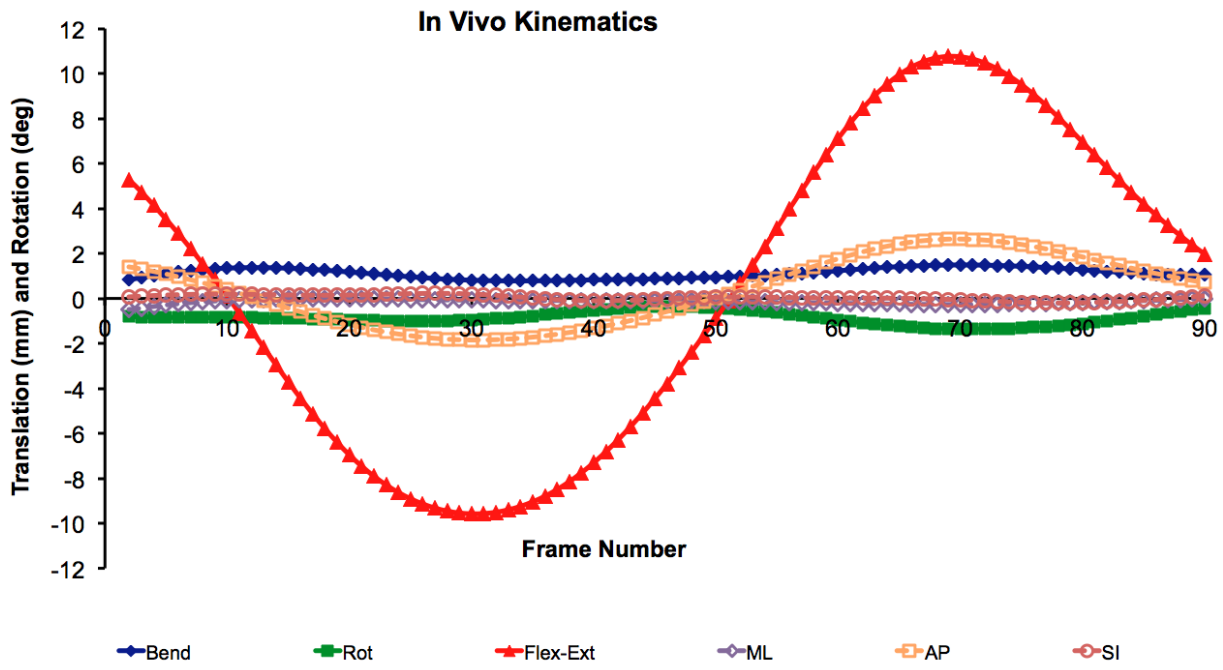

Figure 42: The in vivo 6 DOF kinematics of the C5C6 motion segment.

The genetic algorithm is a stochastic, heuristic algorithm. The ability of the algorithm to correctly converge on a known solution was assessed by applying known forces to the C5 vertebra and running the model in Abaqus. The kinematic output of this model was calculated and used as a reference criterion to assess the precision of the optimization process. The model was then run through the optimizing algorithm, with unknown forces but known criteria kinematics. The force output of this optimization process was compared to the known forces applied initially. This process was repeated three times to assess precision of the algorithm in arriving at the correct solution under various combinations of flexion, extension, compression and distraction forces.

The genetic algorithm was run with 50 individuals in the initial population, and stopping criteria of 25 generations, 3 stall generations, or a change in the minimum error of less than 0.001 over three generations. Lower and upper bounds for the lab-based x, y, and z-components of the force applied to C5 (which roughly corresponded to the anterior-posterior, medial-lateral

and superior-inferior directions) were ±12 N, ±6 N and ±12 N, with the initial guess provided by the optimized solution of the previous frame. Forces applied to C5, based in the laboratory coordinate system, were transformed into the anatomic coordinate system of C5 for analysis. Model validity was assessed by comparing 6 DOF kinematics recorded in vivo to the 6 DOF kinematics output by the model. Average von Mises stress (relative to the static neutral stress) within the anterior annulus, posterior annulus, posterior-lateral annulus, and pressure within the nucleus (relative to the static neutral pressure) was calculated for each frame of the analyzed movement.

4.2.3 Results

4.2.3.1 Convergence Study

Kinematic results were not affected by increasing resolution beyond 864 elements in the disc (Figure 43). Disc stress results were not affected by increasing disc resolution beyond 1800 elements (Figure 43). Therefore, all subsequent disc models included at least 1800 elements.

Kinematics

Resolution Comparison	% Change in SI Translation	% Change in AP Translation	% Change in Flexion-Extension
1 vs. 2	-7.4%	-24.3%	-30.0%
2 vs. 3	1.6%	3.8%	2.4%

Average Stress

Resolution Comparison	% Change in Anterior Annulus	% Change in Posterior Annulus	% Change in Post-Lat Annulus	% Change in Nucleus Pressure
2 vs. 3	2.7%	2.7%	6.5%	-3.4%
3 vs. 4	-3.2%	-2.3%	-4.4%	-1.8%

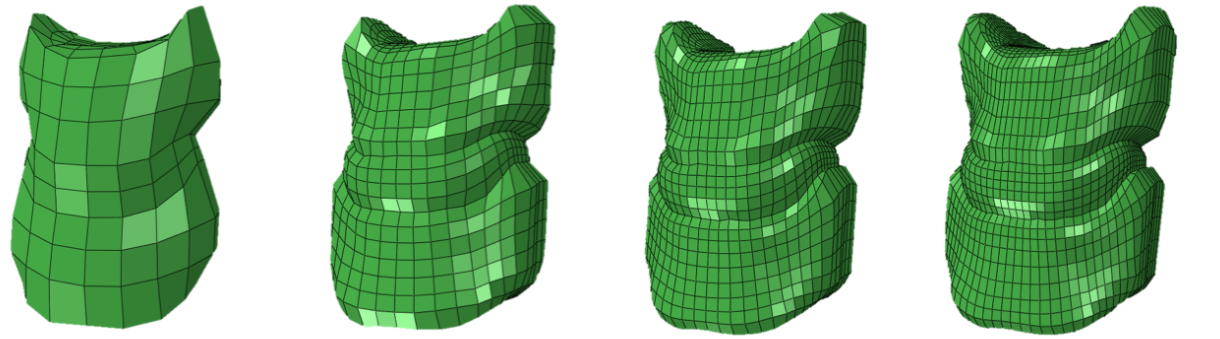

#1 (96 element disc) #2 (864 element disc) #3 (1800 element disc) #4 (4164 element disc)

Figure 43: Model convergence results.

4.2.3.2 Sensitivity Analysis

When anterior-compressive and posterior-compressive loads were applied to the model, the kinematic output was most sensitive to load magnitude and load direction, and to a lesser extent, annulus modulus (Figure 44). After observing that the model was highly sensitive to load magnitude and load direction, these variables were selected as inputs to the optimization algorithm.

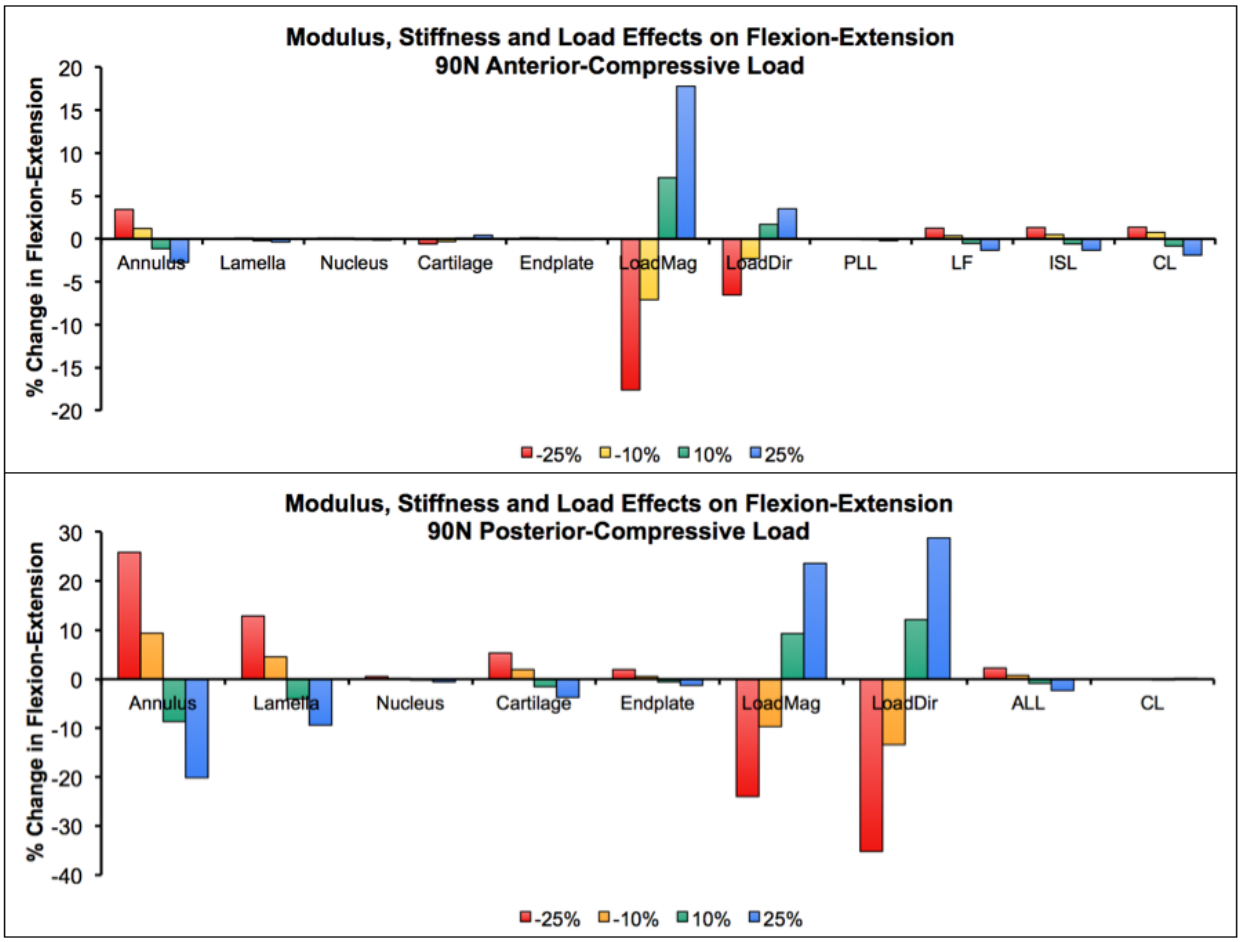

Figure 44: Sensitivity results.

4.2.3.3 Optimization

For a series of known solutions, the genetic algorithm estimated the total force and each component of the known force within 2.2 N, on average. The average difference between the estimated and know force direction was 4.1° (Table 19).

Table 19: Comparison between known forces and forces determined from the optimization process.

Known Applied Force (N)	Estimated Force (N)	Difference in Force Magnitude (N)	Difference in Angle (deg)
F = (6.72, 44.25, 35.67)	F = (5.72, 44.31, 35.64)	-0.08 N	1.0°
F = (7.14, -28.17, -29.06)	F = (3.41, -23.14, -27.73)	-4.82 N	6.3°
F = (-2.05, 31.04, 64.07)	F = (-6.36, 26.31, 63.89)	-1.84 N	5.0°

The absolute value of the difference between the in vivo kinematics and the kinematics output by the optimization process averaged 0.15°, 0.05°, 0.20° for flexion-extension, bend, and twist rotations, respectively, and 0.16 mm, 0.13 mm, 0.12 mm for anterior-posterior, medial-lateral and superior-inferior translation, respectively, over all analyzed frames of movement (Figure 45).

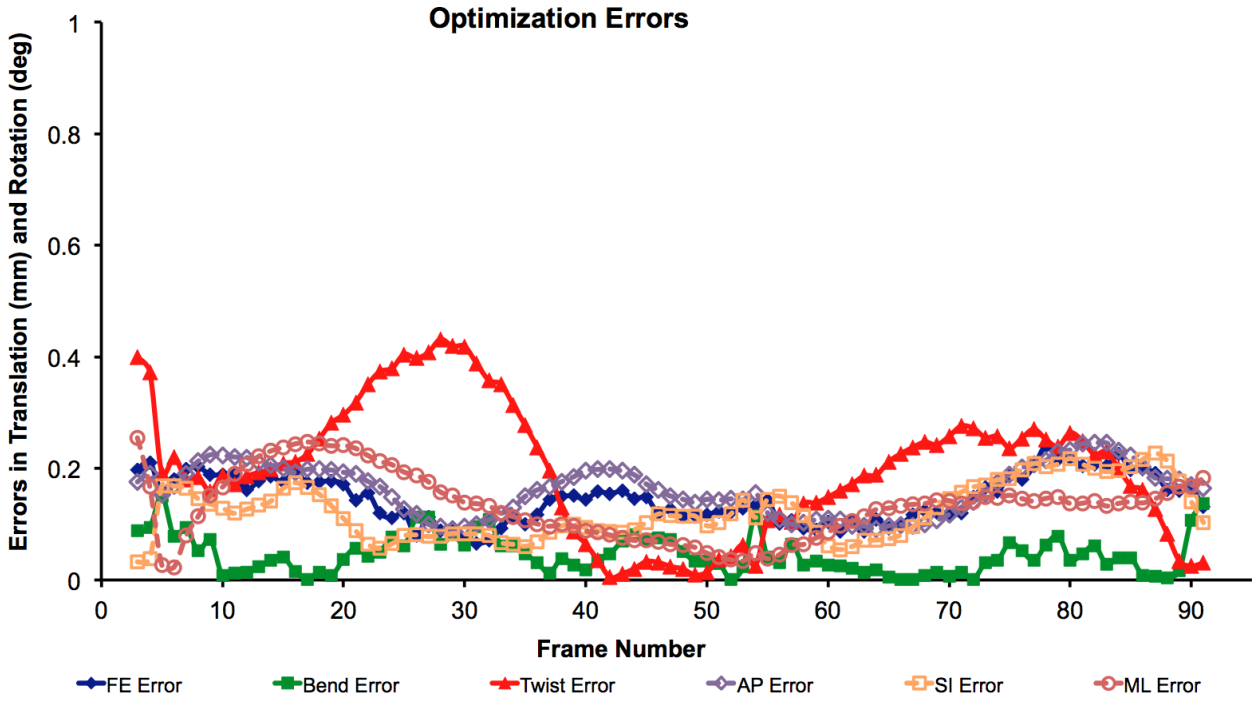

Figure 45: Differences between in vivo and optimized 6 degrees-of-freedom kinematics.

As the head extended, relative to the static neutral position, the posterior shear force increased by approximately 260 N, while the compressive force decreased by approximately 135

N at full extension (Figure 46). As the head moved to full flexion, relative to the static neutral position, the anterior shear force increased by approximately 320 N, while the compressive force decreased by approximately 380 N at full flexion (Figure 46). The peak compressive force (approximately 140 N greater than in the static neutral position, occurred while moving in flexion, midway between full extension and the neutral position

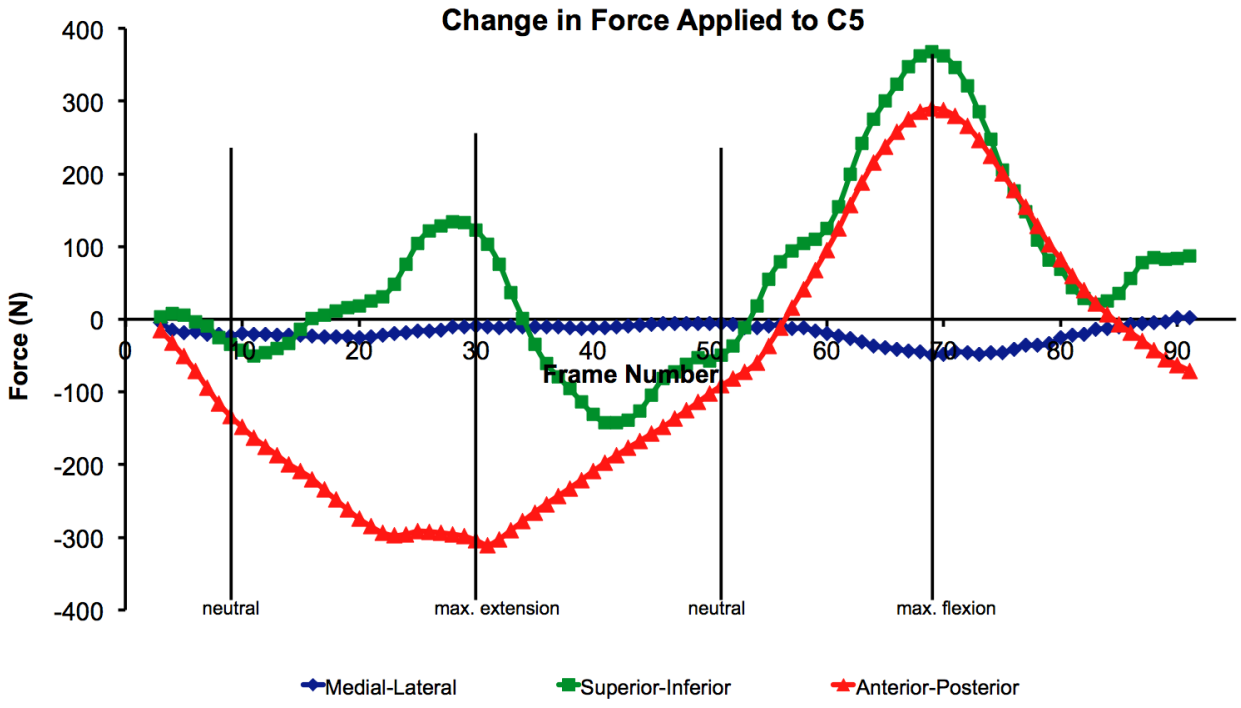

Figure 46: The model-estimated force necessary to reproduce the in vivo kinematics.

Annulus pressure was greatest in the posterior-lateral annulus, posterior annulus and nucleus (0.9 MPa, 0.6 MPa, 0.3 MPa, relative to the static neutral), just after maximum extension as the motion segment began flexion, (Figure 47). Peak pressure in the anterior annulus (0.4 MPa relative to the static neutral pressure) occurred just after maximum flexion, as the motion segment began extension.

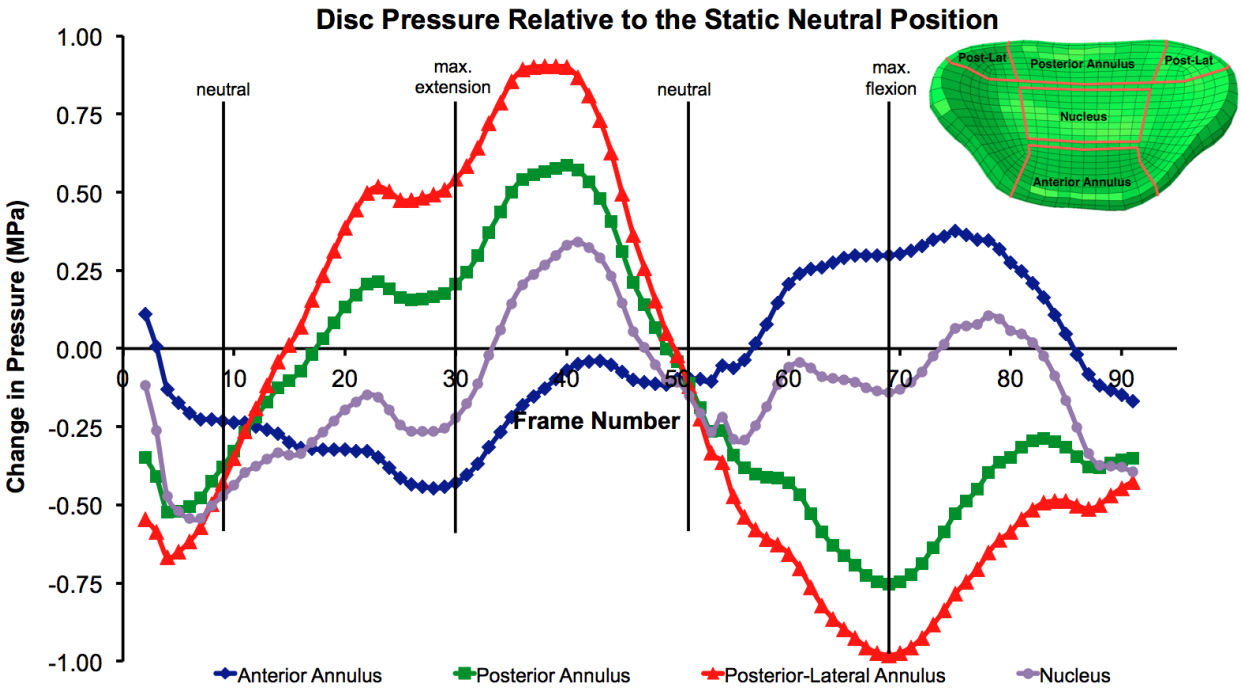

Figure 47: Model-estimated change in pressure within the intervertebral disc.

Stress in the anterior and posterior-lateral annulus at full extension was approximately 1 MPa greater than in the static neutral position (Figure 48). Peak stress in the anterior annulus occurred at full extension, while peak stress in the posterior and posterior-lateral annulus occurred after full extension, as the motion segment moved into flexion. At full flexion, peak stresses in the posterior and posterior-lateral annulus were approximately 0.75 MPa greater than in the static neutral position. Peak stress in the anterior annulus at full flexion was 0.25 MPa greater than in the static, neutral position.

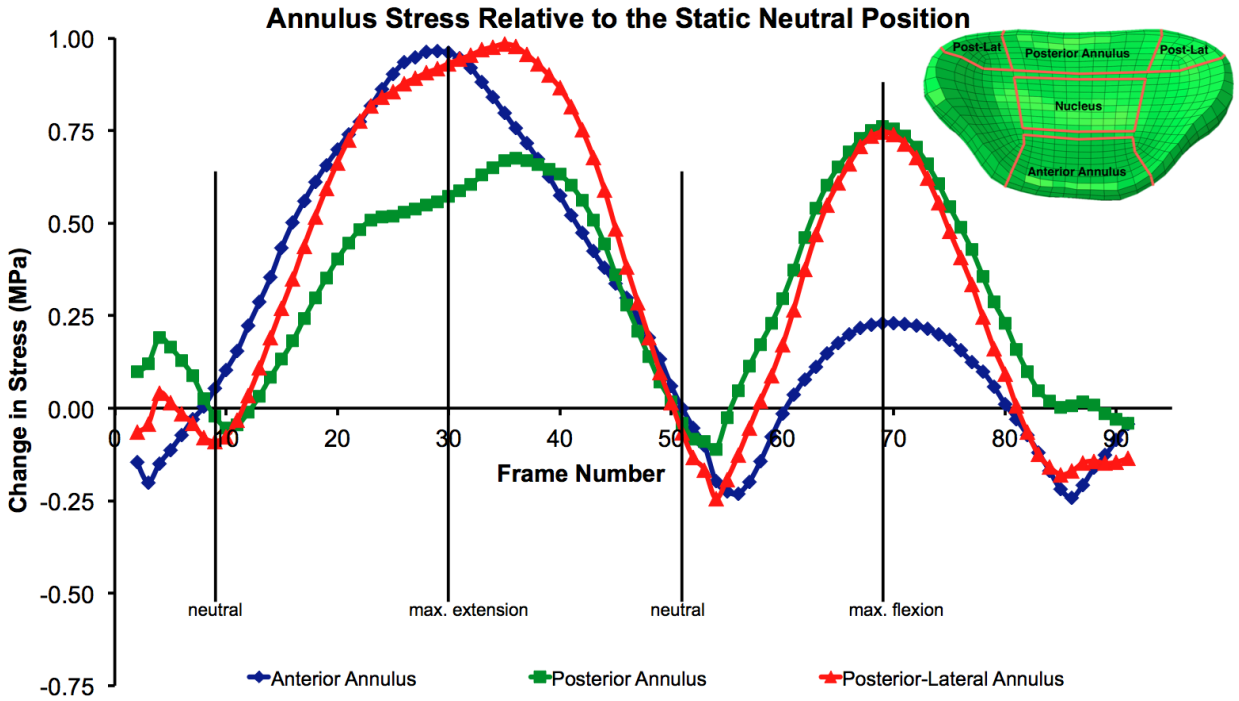

Figure 48: Model-estimated change in stress in the intervertebral disc.

4.2.4 Discussion

This study presents a computational framework for estimating in vivo forces during functional loading. This computational modeling technique applies inverse methods to a finite element model in order to estimate in vivo forces, with highly accurate in vivo subject-specific kinematic data serving as the optimization criteria. This technique may be implemented to estimate in vivo forces for a variety of joints, given the recent proliferation of biplane radiography and fluoroscopy systems that have sub-millimeter accuracy in tracking bone movement in three-dimensions [56,58,202-206].

It was previously demonstrated that the external angular motion and internal stresses of the discs were significantly influenced by variations in the material properties of soft tissues of the cervical spine (disc and ligament), but not by variations in material properties of the hard

tissues (vertebrae and endplates) [207]. The current sensitivity study extended this analysis by assessing the model response to external loads. The results demonstrated that under combined shear and compressive loading, the model was most sensitive to the magnitude and direction of the applied load. These results suggest that, although great efforts have been made to characterize material properties of the bones, endplates and ligaments in the cervical spine [199,200,207], the sensitivity of the model to changes in these material properties is relatively modest in comparison to proportional changes in the applied load.

There are no previous reports of in vivo force and disc loads in the cervical spine during dynamic functional loading that can serve as a benchmark for the finite element model results. However, previous inverse dynamics musculoskeletal models have estimated loading in the cervical spine. The compressive and anterior-posterior shear forces have been estimated to be up to 1164 N and 135 N, respectively, at the level of C4-C5 during isometric contractions in the neutral position [176]. Applying a previously described inverse dynamics model to the participant studied in the current analysis, the peak force applied to C2 was determined, and the compressive and shear components this force projected onto the C5 vertebrae were approximately 300 N and 215 N, respectively, at full extension [193]. Also, given the distance from the point of force application (the top of C5) to the location of the instant center of rotation for the C5/C6 motion segment during flexion (a moment arm of approximately 20 mm) [208], the estimated peak shear forces (280 N in extension and 320 N in flexion) correspond to moments of 5.6 Nm and 6.4 Nm, respectively, applied to the motion segment at full extension and full flexion. While these peak moment values are higher than those typically applied in pure moment loading of cervical spine specimens [90,209] (1.5 Nm and 1.0 Nm, respectively), the range of motion in this relatively young, healthy participant (over 20°) was also much larger than what is commonly reached during in

vitro tests [90,209]. A more appropriate comparison may be the work of Nightingale and colleagues, who applied a 3.5 Nm moment to a series of female C56 motion segments and recorded an average flexion-extension range of motion of 22.8° [210]. In the current study, the forces applied to C5 were estimated by a optimization process that contained many local minimums for the objective function. It is likely that by including a force minimization constraint in the objective function, the optimization process will indicate that much smaller forces may be applied in order to reproduce the in vivo kinematics with sufficient accuracy. Requiring the objective function to minimize muscle stress [211,212], or minimize muscle activation [176] is a constraint commonly applied to musculoskeletal models to estimate in vivo forces.

The changes in pressure estimated by the model are in line with in vitro experiments that recorded C56 disc pressure under a purely compressive load of 200 N (from 0.96 to 1.54 MPa in flexed, neutral and extended postures)[42]. The result indicating that the greatest change in disc pressure occurs in the posterior-lateral annulus coincides well with the frequent clinical observation of disc protrusion into the neural foramen, as found in radiculopathy.

As with any computational model, it is important to understand the assumptions and limitations of the model. The ground substance of the disc was modeled fairly simply, using isotropic, linear mechanical properties. Likewise, ligaments were assigned linear stress-strain behavior. Increasing the model complexity may affect the force and disc stress estimates. The force applied to the superior body (C5) was distributed across only the vertebral body, and not the facet surfaces. This simplification of the distributed load on the motion segment may influence the force estimates, and therefore disc and facet joint cartilage stress. The force and disc stress values reported were relative to the forces and stresses that existed when the spine was in its static, neutral position, and it is not currently practical to measure these forces and stresses

in vivo due to technical and ethical constraints. Finally, it is possible that implementing a local search algorithm after the genetic algorithm could further refine the force estimates calculated by the genetic algorithm.

Accurate knowledge of the internal forces that occur during in vivo functional movement would be invaluable to orthopaedic research. For example, this information may be used to develop in vitro loading regimens to develop and test biologic treatments for cartilage and disc degeneration. In the spine, this technique may be implemented to assess stress in adjacent segments following fusion. This technique may be easily applied to more complex computational models (e.g. multi-segment, nonlinear, anisotropic, etc.) of the cervical motion segment or any of a number of joints in order to estimate in vivo loads applied during dynamic, functional motion.

5.0 CONCLUSION

5.1 SUMMARY OF RESULTS

5.1.1 Kinematics

The results demonstrated that in the asymptomatic control subjects, the location and length of the path of the instant center of rotation is dependent upon motion segment. This finding has implications for cervical arthroplasty. Cervical dis replacements should be designed specifically for each motion segment, or they should allow for variation in the location and path of the center of rotation. Data for the control group indicated that the contributions each motion segment makes to flexion-extension change significantly over the entire range of motion, with cranial motion segments (C23 though C45) making their maximal contributions near the midrange of motion, and caudal motion segments (C56 and C67) making their maximal contributions near the ends of the range of motion. The clinical implication of this is that patients may be advised to avoid movements that require movement to the ends of the range of motion in order to limit the demands placed on the C56 and C67 discs.

The results indicated that total range of motion in adjacent segments was not increased 7 months after fusion surgery. However, the distribution of the flexion-extension motion was shifted toward more extension and posterior translation and less flexion following fusion. A prospective study will be necessary to discern if this difference was related to altered static alignment or alterations in movement patterns following fusion. The data suggest that the

quality of adjacent segment motion (i.e. the path of the ICR) is not altered 7 months after surgery. Although the relative contribution to motion for adjacent segments increases following fusion, this result must be interpreted carefully. Total motion of the cervical spine is decreased after arthrodesis, therefore, the percentage contribution made by each non-fused motion segment must increase after arthrodesis, even if range of motion in the non-fused motion segments does not change.

5.1.2 Arthrokinematics

In asymptomatic subjects, the disc and facet joint capsule deformations are different among motion segments and different among anatomic regions of the cervical spine. This finding suggests that future protocols account for these level-dependent and region-dependent differences when assessing disc and facet joint mechanics.

Single-level anterior arthrodesis alters the compression-distraction deformation of the disc immediately superior to the arthrodesis, suggesting arthrodesis alters the load applied to the superior motion segment. Additionally, adjacent segment facet joint capsule deformation in extension is significantly less in arthrodesis patients in comparison to controls, indicating that arthrodesis affects loading at the facet joints as well as on the discs. Combined, these results provide evidence that suggests arthrodesis affects adjacent segment mechanics. While this data does support the theory that fusion alters adjacent segment mechanics, it is not clear if these mechanical changes are large enough, on their own, to account for all of the degenerative changes that commonly occur in adjacent segments.

5.1.3 Computational Modeling

The computational modeling results indicate that in vitro protocols and finite element models that apply constant loads to the cervical spine do not accurately reflect in vivo cervical spine kinetics during dynamics functional motion. The finite element results indicate that maximum stress and pressure in the intervertebral disc occurs in the posterior-lateral aspect of the annulus. This finding corresponds well with the clinical diagnosis of radiculopathy, where it is believed that bulging of the posterior-lateral annulus decreases the neural foramen area, allowing less space for the nerve root to pass through the foramen.

5.2 FUTURE WORK

The results from the present study provide a basis for a prospective study of single-level and two- level anterior cervical fusion patients. The aim of this study will be to determine to what extent patient-specific factors, iatrogenic factors, and biomechanical factors influence cervical spine mechanics after single-level and two-level fusion. This prospective study will identify the factors that are most closely associated with adjacent segment mechanics. If the results indicate that spine mechanics are influenced primarily by patient-specific and iatrogenic factors, this will provide support for increased attention to patient-specific factors and surgical technique when performing cervical arthrodesis. Alternatively, if the results indicate that adjacent segment mechanics are influenced primarily by increased stress after arthrodesis, this will provide support for increased attention to the design of motion-sparing devices.

APPENDIX A

RANGE OF MOTION SUPPLEMENTARY MATERIAL

A.1 TABLES

Table 20: Rotation range of motion during dynamic flexion-extension.

Group	C2/C3			C3/C4			C4/C5			C5/C6			C6/C7		
	FE	TW	LB	FE	TW	LB	FE	TW	LB	FE	TW	LB	FE	TW	LB
Control	10.2±2.4	1.9±0.8	2.8±1.2	14.2±2.6	1.9±0.8	2.6±1.4	15.9±2.1	1.9±0.7	2.8±1.6	14.6±4.7	1.6±0.7	2.0±0.8	12.5±4.6	1.5±0.5	2.3±1.0
C56 Fusion	N/A	N/A	N/A	13.2±3.1	2.1±0.8	2.5±0.9	16.7±2.9	2.4±0.9	2.7±1.2	2.9±0.9*	2.2±1.1	2.5±1.2	12.6±4.2	2.6±0.9*	3.3±0.9
Difference	N/A	N/A	N/A	-1.0	0.2	-0.2	0.8	0.5	-0.0	-11.8	0.6	0.5	0.1	1.1	1.0
95% CI	N/A	N/A	N/A	-3.2 to 1.2	-0.5 to 0.8	-1.1 to 0.8	-1.1 to 2.7	-0.2 to 1.1	-1.2 to 1.1	-14.9 to -8.7	-0.1 to 1.3	-0.2 to 1.3	-3.5 to 3.6	0.5 to 1.6	0.2 to 1.8

Table 21: Flexion and extension components of total range of motion.

Group	C2/C3		C3/C4		C4/C5		C5/C6		C6/C7	
	Flexion	Extension	Flexion	Extension	Flexion	Extension	Flexion	Extension	Flexion	Extension
Control	5.9±2.4	4.2±2.2	7.9±3.6	6.3±3.3	8.0±2.6	7.9±3.3	7.4±2.9	7.3±3.8	7.1±3.9	5.4±2.3
C56 Fusion	N/A	N/A	6.1±3.1	7.1±2.2	5.1±3.7*	11.7±4.1*	2.2±1.1*	0.6±1.4*	5.9±3.1	6.7±3.0
Difference	N/A	N/A	-1.8	0.8	-2.9	3.8	-5.2	-6.7	-1.2	1.3
95% CI	N/A	N/A	-4.5 to 0.9	-1.5 to 3.2	-5.3 to -0.5	0.9 to 6.6	-7.1 to -3.2	-9.2 to -4.1	-4.1 to 1.7	-1.1 to 3.6

Table 22: Translation range of motion during dynamic flexion-extension.

Group	C2/C3			C3/C4			C4/C5			C5/C6			C6/C7		
	ML	SI	AP	ML	SI	AP	ML	SI	AP	ML	SI	AP	ML	SI	AP
Control	0.6±0.2	0.7±0.3	3.8±1.1	0.6±0.4	0.7±0.3	3.8±0.8	0.6±0.3	0.6±0.3	3.9±0.7	0.6±0.5	0.6±0.3	3.2±1.3	0.7±0.6	0.7±0.4	2.4±1.0
C56 Fusion	N/A	N/A	N/A	0.8±0.3	0.7±0.3	3.7±0.8	0.7±0.3	1.0±0.5	4.5±0.9	1.0±0.5	0.7±0.3	0.6±0.3*	1.3±0.9	0.9±0.4	2.9±0.8
Difference	N/A	N/A	N/A	0.2	-0.0	-0.0	0.1	0.4	0.6	0.4	0.0	-2.6	0.6	0.2	0.4
95% CI	N/A	N/A	N/A	-0.1 to 0.5	-0.2 to 0.2	-0.7 to 0.6	-0.1 to 0.4	0.0 to 0.8	-0.0 to 1.2	0.0 to 0.8	-0.2 to 0.3	-3.2 to -2.0	0.1 to 1.1	-0.1 to 0.5	-0.4 to 1.2

Table 23: Anterior and posterior components of translation range of motion.

Group	C2/C3		C3/C4		C4/C5		C5/C6		C6/C7	
	Anterior	Posterior	Anterior	Posterior	Anterior	Posterior	Anterior	Posterior	Anterior	Posterior
Control	2.2±1.0	1.7±1.0	2.0±1.1	1.7±0.9	1.9±0.8	2.0±0.8	1.6±0.7	1.5±1.0	1.4±0.8	1.0±0.5
C56 Fusion	N/A	N/A	1.6±1.1	2.0±0.7	1.7±1.4	2.7±1.3	0.4±0.3*	0.3±0.3*	1.2±0.8	1.4±0.5*
Difference	N/A	N/A	-0.4	0.3	-0.2	0.8	-1.2	-1.3	-0.1	0.4
95% CI	N/A	N/A	-1.2 to 0.5	-0.3 to 1.0	-1.0 to 0.6	-0.0 to 1.6	-1.6 to -0.9	-1.7 to -0.8	-0.8 to 0.5	0.0 to 0.8

Table 24: Differences between dynamic and static rotation range of motion during flexion-extension.

Group	C2/C3			C3/C4			C4/C5			C5/C6			C6/C7		
	FE	TW	LB	FE	TW	LB	FE	TW	LB	FE	TW	LB	FE	TW	LB
Control	**1.1±0.6**	**1.3±0.6**	**1.2±0.6**	**0.9±1.1**	**1.1±1.0**	**1.5±1.2**	**1.2±1.9**	**1.0±0.5**	**1.5±0.9**	0.4±2.4	**1.0±0.8**	**1.2±0.7**	-0.3±4.0	0.6±1.2	**1.1±1.1**
C56 Fusion	N/A	N/A	N/A	3.1±4.1	**1.4±0.6**	**1.4±1.1**	**2.8±2.9**	**2.1±1.2**	**2.0±1.7**	**1.8±0.9**	**0.9±1.0**	**1.8±0.9**	1.6±2.1	1.2±1.4	**2.0±1.4**
95% CI	0.9 to 1.5	0.9 to 1.5	0.9 to 2.2	0.5 to 3.1	0.9 to 1.6	1.0 to 2.1	0.8 to 2.7	0.9 to 2.1	1.0 to 2.3	0.7 to 1.8	-0.1 to 2.0	1.1 to 2.2	-1.4 to 1.9	0.2 to 1.7	0.9 to 2.2

Table 25: Difference between dynamic and static translation range of motion during flexion-extension.

Group	C2/C3			C3/C4			C4/C5			C5/C6			C6/C7		
	ML	SI	AP	ML	SI	AP	ML	SI	AP	ML	SI	AP	ML	SI	AP
Control	**0.3±0.2**	**0.3±0.2**	**0.4±0.3**	**0.4±0.3**	**0.3±0.3**	**0.2±0.3**	**0.4±0.4**	**0.3±0.2**	**0.2±0.3**	**0.4±0.3**	**0.2±0.3**	0.0±0.6	**0.3±0.2**	**0.3±0.4**	-0.1±0.8
C56 Fusion	N/A	N/A	N/A	**0.5±0.4**	**0.4±0.3**	0.8±1.0	**0.4±0.2**	**0.7±0.7**	0.8±1.2	**0.6±0.5**	**0.6±0.3**	0.2±0.4	**0.7±0.4***	**0.6±0.3**	**0.7±0.6**
95% CI	0.2 to 0.5	0.2 to 0.4	0.2 to 0.5	0.3 to 0.6	0.2 to 0.5	0.1 to 0.7	0.3 to 0.5	0.3 to 0.6	0.1 to 0.8	0.3 to 0.6	0.2 to 0.5	-0.1 to 0.3	0.3 to 0.5	0.3 to 0.6	-0.1 to 0.5

Table 26: Disc height by vertebral level and anatomic location.

Group	C23			C34			C45			C56			C67		
	AA	N	PA	AA	N	PA	AA	N	PA	AA	N	PA	AA	N	PA
Control	4.0±0.9	4.6±0.7	3.3±0.5	3.9±0.6	4.4±0.7	3.0±0.6	4.0±1.0	4.4±0.8	3.1±0.6	3.6±1.1	4.0±1.2	2.7±1.0	3.8±1.3	4.4±1.3	3.0±1.1
C56 Fusion	N/A	N/A	N/A	4.3±0.9	4.8±0.5	3.2±0.7	4.3±0.9	4.7±0.9	3.8±0.9	N/A	N/A	N/A	4.5±0.8	5.2±0.5	3.9±0.6
Difference	N/A	N/A	N/A	0.4	0.4	0.2	0.3	0.3	0.8	N/A	N/A	N/A	0.7	0.8	0.9
95% CI	N/A	N/A	N/A	-0.2 to 1.0	-0.1 to 0.9	-0.3 to 0.7	-0.5 to 1.0	-0.4 to 1.0	0.2 to 1.3	N/A	N/A	N/A	-0.3 to 1.6	-0.1 to 1.7	0.2 to 1.7

APPENDIX B

CONTINUOUS KINEMATICS SUPPLEMENTARY MATERIAL

B.1 MATERIALS AND METHODS

B.1.1 Relationship Between Disc Height and Range of Motion

Pearson correlation was used to identify significant relationships between disc height and flexion-extension range of motion and between static orientation and average flexion-extension angle during the dynamic movement for control subjects. A regression equation relating disc height and flexion-extension ROM at each disc level was determined when significant correlations between these two variables were identified. This regression equation was used to predict ROM at each motion segment given the disc height. A vertebral level-specific scale factor was then calculated for each motion segment for every subject using the predicted and actual ROM using the following equation: *ScaleFactor = (Predicted_ROM – Actual_ROM) / Actual_ROM* (1). The scale factor and average flexion-extension angle over the entire flexion (or extension) movement were then input to equation (2), below, to determine the adjusted intervertebral flexion-extension angle at each 1% interval of C2/C7 ROM.

$$Adjusted\_Angle = Measured\_Angle + (Measured\_Angle - Average\_Angle) * ScaleFactor \quad (2)$$

In this way, the slope of the segmental flexion-extension angle versus percent of C2/C7 ROM curves were adjusted to account for inter-subject differences in disc height (Figure 42).

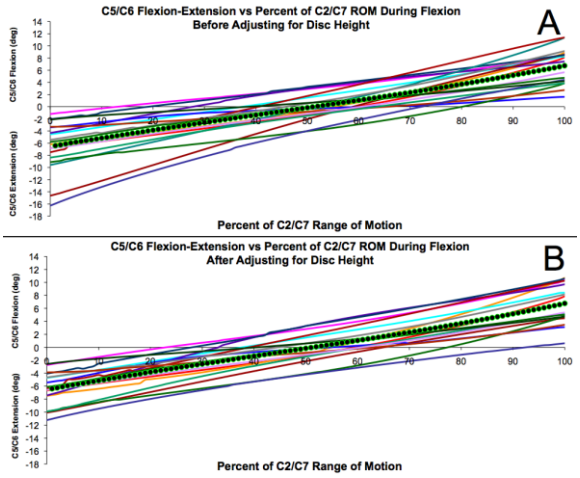

Figure 49: C5/C6 flexion-extension curves before (A) and after (B) adjusting for disc height during the flexion motion.

B.1.2 Relationship Between Static Orientation and Average Flexion-Extension Angle

A second regression equation relating static orientation and average flexion-extension angle at each motion segment was determined when significant correlations between these two variables were identified. This regression equation was used to predict the average intervertebral flexion-extension angle at each motion segment given the static orientation angle. A vertebral level-specific offset value was then calculated for each motion segment for every subject using the predicted and actual average flexion-extension angle using the following equation: $OffsetValue = Measured\_Average\_Angle - Predicted\_Average\_Angle$ (3). The offset value was then used to determine the adjusted intervertebral flexion-extension angle at each 1% interval of C2/C7 ROM using the equation: $Adjusted\_Angle = Measured\_Angle - OffsetValue$ (4). In this way, segmental flexion-extension angle versus percent C2/C7 ROM curves were adjusted to account

for inter-subject differences in static orientation (Figure 43). After segmental flexion-extension angles were adjusted to account for disc height and static orientation, as just described, a 3rd order polynomial was fit to the group mean flexion-extension angle versus percent of C2/C7 ROM curve for each motion segment.

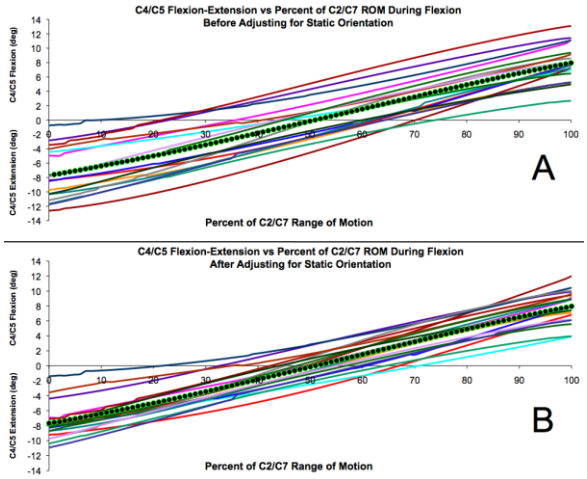

Figure 50: C4/C5 flexion-extension curves before (A) and after (B) adjusting for static orientation during the flexion motion.

The process described above was repeated using anterior-posterior translation curves in place of flexion-extension rotation curves to more precisely define the anterior-posterior translation motion path during flexion-extension.

B.2 RESULTS

Applying regression equations relating disc height to ROM reduced inter-subject variability in C5/C6 and C6/C7 flexion-extension curves by adjusting the slope of the flexion-extension curve for each participant (Figure 42).

Applying regression equations relating static orientation to average flexion-extension angle reduced inter-subject variability in C2/C3, C3/C4, C4/C5 and C5/C6 flexion extension curves by adjusting the mean value of the flexion-extension curve for each participant (Figure 43).

Third-order polynomials fit to flexion-extension versus percent of C2/C7 rotation ROM precisely described the mean continuous flexion-extension motion path at each motion segment for the control group (all $R^2 > .99$) (Table 12). Third-order polynomials fit to anterior-posterior translation versus percent of C2/C7 rotation ROM precisely described the mean AP translation motion path at each motion segment for the control group (all $R^2 > .99$) (Table 13).

Table 27: Third-order polynomial equations to describe flexion-extension angle versus C2/C7 percent range of motion during flexion and extension.

Motion Segment	Flexion Motion Path	Extension Motion Path
C2/C3	Angle = -4.433E-06x³ + 4.926E-04x² + 8.916E-02x - 3.901	Angle = 5.870E-06x³ - 4.961E-04x² - 1.040E-01x + 5.524
C3/C4	Angle = -8.242E-06x³ + 1.266E-03x² + 9.332E-02x - 6.209	Angle = 9.543E-06x³ - 1.247E-03x² - 1.063E-01x + 7.375
C4/C5	Angle = -4.947E-06x³ + 8.621E-04x² + 1.200E-01x - 7.690	Angle = 2.469E-06x³ - 6.047E-04x² - 1.204E-01x + 7.831
C5/C6	Angle = 4.971E-06x³ - 6.346E-04x² + 1.467E-01x - 6.544	Angle = -7.662E-06x³ + 9.068E-04x² - 1.464E-01x + 6.789
C6/C7	Angle = 1.511E-05x³ - 2.185E-03x² + 1.720E-01x - 4.535	Angle = -1.277E-05x³ + 1.858E-03x² - 1.672E-01x + 6.334

Table 28: Third-order polynomial equations to describe anterior-posterior translation versus C2/C7 percent range of motion during flexion and extension.

Motion Segment	Flexion Motion Path	Extension Motion Path
C2/C3	Translation = -9.827E-07x³ + 5.834E-05x² + 3.919E-02x - 1.494	Translation = 1.515E-06x³ - 1.173E-04x² - 3.924E-02x + 2.040
C3/C4	Translation = -1.724E-06x³ + 2.405E-04x² + 2.973E-02x - 1.816	Translation = 2.063E-06x³ - 2.870E-04x² - 2.822E-02x + 1.811
C4/C5	Translation = -1.032E-06x³ + 1.730E-04x² + 3.265E-02x - 1.967	Translation = 3.144E-07x³ - 1.203E-04x² - 3.091E-02x + 1.962
C5/C6	Translation = 1.115E-06x³ - 1.424E-04x² + 3.254E-02x - 1.431	Translation = -1.821E-06x³ + 2.227E-04x² - 3.358E-02x + 1.526
C6/C7	Translation = 3.029E-06x³ - 4.398E-04x² + 3.388E-02x - 8.437	Translation = -2.563E-06x³ + 3.740E-04x² - 3.309E-02x + 1.282

BIBLIOGRAPHY

1. Smith GW, Robinson RA. The treatment of certain cervical-spine disorders by anterior removal of the intervertebral disc and interbody fusion. J Bone Joint Surg Am. 1958;**40-A(3)**: 607-24.

2. Patil PG, Turner DA, Pietrobon R. National trends in surgical procedures for degenerative cervical spine disease: 1990-2000. Neurosurgery. 2005;**57(4)**: 753-8; discussion 753-8.

3. Davis H. Increasing rates of cervical and lumbar spine surgery in the United States, 1979-1990. Spine (Phila Pa 1976). 1994;**19(10)**: 1117-23; discussion 1123-4.

4. Angevine PD, Arons RR, McCormick PC. National and regional rates and variation of cervical discectomy with and without anterior fusion, 1990-1999. Spine (Phila Pa 1976). 2003;**28(9)**: 931-9; discussion 940.

5. Gore DR, Sepic SB. Anterior discectomy and fusion for painful cervical disc disease. A report of 50 patients with an average follow-up of 21 years. Spine (Phila Pa 1976). 1998;**23(19)**: 2047-51.

6. Ishihara H, Kanamori M, Kawaguchi Y, Nakamura H, Kimura T. Adjacent segment disease after anterior cervical interbody fusion. Spine J. 2004;**4(6)**: 624-8.

7. Hilibrand AS, Carlson GD, Palumbo MA, Jones PK, Bohlman HH. Radiculopathy and myelopathy at segments adjacent to the site of a previous anterior cervical arthrodesis. J Bone Joint Surg Am. 1999;**81(4)**: 519-28.

8. Kulkarni V, Rajshekhar V, Raghuram L. Accelerated spondylotic changes adjacent to the fused segment following central cervical corpectomy: magnetic resonance imaging study evidence. J Neurosurg. 2004;**100(1 Suppl Spine)**: 2-6.

9. Hunter LY, Braunstein EM, Bailey RW. Radiographic changes following anterior cervical fusion. Spine (Phila Pa 1976). 1980;**5(5)**: 399-401.

10. Baba H, Furusawa N, Imura S, Kawahara N, Tsuchiya H, Tomita K. Late radiographic findings after anterior cervical fusion for spondylotic myeloradiculopathy. Spine. 1993;**18(15)**: 2167-73.

11. Goffin J, Geusens E, Vantomme N, Quintens E, Waerzeggers Y, Depreitere B, Van Calenbergh F, van Loon J. Long-term follow-up after interbody fusion of the cervical spine. J Spinal Disord Tech. 2004;**17(2)**: 79-85.

12. Schwab JS, Diangelo DJ, Foley KT. Motion compensation associated with single-level cervical fusion: where does the lost motion go? Spine. 2006;**31(21)**: 2439-48.

13. Kolstad F, Nygaard OP, Leivseth G. Segmental motion adjacent to anterior cervical arthrodesis: a prospective study. Spine (Phila Pa 1976). 2007;**32(5)**: 512-7.

14. Fuller DA, Kirkpatrick JS, Emery SE, Wilber RG, Davy DT. A kinematic study of the cervical spine before and after segmental arthrodesis. Spine. 1998;**23(15)**: 1649-56.

15. Fielding JW. Normal and Selected Abnormal Motion of the Cervical Spine from the Second Cervical Vertebra to the Seventh Cervical Vertebra Based on Cineroentgenography. J Bone Joint Surg Am. 1964;**46**: 1779-81.

16. Dunsker SB, Colley DP, Mayfield FH. Kinematics of the cervical spine. Clin Neurosurg. 1978;**25**: 174-83.

17. Matsunaga S, Kabayama S, Yamamoto T, Yone K, Sakou T, Nakanishi K. Strain on intervertebral discs after anterior cervical decompression and fusion. Spine. 1999;**24(7)**: 670-5.

18. Buetti-Bauml C. Funktionelle rontgendiagnostik der halswirbelsaule. Thieme, Stuttgart, Fortschritte auf dem gebiete der roentgenstrahlen vereinigt mit roentgenpraxis. Erganzungsband. 1954: 70: Data presented in Dvorak, 1988.

19. Bakke S. Rontgenologishe beobachtungen uber die bewegungen der halswirbelsaule. Acta Radiol [Suppl] (Stockh). 1931;**13**: : Data presented in Dvorak, 1988.

20. De Seze C, Djian A, Abdelmaola M. Etude radiologique de la dynamique cervicale dans le plain sagittal. (Une contribution radiophysiologique a l'etude pathogenique des artheoses cervicales). Revue Du Rhumatismer. 1951;**18**: 37-46 Data presented in Dvorak, 1988.

21. White AA, 3rd, Panjabi MM. The basic kinematics of the human spine. A review of past and current knowledge. Spine. 1978;**3(1)**: 12-20.

22. Dvorak J, Froehlich D, Penning L, Baumgartner H, Panjabi MM. Functional radiographic diagnosis of the cervical spine: flexion/extension. Spine 1988;**13(7)**: 748-55.

23. Frobin W, Leivseth G, Biggemann M, Brinckmann P. Sagittal plane segmental motion of the cervical spine. A new precision measurement protocol and normal motion data of healthy adults. Clin Biomech 2002;**17(1)**: 21-31.

24. Hino H, Abumi K, Kanayama M, Kaneda K. Dynamic motion analysis of normal and unstable cervical spines using cineradiography. An in vivo study. Spine (Phila Pa 1976). 1999;**24(2)**: 163-8.

25. Wu SK, Kuo LC, Lan HC, Tsai SW, Chen CL, Su FC. The quantitative measurements of the intervertebral angulation and translation during cervical flexion and extension. Eur Spine J. 2007;**16(9)**: 1435-44.

26. van Mameren H, Sanches H, Beursgens J, Drukker J. Cervical spine motion in the sagittal plane. II. Position of segmental averaged instantaneous centers of rotation--a cineradiographic study. Spine (Phila Pa 1976). 1992;**17(5)**: 467-74.

27. Reitman CA, Mauro KM, Nguyen L, Ziegler JM, Hipp JA. Intervertebral motion between flexion and extension in asymptomatic individuals. Spine 2004;**29(24)**: 2832-43.

28. Mimura M, Moriya H, Watanabe T, Takahashi K, Yamagata M, Tamaki T. Three-dimensional motion analysis of the cervical spine with special reference to the axial rotation. Spine 1989;**14(11)**: 1135-9.

29. Iai H, Moriya H, Goto S, Takahashi K, Yamagata M, Tamaki T. Three-dimensional motion analysis of the upper cervical spine during axial rotation. Spine 1993;**18(16)**: 2388-92.

30. Bogduk N, Mercer S. Biomechanics of the cervical spine. I: Normal kinematics. Clin Biomech 2000;**15(9)**: 633-48.

31. Ishii T, Mukai Y, Hosono N, Sakaura H, Fujii R, Nakajima Y, Tamura S, Sugamoto K, Yoshikawa H. Kinematics of the subaxial cervical spine in rotation in vivo three-dimensional analysis. Spine 2004;**29(24)**: 2826-31.

32. Ishii T, Mukai Y, Hosono N, Sakaura H, Fujii R, Nakajima Y, Tamura S, Iwasaki M, Yoshikawa H, Sugamoto K. Kinematics of the cervical spine in lateral bending: in vivo three-dimensional analysis. Spine 2006;**31(2)**: 155-60.

33. Goel VK, Pope MH. Biomechanics of fusion and stabilization. Spine. 1995;**20(24 Suppl)**: 85S-99S.

34. Van Mameren H, Drukker J, Sanches H, Beursgens J. Cervical spine motion in the sagittal plane (I) range of motion of actually performed movements, an X-ray cinematographic study. Eur J Morphol. 1990;**28(1)**: 47-68.

35. Nissan M, Gilad I. The cervical and lumbar vertebrae--an anthropometric model. Eng Med. 1984;**13(3)**: 111-4.

36. Gilad I, Nissan M. A study of vertebra and disc geometric relations of the human cervical and lumbar spine. Spine (Phila Pa 1976). 1986;**11(2)**: 154-7.

37. Anderson AE, Ellis BJ, Weiss JA. Verification, validation and sensitivity studies in computational biomechanics. Comput Methods Biomech Biomed Engin. 2007;**10(3)**: 171-84.

38. Schmidt H, Kettler A, Heuer F, Simon U, Claes L, Wilke HJ. Intradiscal pressure, shear strain, and fiber strain in the intervertebral disc under combined loading. Spine (Phila Pa 1976). 2007;**32(7)**: 748-55.

39. Adams MA, Dolan P, McNally DS. The internal mechanical functioning of intervertebral discs and articular cartilage, and its relevance to matrix biology. Matrix Biol. 2009;**28(7)**: 384-9.

40. Urban JP, Holm S, Maroudas A, Nachemson A. Nutrition of the intervertebral disk. An in vivo study of solute transport. Clin Orthop Relat Res. 1977;**(129)**: 101-14.

41. Urban JP, Holm S, Maroudas A, Nachemson A. Nutrition of the intervertebral disc: effect of fluid flow on solute transport. Clin Orthop Relat Res. 1982;**(170)**: 296-302.

42. Skrzypiec DM, Pollintine P, Przybyla A, Dolan P, Adams MA. The internal mechanical properties of cervical intervertebral discs as revealed by stress profilometry. Eur Spine J. 2007;**16(10)**: 1701-9.

43. Perie DS, Maclean JJ, Owen JP, Iatridis JC. Correlating material properties with tissue composition in enzymatically digested bovine annulus fibrosus and nucleus pulposus tissue. Ann Biomed Eng. 2006;**34(5)**: 769-77.

44. Boxberger JI, Sen S, Yerramalli CS, Elliott DM. Nucleus pulposus glycosaminoglycan content is correlated with axial mechanics in rat lumbar motion segments. J Orthop Res. 2006;**24(9)**: 1906-15.

45. Bohlman HH, Emery SE, Goodfellow DB, Jones PK. Robinson anterior cervical discectomy and arthrodesis for cervical radiculopathy. Long-term follow-up of one hundred and twenty-two patients. J Bone Joint Surg Am. 1993;**75(9)**: 1298-307.

46. Gore DR, Sepic SB. Anterior cervical fusion for degenerated or protruded discs. A review of one hundred forty-six patients. Spine (Phila Pa 1976). 1984;**9(7)**: 667-71.

47. Watters WC, 3rd, Levinthal R. Anterior cervical discectomy with and without fusion. Results, complications, and long-term follow-up. Spine (Phila Pa 1976). 1994;**19(20)**: 2343-7.

48. Hilibrand AS, Yoo JU, Carlson GD, Bohlman HH. The success of anterior cervical arthrodesis adjacent to a previous fusion. Spine (Phila Pa 1976). 1997;**22(14)**: 1574-9.

49. Matsumoto M, Okada E, Ichihara D, Watanabe K, Chiba K, Toyama Y, Fujiwara H, Momoshima S, Nishiwaki Y, Hashimoto T, and Takahata T. Age-related changes of thoracic and cervical intervertebral discs in asymptomatic subjects. Spine (Phila Pa 1976). 2010;**35(14)**: 1359-64.

50. Song KJ, Choi BW, Jeon TS, Lee KB, Chang H. Adjacent segment degenerative disease: is it due to disease progression or a fusion-associated phenomenon? Comparison between segments adjacent to the fused and non-fused segments. Eur Spine J. 2011;**20(11)**: 1940-5.

51. Penning L, *Functioneel rontgenonderzoek bij degenerative en traumatische afwijkingen der laag-cervicale bewegingssegmenten*. 1960, University of Groningen: Groningen, The Netherlands.

52. Simpson AK, Biswas D, Emerson JW, Lawrence BD, Grauer JN. Quantifying the effects of age, gender, degeneration, and adjacent level degeneration on cervical spine range of motion using multivariate analyses. Spine (Phila Pa 1976). 2008;**33(2)**: 183-6.

53. Thorhauer E, Miyawaki M, Illingworth K, Holmes A, Anderst W (2010). Accuracy of bone and cartilage models obtained from ct and mri. *American Society of Biomechanics*. Providence, RI.

54. Treece G, Prager, RW, Gee, AH. Regularized marching tetrahedra: improved iso-surface extraction. Computers and Graphics. 1999;**23**: 583-598.

55. Anderst WJ, Baillargeon E, Donaldson WF, 3rd, Lee JY, Kang JD. Validation of a noninvasive technique to precisely measure in vivo three-dimensional cervical spine movement. Spine (Phila Pa 1976). 2011;**36(6)**: E393-400.

56. Bey MJ, Zauel R, Brock SK, Tashman S. Validation of a new model-based tracking technique for measuring three-dimensional, in vivo glenohumeral joint kinematics. J Biomech Eng. 2006;**128(4)**: 604-9.

57. Martin DE, Greco NJ, Klatt BA, Wright VJ, Anderst WJ, Tashman S. Model-based tracking of the hip: implications for novel analyses of hip pathology. J Arthroplasty. 2011;**26(1)**: 88-97.

58. Anderst W, Zauel R, Bishop J, Demps E, Tashman S. Validation of three-dimensional model-based tibio-femoral tracking during running. Med Eng Phys. 2009;**31(1)**: 10-16.

59. Winter DA. Biomechanics and Motor Control of Human Movement (4th Edition).2009 **Vol.** Hoboken, New Jersey: Wiley.

60. Wu G, Siegler S, Allard P, Kirtley C, Leardini A, Rosenbaum D, Whittle M, D'Lima DD, Cristofolini L, Witte H, Schmid O, and Stokes I. ISB recommendation on definitions of joint coordinate system of various joints for the reporting of human joint motion--part I: ankle, hip, and spine. International Society of Biomechanics. J Biomech. 2002;**35(4)**: 543-8.

61. Kane T, Likins P, Leivseth G. Spacecraft dynamics.1983 **Vol.** New York: McGraw-Hill.

62. Park DK, Lin EL, Phillips FM. Index and adjacent level kinematics after cervical disc replacement and anterior fusion: in vivo quantitative radiographic analysis. Spine (Phila Pa 1976). 2011;**36(9)**: 721-30.

63. Pagano R. Understanding statistics in the behavioral sciences. 3rd ed.1990 **Vol.** New York: West Publishing Co.

64. Benjamini Y, Hochberg Y. Controlling the false discovery rate: a practical and powerful approach to multiple testing. Journal Royal Statistical Society, Series B. 1995;**57(1)**: 289-300.

65. Reitman CA, Hipp JA, Nguyen L, Esses SI. Changes in segmental intervertebral motion adjacent to cervical arthrodesis: a prospective study. Spine. 2004;**29(11)**: E221-6.

66. Liu F, Cheng J, Komistek RD, Mahfouz MR, Sharma A. In vivo evaluation of dynamic characteristics of the normal, fused, and disc replacement cervical spines. Spine (Phila Pa 1976). 2007;**32(23)**: 2578-84.

67. Finn MA, Brodke DS, Daubs M, Patel A, Bachus KN. Local and global subaxial cervical spine biomechanics after single-level fusion or cervical arthroplasty. Eur Spine J. 2009;**18(10)**: 1520-7.

68. Eck JC, Humphreys SC, Lim TH, Jeong ST, Kim JG, Hodges SD, An HS. Biomechanical study on the effect of cervical spine fusion on adjacent-level intradiscal pressure and segmental motion. Spine (Phila Pa 1976). 2002;**27(22)**: 2431-4.

69. Dmitriev AE, Cunningham BW, Hu N, Sell G, Vigna F, McAfee PC. Adjacent level intradiscal pressure and segmental kinematics following a cervical total disc arthroplasty: an in vitro human cadaveric model. Spine (Phila Pa 1976). 2005;**30(10)**: 1165-72.

70. DiAngelo DJ, Roberston JT, Metcalf NH, McVay BJ, Davis RC. Biomechanical testing of an artificial cervical joint and an anterior cervical plate. J Spinal Disord Tech. 2003;**16(4)**: 314-23.

71. Benoist M. Natural history of the aging spine. Eur Spine J. 2003;**12 Suppl 2**: S86-9.

72. White AA, 3rd, Johnson RM, Panjabi MM, Southwick WO. Biomechanical analysis of clinical stability in the cervical spine. Clin Orthop Relat Res. 1975;**(109)**: 85-96.

73. Boden SD, McCowin PR, Davis DO, Dina TS, Mark AS, Wiesel S. Abnormal magnetic-resonance scans of the cervical spine in asymptomatic subjects. A prospective investigation. J Bone Joint Surg Am. 1990;**72(8)**: 1178-84.

74. Ferguson SJ, Steffen T. Biomechanics of the aging spine. Eur Spine J. 2003;**12 Suppl 2**: S97-S103.

75. Nunley PD, Jawahar A, Kerr EJ, 3rd, Gordon CJ, Cavanaugh DA, Birdsong EM, Stocks M, Danielson G. Factors affecting the incidence of symptomatic adjacent-level disease in cervical spine after total disc arthroplasty: 2- to 4-year follow-up of 3 prospective randomized trials. Spine (Phila Pa 1976). 2012;**37(6)**: 445-51.

76. Amevo B, Aprill C, Bogduk N. Abnormal instantaneous axes of rotation in patients with neck pain. Spine (Phila Pa 1976). 1992;**17(7)**: 748-56.

77. Wu SK, Kuo LC, Lan HC, Tsai SW, Su FC. Segmental percentage contributions of cervical spine during different motion ranges of flexion and extension. J Spinal Disord Tech. 2010;**23(4)**: 278-84.

78. Lind B, Sihlbom H, Nordwall A, Malchau H. Normal range of motion of the cervical spine. Arch Phys Med Rehabil. 1989;**70(9)**: 692-5.

79. Bible JE, Biswas D, Miller CP, Whang PG, Grauer JN. Normal functional range of motion of the cervical spine during 15 activities of daily living. J Spinal Disord Tech. 2010;**23(1)**: 15-21.

80. Cobian DG, Sterling AC, Anderson PA, Heiderscheit BC. Task-specific frequencies of neck motion measured in healthy young adults over a five-day period. Spine (Phila Pa 1976). 2009;**34(6)**: E202-7.

81. Brodke DS, Klimo P, Jr., Bachus KN, Braun JT, Dailey AT. Anterior cervical fixation: analysis of load-sharing and stability with use of static and dynamic plates. J Bone Joint Surg Am. 2006;**88(7)**: 1566-73.

82. Davies MA, Bryant SC, Larsen SP, Murrey DB, Nussman DS, Laxer EB, Darden BV. Comparison of cervical disk implants and cervical disk fusion treatments in human cadaveric models. J Biomech Eng. 2006;**128(4)**: 481-6.

83. Brolin K, Halldin P. Development of a finite element model of the upper cervical spine and a parameter study of ligament characteristics. Spine (Phila Pa 1976). 2004;**29(4)**: 376-85.

84. del Palomar AP, Calvo B, Doblare M. An accurate finite element model of the cervical spine under quasi-static loading. J Biomech. 2008;**41(3)**: 523-31.

85. Kallemeyn N, Gandhi A, Kode S, Shivanna K, Smucker J, Grosland N. Validation of a C2-C7 cervical spine finite element model using specimen-specific flexibility data. Med Eng Phys. 2010;**32(5)**: 482-9.

86. Maiman DJ, Kumaresan S, Yoganandan N, Pintar FA. Biomechanical effect of anterior cervical spine fusion on adjacent segments. Biomed Mater Eng. 1999;**9(1)**: 27-38.

87. Womack W, Leahy PD, Patel VV, Puttlitz CM. Finite element modeling of kinematic and load transmission alterations due to cervical intervertebral disc replacement. Spine (Phila Pa 1976). 2011.

88. DiAngelo DJ, Foley KT. An improved biomechanical testing protocol for evaluating spinal arthroplasty and motion preservation devices in a multilevel human cadaveric cervical model. Neurosurg Focus. 2004;**17(3)**: E4.

89. Miura T, Panjabi MM, Cripton PA. A method to simulate in vivo cervical spine kinematics using in vitro compressive preload. Spine (Phila Pa 1976). 2002;**27(1)**: 43-8.

90. Panjabi MM, Crisco JJ, Vasavada A, Oda T, Cholewicki J, Nibu K, Shin E. Mechanical properties of the human cervical spine as shown by three-dimensional load-displacement curves. Spine (Phila Pa 1976). 2001;**26(24)**: 2692-700.

91. Biswas D, Bible JE, Bohan M, Simpson AK, Whang PG, Grauer JN. Radiation exposure from musculoskeletal computerized tomographic scans. J Bone Joint Surg Am. 2009;**91(8)**: 1882-9.

92. Fazel R, Krumholz HM, Wang Y, Ross JS, Chen J, Ting HH, Shah ND, Nasir K, Einstein AJ, Nallamothu BK. Exposure to low-dose ionizing radiation from medical imaging procedures. N Engl J Med. 2009;**361(9)**: 849-57.

93. Anderst W, Donaldson W, Lee J, Kang J. Six Degree of Freedom Cervical Spine Range of Motion During Dynamic Flexion-Extension in Single-Level Anterior Arthrodesis Patients and Asymptomatic Controls. Journal of Bone and Joint Surgery. In Press.

94. Pooni JS, Hukins DW, Harris PF, Hilton RC, Davies KE. Comparison of the structure of human intervertebral discs in the cervical, thoracic and lumbar regions of the spine. Surg Radiol Anat. 1986;**8(3)**: 175-82.

95. Rabin D, Pickett GE, Bisnaire L, Duggal N. The kinematics of anterior cervical discectomy and fusion versus artificial cervical disc: a pilot study. Neurosurgery. 2007;**61(3 Suppl)**: 100-4; discussion 104-5.

96. Sasso RC, Best NM. Cervical kinematics after fusion and bryan disc arthroplasty. J Spinal Disord Tech. 2008;**21(1)**: 19-22.

97. Sasso RC, Anderson PA, Riew KD, Heller JG. Results of cervical arthroplasty compared with anterior discectomy and fusion: four-year clinical outcomes in a prospective, randomized controlled trial. J Bone Joint Surg Am. 2011;**93(18)**: 1684-92.

98. Jawahar A, Cavanaugh DA, Kerr EJ, 3rd, Birdsong EM, Nunley PD. Total disc arthroplasty does not affect the incidence of adjacent segment degeneration in cervical spine: results of 93 patients in three prospective randomized clinical trials. Spine J. 2010;**10(12)**: 1043-8.

99. McAfee PC, Reah C, Gilder K, Eisermann L, Cunningham B. A Meta-Analysis of Comparative Outcomes Following Cervical Arthroplasty or Anterior Cervical Fusion: Results from Four Prospective Multi-center Randomized Clinical Trials and up to 1226 Patients. Spine (Phila Pa 1976). 2011.

100. Kelly MP, Mok JM, Frisch RF, Tay BK. Adjacent segment motion after anterior cervical discectomy and fusion versus Prodisc-c cervical total disk arthroplasty: analysis from a randomized, controlled trial. Spine (Phila Pa 1976). 2011;**36(15)**: 1171-9.

101. Auerbach JD, Anakwenze OA, Milby AH, Lonner BS, Balderston RA. Segmental contribution toward total cervical range of motion: a comparison of cervical disc arthroplasty and fusion. Spine (Phila Pa 1976). 2011;**36(25)**: E1593-9.

102. Holmes A, Wang C, Han ZH, Dang GT. The range and nature of flexion-extension motion in the cervical spine. Spine (Phila Pa 1976). 1994;**19(22)**: 2505-10.

103. Miyazaki M, Hong SW, Yoon SH, Zou J, Tow B, Alanay A, Abitbol JJ, Wang JC. Kinematic analysis of the relationship between the grade of disc degeneration and motion unit of the cervical spine. Spine (Phila Pa 1976). 2008;**33(2)**: 187-93.

104. Friedenberg ZB, Miller WT. Degenerative Disc Disease of the Cervical Spine. J Bone Joint Surg Am. 1963;**45**: 1171-8.

105. Okada E, Matsumoto M, Ichihara D, Chiba K, Toyama Y, Fujiwara H, Momoshima S, Nishiwaki Y, Hashimoto T, Ogawa J, Watanabe M, and Takahata T. Aging of the cervical spine in healthy volunteers: a 10-year longitudinal magnetic resonance imaging study. Spine (Phila Pa 1976). 2009;**34(7)**: 706-12.

106. Dvorak J, Panjabi MM, Novotny JE, Antinnes JA. In vivo flexion/extension of the normal cervical spine. J Orthop Res. 1991;**9(6)**: 828-34.

107. Amevo B, Worth D, Bogduk N. Instantaneous axes of rotation of the typical cervical motion segments: a study in normal volunteers. Clinical Biomechanics. 1991;**6**: 111-117.

108. Barrey C, Champain S, Campana S, Ramadan A, Perrin G, Skalli W. Sagittal alignment and kinematics at instrumented and adjacent levels after total disc replacement in the cervical spine. Eur Spine J. 2012;**21(8)**: 1648-59.

109. Bogduk N, Amevo B, Pearcy M. A biological basis for instantaneous centres of rotation of the vertebral column. Proc Inst Mech Eng H. 1995;**209(3)**: 177-83.

110. An KN, Chao EY. Kinematic analysis of human movement. Ann Biomed Eng. 1984;**12(6)**: 585-97.

111. Soudan K, Van Audekercke R, Martens M. Methods, difficulties and inaccuracies in the study of human joint kinematics and pathokinematics by the instant axis concept. Example: the knee joint. J Biomech. 1979;**12(1)**: 27-33.

112. King GJ, McMurtry RY, Rubenstein JD, Gertzbein SD. Kinematics of the distal radioulnar joint. J Hand Surg Am. 1986;**11(6)**: 798-804.

113. Blankevoort L, Huiskes R, de Lange A. Helical axes of passive knee joint motions. J Biomech. 1990;**23(12)**: 1219-29.

114. van den Bogert AJ, Reinschmidt C, Lundberg A. Helical axes of skeletal knee joint motion during running. J Biomech. 2008;**41(8)**: 1632-8.

115. Sheehan FT. The finite helical axis of the knee joint (a non-invasive in vivo study using fast-PC MRI). J Biomech. 2007;**40(5)**: 1038-47.

116. Ogston NG, King GJ, Gertzbein SD, Tile M, Kapasouri A, Rubenstein JD. Centrode patterns in the lumbar spine. Baseline studies in normal subjects. Spine (Phila Pa 1976). 1986;**11(6)**: 591-5.

117. Sawers A, Hahn ME. Trajectory of the center of rotation in non-articulated energy storage and return prosthetic feet. J Biomech. 2011;**44(9)**: 1673-7.

118. Sheehan FT. The instantaneous helical axis of the subtalar and talocrural joints: a non-invasive in vivo dynamic study. J Foot Ankle Res. 2010;**3**: 13.

119. Murrey D, Janssen M, Delamarter R, Goldstein J, Zigler J, Tay B, Darden B. Results of the prospective, randomized, controlled multicenter Food and Drug Administration investigational device exemption study of the ProDisc-C total disc replacement versus anterior discectomy and fusion for the treatment of 1-level symptomatic cervical disc disease. Spine J. 2009;**9(4)**: 275-86.

120. Coric D, Nunley PD, Guyer RD, Musante D, Carmody CN, Gordon CR, Lauryssen C, Ohnmeiss DD, Boltes MO. Prospective, randomized, multicenter study of cervical arthroplasty: 269 patients from the Kineflex|C artificial disc investigational device exemption study with a minimum 2-year follow-up: clinical article. J Neurosurg Spine. 2011;**15(4)**: 348-58.

121. Crisco JJ, 3rd, Chen X, Panjabi MM, Wolfe SW. Optimal marker placement for calculating the instantaneous center of rotation. J Biomech. 1994;**27(9)**: 1183-7.

122. Metzger MF, Faruk Senan NA, O'Reilly OM, Lotz JC. Minimizing errors associated with calculating the location of the helical axis for spinal motions. J Biomech. 2010;**43(14)**: 2822-9.

123. Panjabi MM, Goel VK, Walter SD, Schick S. Errors in the center and angle of rotation of a joint: an experimental study. J Biomech Eng. 1982;**104(3)**: 232-7.

124. Halvorsen K, Lesser M, Lundberg A. A new method for estimating the axis of rotation and the center of rotation. J Biomech. 1999;**32(11)**: 1221-7.

125. Spoor CW, Veldpaus FE. Rigid body motion calculated from spatial co-ordinates of markers. J Biomech. 1980;**13(4)**: 391-3.

126. Curatolo M, Bogduk N, Ivancic PC, McLean SA, Siegmund GP, Winkelstein BA. The role of tissue damage in whiplash-associated disorders: discussion paper 1. Spine (Phila Pa 1976). 2011;**36(25 Suppl)**: S309-15.

127. Page A, De Rosario H, Mata V, Hoyos JV, Porcar R. Effect of marker cluster design on the accuracy of human movement analysis using stereophotogrammetry. Med Biol Eng Comput. 2006;**44(12)**: 1113-9.

128. Panjabi MM. Centers and angles of rotation of body joints: a study of errors and optimization. J Biomech. 1979;**12(12)**: 911-20.

129. Woltring HJ, Long K, Osterbauer PJ, Fuhr AW. Instantaneous helical axis estimation from 3-D video data in neck kinematics for whiplash diagnostics. J Biomech. 1994;**27(12)**: 1415-32.

130. White AP, Biswas D, Smart LR, Haims A, Grauer JN. Utility of flexion-extension radiographs in evaluating the degenerative cervical spine. Spine (Phila Pa 1976). 2007;**32(9)**: 975-9.

131. Powell JW, Sasso RC, Metcalf NH, Anderson PA, Hipp JA. Quality of spinal motion with cervical disk arthroplasty: computer-aided radiographic analysis. J Spinal Disord Tech. 2010;**23(2)**: 89-95.

132. Park JJ, Quirno M, Cunningham MR, Schwarzkopf R, Bendo JA, Spivak JM, Goldstein JA. Analysis of segmental cervical spine vertebral motion after prodisc-C cervical disc replacement. Spine (Phila Pa 1976). 2010;**35(8)**: E285-9.

133. Baillargeon E, Anderst W. Sensitivity, Reliability and Accuracy of the Instant Center of Rotation Calculation in the Cervical Spine During In Vivo Dynamic Flexion-Extension. Journal of Biomechanics. In Press.

134. Erdfelder E, Faul F, Buchner A. G*Power: A general power analysis program. Behavior Research Methods, Instruments, & Computers. 1996;**28**: 1-11.

135. Anderson PA, Sasso RC, Hipp J, Norvell DC, Raich A, Hashimoto R. Kinematics of the cervical adjacent segments after disc arthroplasty compared with anterior discectomy and fusion: a systematic review and meta-analysis. Spine (Phila Pa 1976). 2012;**37(22 Suppl)**: S85-95.

136. Song KJ, Choi BW, Jeon TS, Lee KB, Chang H. Adjacent segment degenerative disease: is it due to disease progression or a fusion-associated phenomenon? Comparison between segments adjacent to the fused and non-fused segments. Eur Spine J. 2011.

137. Stokes IA. Surface strain on human intervertebral discs. J Orthop Res. 1987;**5(3)**: 348-55.

138. O'Connell GD, Johannessen W, Vresilovic EJ, Elliott DM. Human internal disc strains in axial compression measured noninvasively using magnetic resonance imaging. Spine (Phila Pa 1976). 2007;**32(25)**: 2860-8.

139. Kanayama M, Tadano S, Kaneda K, Ukai T, Abumi K, Ito M. A cineradiographic study on the lumbar disc deformation during flexion and extension of the trunk. Clin Biomech (Bristol, Avon). 1995;**10(4)**: 193-199.

140. Anderst W, Donaldson W, Lee J, Kang J. Six-Degrees-of-Freedom Cervical Spine Range of Motion During Dynamic Flexion-ExtensionAfter Single-Level Anterior Arthrodesis: Comparison with Asymptomatic Control Subjects. Journal of Bone and Joint Surgery. 2013;**95(6)**: 497-506.

141. O'Connell GD, Vresilovic EJ, Elliott DM. Human intervertebral disc internal strain in compression: the effect of disc region, loading position, and degeneration. J Orthop Res. 2011;**29(4)**: 547-55.

142. Guehring T, Nerlich A, Kroeber M, Richter W, Omlor GW. Sensitivity of notochordal disc cells to mechanical loading: an experimental animal study. Eur Spine J. 2010;**19(1)**: 113-21.

143. Iatridis JC, MaClean JJ, Ryan DA. Mechanical damage to the intervertebral disc annulus fibrosus subjected to tensile loading. J Biomech. 2005;**38(3)**: 557-65.

144. Maclean JJ, Lee CR, Alini M, Iatridis JC. Anabolic and catabolic mRNA levels of the intervertebral disc vary with the magnitude and frequency of in vivo dynamic compression. J Orthop Res. 2004;**22(6)**: 1193-200.

145. MacLean JJ, Lee CR, Alini M, Iatridis JC. The effects of short-term load duration on anabolic and catabolic gene expression in the rat tail intervertebral disc. J Orthop Res. 2005;**23(5)**: 1120-7.

146. MacLean JJ, Lee CR, Grad S, Ito K, Alini M, Iatridis JC. Effects of immobilization and dynamic compression on intervertebral disc cell gene expression in vivo. Spine (Phila Pa 1976). 2003;**28(10)**: 973-81.

147. Walsh AJ, Lotz JC. Biological response of the intervertebral disc to dynamic loading. J Biomech. 2004;**37(3)**: 329-37.

148. Wuertz K, Godburn K, MacLean JJ, Barbir A, Donnelly JS, Roughley PJ, Alini M, Iatridis JC. In vivo remodeling of intervertebral discs in response to short- and long-term dynamic compression. J Orthop Res. 2009;**27(9)**: 1235-42.

149. Campbell JJ, Lee DA, Bader DL. Dynamic compressive strain influences chondrogenic gene expression in human mesenchymal stem cells. Biorheology. 2006;**43(3-4)**: 455-70.

150. Kisiday JD, Frisbie DD, McIlwraith CW, Grodzinsky AJ. Dynamic compression stimulates proteoglycan synthesis by mesenchymal stem cells in the absence of chondrogenic cytokines. Tissue Eng Part A. 2009;**15(10)**: 2817-24.

151. Yoganandan N, Kumaresan S, Pintar FA. Biomechanics of the cervical spine Part 2. Cervical spine soft tissue responses and biomechanical modeling. Clin Biomech (Bristol, Avon). 2001;**16(1)**: 1-27.

152. Anderst W, Baillargeon E, Donaldson W, Lee J, Kang J. Motion Path of the Instant Center of Rotation in the Cervical Spine During In Vivo Dynamic Flexion-Extension: Implications for Artificial Disc Design and Evaluation of Motion Quality Following Arthrodesis. Spine (Phila Pa 1976). 2013.

153. Boden SD, Davis DO, Dina TS, Patronas NJ, Wiesel SW. Abnormal magnetic-resonance scans of the lumbar spine in asymptomatic subjects. A prospective investigation. J Bone Joint Surg Am. 1990;**72(3)**: 403-8.

154. Bogduk N, Marsland A. The cervical zygapophysial joints as a source of neck pain. Spine (Phila Pa 1976). 1988;**13(6)**: 610-7.

155. Barnsley L, Lord S, Bogduk N. Comparative local anaesthetic blocks in the diagnosis of cervical zygapophysial joint pain. Pain. 1993;**55(1)**: 99-106.

156. Winkelstein BA, Nightingale RW, Richardson WJ, Myers BS. The cervical facet capsule and its role in whiplash injury: a biomechanical investigation. Spine (Phila Pa 1976). 2000;**25(10)**: 1238-46.

157. Barnsley L, Lord SM, Wallis BJ, Bogduk N. The prevalence of chronic cervical zygapophysial joint pain after whiplash. Spine (Phila Pa 1976). 1995;**20(1)**: 20-5; discussion 26.

158. Bogduk N. On cervical zygapophysial joint pain after whiplash. Spine (Phila Pa 1976). 2011;**36(25 Suppl)**: S194-9.

159. Lord SM, Barnsley L, Wallis BJ, Bogduk N. Chronic cervical zygapophysial joint pain after whiplash. A placebo-controlled prevalence study. Spine (Phila Pa 1976). 1996;**21(15)**: 1737-44; discussion 1744-5.

160. Carroll LJ, Holm LW, Hogg-Johnson S, Cote P, Cassidy JD, Haldeman S, Nordin M, Hurwitz EL, Carragee EJ, van der Velde G, Peloso PM, Guzman J, Bone, Joint Decade - Task Force on Neck P, and Its Associated D. Course and prognostic factors for neck pain in whiplash-associated disorders (WAD): results of the Bone and Joint Decade 2000-2010 Task Force on Neck Pain and Its Associated Disorders. Spine (Phila Pa 1976). 2008;**33(4 Suppl)**: S83-92.

161. Inami S, Kaneoka K, Hayashi K, Ochiai N. Types of synovial fold in the cervical facet joint. J Orthop Sci. 2000;**5(5)**: 475-80.

162. Pearson AM, Ivancic PC, Ito S, Panjabi MM. Facet joint kinematics and injury mechanisms during simulated whiplash. Spine (Phila Pa 1976). 2004;**29(4)**: 390-7.

163. Siegmund GP, Myers BS, Davis MB, Bohnet HF, Winkelstein BA. Mechanical evidence of cervical facet capsule injury during whiplash: a cadaveric study using combined shear, compression, and extension loading. Spine (Phila Pa 1976). 2001;**26(19)**: 2095-101.

164. Stemper BD, Yoganandan N, Gennarelli TA, Pintar FA. Localized cervical facet joint kinematics under physiological and whiplash loading. J Neurosurg Spine. 2005;**3(6)**: 471-6.

165. Anderst WJ, Donaldson WF, 3rd, Lee JY, Kang JD. Cervical Motion Segment Percent Contributions to Flexion-Extension During Continuous Functional Movement in Control Subjects and Arthrodesis Patients. Spine (Phila Pa 1976). 2013.

166. Panjabi MM, Oxland TR, Parks EH. Quantitative anatomy of cervical spine ligaments. Part II. Middle and lower cervical spine. J Spinal Disord. 1991;**4(3)**: 277-85.

167. Sterling M, McLean SA, Sullivan MJ, Elliott JM, Buitenhuis J, Kamper SJ. Potential processes involved in the initiation and maintenance of whiplash-associated disorders: discussion paper 3. Spine (Phila Pa 1976). 2011;**36(25 Suppl)**: S322-9.

168. Panjabi MM, Cholewicki J, Nibu K, Grauer J, Babat LB, Dvorak J. Critical load of the human cervical spine: an in vitro experimental study. Clin Biomech (Bristol, Avon). 1998;**13(1)**: 11-17.

169. Yoganandan N, Pintar FA, Zhang J, Baisden JL. Physical properties of the human head: mass, center of gravity and moment of inertia. J Biomech. 2009;**42(9)**: 1177-92.

170. Patwardhan AG, Havey RM, Ghanayem AJ, Diener H, Meade KP, Dunlap B, Hodges SD. Load-carrying capacity of the human cervical spine in compression is increased under a follower load. Spine (Phila Pa 1976). 2000;**25(12)**: 1548-54.

171. Patwardhan AG, Havey RM, Meade KP, Lee B, Dunlap B. A follower load increases the load-carrying capacity of the lumbar spine in compression. Spine (Phila Pa 1976). 1999;**24(10)**: 1003-9.

172. Seacrist T, Arbogast KB, Maltese MR, Garcia-Espana JF, Lopez-Valdes FJ, Kent RW, Tanji H, Higuchi K, Balasubramanian S. Kinetics of the cervical spine in pediatric and adult volunteers during low speed frontal impacts. J Biomech. 2012;**45(1)**: 99-106.

173. Pintar FA, Yoganandan N, Baisden J. Characterizing occipital condyle loads under high-speed head rotation. Stapp Car Crash J. 2005;**49**: 33-47.

174. Pintar FA, Yoganandan N, Maiman DJ. Lower cervical spine loading in frontal sled tests using inverse dynamics: potential applications for lower neck injury criteria. Stapp Car Crash J. 2010;**54**: 133-66.

175. Ivancic PC, Panjabi MM, Ito S. Cervical spine loads and intervertebral motions during whiplash. Traffic Inj Prev. 2006;**7(4)**: 389-99.

176. Moroney SP, Schultz AB, Miller JA. Analysis and measurement of neck loads. J Orthop Res. 1988;**6(5)**: 713-20.

177. Siegmund GP, Blouin JS, Brault JR, Hedenstierna S, Inglis JT. Electromyography of superficial and deep neck muscles during isometric, voluntary, and reflex contractions. J Biomech Eng. 2007;**129(1)**: 66-77.

178. Iowa Uo. *https://mri.radiology.uiowa.edu/visible_human_datasets.html*. downloaded 03/29/2012.

179. Chancey VC, Nightingale RW, Van Ee CA, Knaub KE, Myers BS. Improved estimation of human neck tensile tolerance: reducing the range of reported tolerance using anthropometrically correct muscles and optimized physiologic initial conditions. Stapp Car Crash J. 2003;**47**: 135-53.

180. Ackland DC, Merritt JS, Pandy MG. Moment arms of the human neck muscles in flexion, bending and rotation. J Biomech. 2011;**44(3)**: 475-86.

181. Oi N, Pandy MG, Myers BS, Nightingale RW, Chancey VC. Variation of neck muscle strength along the human cervical spine. Stapp Car Crash J. 2004;**48**: 397-417.

182. Andrade AV, Gomes PF, Teixeira-Salmela LF. Cervical spine alignment and hyoid bone positioning with temporomandibular disorders. J Oral Rehabil. 2007;**34(10)**: 767-72.

183. Zheng L, Jahn J, Vasavada AN. Sagittal plane kinematics of the adult hyoid bone. J Biomech. 2012;**45(3)**: 531-6.

184. Anderst W, Schafman M, Donaldson W, Lee J, Kang J (2011). Cervical Spine Movement Sequencing During Flexion-Extension. *ASME 2011 Summer Bioengineering Conference*. Farmington, PA, USA.

185. Hattori S, Oda H, Kawai U. Cervical intradiscal pressure in movements and traction of the cervical spine. Z. Orthop. 1981;**119**: 568-569.

186. Vasavada AN, Li S, Delp SL. Influence of muscle morphometry and moment arms on the moment-generating capacity of human neck muscles. Spine (Phila Pa 1976). 1998;**23(4)**: 412-22.

187. Iatridis JC, MacLean JJ, Roughley PJ, Alini M. Effects of mechanical loading on intervertebral disc metabolism in vivo. J Bone Joint Surg Am. 2006;**88 Suppl 2**: 41-6.

188. Setton LA, Chen J. Mechanobiology of the intervertebral disc and relevance to disc degeneration. J Bone Joint Surg Am. 2006;**88 Suppl 2**: 52-7.

189. Nachemson AL. Disc pressure measurements. Spine (Phila Pa 1976). 1981;**6(1)**: 93-7.

190. Wilke HJ, Neef P, Caimi M, Hoogland T, Claes LE. New in vivo measurements of pressures in the intervertebral disc in daily life. Spine (Phila Pa 1976). 1999;**24(8)**: 755-62.

191. Panzer MB, Cronin DS. C4-C5 segment finite element model development, validation, and load-sharing investigation. J Biomech. 2009;**42(4)**: 480-90.

192. Kumaresan S, Yoganandan N, Pintar FA, Maiman DJ. Finite element modeling of the cervical spine: role of intervertebral disc under axial and eccentric loads. Med Eng Phys. 1999;**21(10)**: 689-700.

193. Anderst WJ, Donaldson WF, Lee JY, Kang JD. Subject-specific inverse dynamics of the head and cervical spine during in vivo dynamic flexion-extension. J Biomech Eng. 2013;**135(6)**: 61007-8.

194. Anderst WJ, Donaldson WF, 3rd, Lee JY, Kang JD. Continuous cervical spine kinematics during in vivo dynamic flexion-extension. Spine J. 2013.

195. Hussain M, Natarajan RN, An HS, Andersson GB. Motion changes in adjacent segments due to moderate and severe degeneration in C5-C6 disc: a poroelastic C3-T1 finite element model study. Spine (Phila Pa 1976). 2010;**35(9)**: 939-47.

196. Wheeldon JA, Stemper BD, Yoganandan N, Pintar FA. Validation of a finite element model of the young normal lower cervical spine. Ann Biomed Eng. 2008;**36(9)**: 1458-69.

197. Anderst WJ, Lee JY, Donaldson WF, 3rd, Kang JD. Six-degrees-of-freedom cervical spine range of motion during dynamic flexion-extension after single-level anterior arthrodesis: comparison with asymptomatic control subjects. J Bone Joint Surg Am. 2013;**95(6)**: 497-506.

198. Womack W, Woldtvedt D, Puttlitz CM. Lower cervical spine facet cartilage thickness mapping. Osteoarthritis Cartilage. 2008;**16(9)**: 1018-23.

199. Mattucci SF, Moulton JA, Chandrashekar N, Cronin DS. Strain rate dependent properties of younger human cervical spine ligaments. J Mech Behav Biomed Mater. 2012;**10**: 216-26.

200. Yoganandan N, Kumaresan S, Pintar FA. Geometric and mechanical properties of human cervical spine ligaments. J Biomech Eng. 2000;**122(6)**: 623-9.

201. Jones AC, Wilcox RK. Finite element analysis of the spine: towards a framework of verification, validation and sensitivity analysis. Med Eng Phys. 2008;**30(10)**: 1287-304.

202. Anderst W, Donaldson W, Lee J, Kang J (2009). Validation of a Non-Invasive Technique to Precisely Measure In Vivo Three-Dimensional Cervical Spine Movement. *37th Annual Meeting of the Cervical Spine Research Society*.

203. Li G, Van de Velde SK, Bingham JT. Validation of a non-invasive fluoroscopic imaging technique for the measurement of dynamic knee joint motion. J Biomech. 2008;**41(7)**: 1616-22.

204. Defrate LE, Papannagari R, Gill TJ, Moses JM, Pathare NP, Li G. The 6 degrees of freedom kinematics of the knee after anterior cruciate ligament deficiency: an in vivo imaging analysis. Am J Sports Med. 2006;**34(8)**: 1240-6.

205. Iaquinto JM, Tsai R, Haynor DR, Fassbind MJ, Sangeorzan BJ, Ledoux WR. Marker-based validation of a biplane fluoroscopy system for quantifying foot kinematics. Med Eng Phys. 2014;**36(3)**: 391-6.

206. Miranda DL, Schwartz JB, Loomis AC, Brainerd EL, Fleming BC, Crisco JJ. Static and dynamic error of a biplanar videoradiography system using marker-based and markerless tracking techniques. J Biomech Eng. 2011;**133(12)**: 121002.

207. Kumaresan S, Yoganandan N, Pintar FA. Finite element analysis of the cervical spine: a material property sensitivity study. Clin Biomech (Bristol, Avon). 1999;**14(1)**: 41-53.

208. Anderst W, Baillargeon E, Donaldson W, Lee J, Kang J. Motion path of the instant center of rotation in the cervical spine during in vivo dynamic flexion-extension: implications for artificial disc design and evaluation of motion quality after arthrodesis. Spine (Phila Pa 1976). 2013;**38(10)**: E594-601.

209. Dvorak MF, Pitzen T, Zhu Q, Gordon JD, Fisher CG, Oxland TR. Anterior cervical plate fixation: a biomechanical study to evaluate the effects of plate design, endplate preparation, and bone mineral density. Spine (Phila Pa 1976). 2005;**30(3)**: 294-301.

210. Nightingale RW, Winkelstein BA, Knaub KE, Richardson WJ, Luck JF, Myers BS. Comparative strengths and structural properties of the upper and lower cervical spine in flexion and extension. J Biomech. 2002;**35(6)**: 725-32.

211. Stokes IA, Gardner-Morse M. Lumbar spine maximum efforts and muscle recruitment patterns predicted by a model with multijoint muscles and joints with stiffness. J Biomech. 1995;**28(2)**: 173-86.

212. Galbusera F, Wilke HJ, Brayda-Bruno M, Costa F, Fornari M. Influence of sagittal balance on spinal lumbar loads: a numerical approach. Clin Biomech (Bristol, Avon). 2013;**28(4)**: 370-7.